D I P L O M A R B E I T

M A S T E R ' S T H E S I S

Review of stochastic Finite-Element approaches and assessment of their applicability to wood-based products

ausgeführt zum Zwecke der Erlangung des akademischen
Grades eines Diplom-Ingenieurs

unter der Anleitung von

Univ. Ass. Dipl.-Ing. Dr. techn. **Josef Füssl**
Institut für Mechanik der Werkstoffe und Strukturen
Fakultät für Bauingenieurwesen
Technische Universität Wien

und

Univ. Prof. Dipl.-Ing. Dr. techn. DDr. h.c. **Josef Eberhardsteiner**
Institut für Mechanik der Werkstoffe und Strukturen
Fakultät für Bauingenieurwesen
Technische Universität Wien

eingereicht an der Technischen Universität Wien
Fakultät für Bauingenieurwesen

von

Georg Kandler

Matr.Nr.: 06 26 144
Webgasse 22/2/4
A - 1060 Wien

Wien, im Februar 2012

Danksagung

Mein Dank richtet sich an alle Mitarbeiter des Instituts für Mechanik der Werkstoffe und Strukturen. Dekan Univ.-Prof. Dipl.-Ing. Dr. techn. DDr. h.c. Josef Eberhardsteiner möchte ich dafür danken, dass ich am IMWS der TU Wien meine Diplomarbeit verfassen konnte, und ich mich anschließend an diesem Institut der Forschung widmen darf.

Meinen herzlichsten Dank möchte ich meinem Betreuer Dipl.-Ing. Dr. techn. Josef Füssl aussprechen. Seine erstklassige Betreuung ging, sowohl Kompetenz als auch Engagement betreffend, weit über das zu erwartende Maß hinaus. Auch für die Bereitstellung eines Arbeitsplatzes möchte ich mich bedanken. Das Arbeiten in diesem konstruktivem Umfeld gemeinsam mit der intensiven Betreuung hat den einwandfreien Ablauf dieser Arbeit erst ermöglicht.

Auch möchte ich Dipl.-Ing. Dr. techn. Johannes Eitelberger danken, ohne den ich nicht zu dieser Diplomarbeit gekommen wäre. Auch stand er mir immer wieder mit guten Ratschlägen zur Seite.

Bei Univ.Prof. Dipl.-Ing. Dr.techn. Christian Bucher bedanke ich mich für die eigens gehaltene Lehrveranstaltung zur Einführung in die stochastische Mechanik. Auf den in dieser Lehrveranstaltung vermittelten Grundlagen baut diese Arbeit auf.

Ich möchte mich bei meiner Familie, meinen Freunden und Studienkollegen für die ständige Unterstützung während der Studienzeit und auch davor bedanken. Meiner Freundin Luise danke ich für ihr Verständnis und ihre Unterstützung gerade in der letzten stressigen Zeit.

Kurzfassung

Das natürliche Wachstum von Holz führt zu nicht konstanten Dichteverteilungen und unterschiedlichen Astgruppen in Bauholz, das in den verschiedensten Formen, zum Beispiel als Konstruktionsvollholz (KVH), Brettschichtholz (BSH) oder Brettsperrholz, genutzt wird. Die aktuell angewandten Bemessungs- und Berechnungsverfahren basieren jedoch hauptsächlich auf deterministischen Konzepten und empirisch hergeleiteten Materialparametern, die die in der Realität auftretende Streuung der Materialeingangswerte nicht ausreichend berücksichtigen. Das Resultat sind teilweise unwirtschaftliche Konstruktionen, die aber trotz hoher Sicherheitsbeiwerte die Gebrauchstauglichkeit nicht unbedingt gewährleisten.

Daher ist das Ziel dieser Arbeit, den Einfluss der räumlich zufällig variierenden Steifigkeit eines Brettes auf die Gesamtsteifigkeit des Endprodukts BSH zu quantifizieren. Die zufälligen Materialeigenschaften werden durch Zufallsvariablen, -prozesse und -felder modelliert. Um daraus die mechanischen Eigenschaften von BSH ableiten zu können, werden unterschiedliche Verfahren der so genannten Stochastischen Finite Elemente Methode (SFEM) vorgestellt, die hauptsächlich in den letzten drei Jahrzehnten entwickelt wurden. Zur Berechnung des Mittelwerts und der Standardabweichung der Struktureigenschaften eignen sich vor allem die Monte Carlo Simulation, die "Perturbation" Methode basierend auf der Taylorreihenentwicklung und die Spektrale Stochastische Finite Elemente Methode. Diese Methoden werden mit der Mittelpunktsdiskretisierung und der Karhunen-Loève Reihenentwicklung kombiniert und auf BSH mit bis zu vier Brettlagen angewendet. Schlußendlich wird in einer Parameterstudie die Genauigkeit der Methoden verglichen, und vor allem der oben genannte Einfluss einzelner Bretter auf die Gesamtsteifigkeit verdeutlicht.

An den Ergebnissen kann man sehen, dass die Monte Carlo Simulation zwar eine flexible und genaue Methode, dafür aber auch sehr rechenintensiv ist. Im Gegensatz dazu benötigen die "Perturbation" Methode und die Spektrale Stochastische Finite Elemente Methode einen Bruchteil an Rechenzeit. Während mit letzterer genaue Resultate für einzelne Bretter gewonnen werden können, liefert die "Perturbation" Methode vor allem bei mehreren Brettern gute Ergebnisse.

Zusammenfassend lässt sich sagen, dass mit der Stochastischen Finite Elemente Methode sehr effizient und genau auf die Streuung der mechanischen Eigenschaften von holz-basierten Produkten geschlossen werden kann. Daher liegt es nahe, dass die darauf basierenden Resultate stark an Bedeutung gewinnen werden, sei es bei der Sortierung von Bauholz, der Optimierung von Holzprodukten oder in zukünftigen Bemessungsansätzen für Holzkonstruktionen.

Abstract

Considering timber elements, a high variability of their effective properties is induced by uncertain density distributions and the existence of different knot groups. However, dimensioning practice and many existing design rules for glued-laminated-timber (GLT) are still based on deterministic calculation methods. The stochastic aspect is only considered by empirically determined parameters, which often leads to unsatisfactory results in terms of efficiency and reliability of wood-based products and timber structures.

This thesis aims at giving an idea of how the spatial stiffness variability of timber influences the performance of wood-based products, in this case GLT. The variability is captured using the framework of random variables, processes, and fields. To place these uncertain quantities into a mechanical context, different Stochastic-Finite-Element Methods (SFEM), which have been mainly developed within the last three decades, are reviewed. For obtaining the mean value and standard deviation of the structural response, the most promising approaches are the Monte Carlo simulation, the Perturbation Method and the Spectral-Stochastic-Finite-Element Method. The application of these methods to a GLT beam with up to four laminations is presented and discussed in detail. Thereby, the random field is approximated either with discrete elements (midpoint method) or by using series expansions (Karhunen-Loève expansion). Finally, in a parameter study the performance of the different approaches is compared and, in particular, the influence of the variability of the "raw" material on the structural response is shown.

Well known effects, such as the decrease of the variability of effective properties of GLT with increasing number of laminations, are numerically reproduced and quantified. Moreover, a significant influence of the correlation length, specifying the rate of material-property fluctuation, on the "overall" stiffness is demonstrated.

Regarding the different approaches, the Monte Carlo simulation, on the one hand, is an universally applicable method and suitable for obtaining reference results. However, the computational effort is huge compared to the Perturbation- and the Spectral-Stochastic-Finite-Element Method, respectively, which provide results of equal quality, when used in the right context.

Summarized, it can be said that the Stochastic-Finite-Element Method is a powerful and valuable tool to gain understanding of the variability of the mechanical behaviour of wood-based products. Results, based on this methods, will become important in many fields, from grading and optimization of wood-based products to engineering design of wooden structures.

Contents

Chapter 1

Introduction

1.1 Motivation

Wood is a naturally renewable material and is consequently gaining importance for a number of reasons. Most importantly, forestry and wood products play a major role in combating climate changes and can help European countries to achieve their Kyoto targets, not only by increasing the carbon sink of wood-based products and growing forests, but also by decreasing carbon sources through substituting energy-intensive products by wood-based products. Not least because of its evident ecological advantages, its share on the building market is constantly increasing, and volume consumption is facing enormous growth rates.

Nevertheless, dimensioning practice and many existing design rules are still based on an empirical background, which often gives unsatisfactory results in terms of efficiency and reliability. Developing the design concepts of wood-based products and improving analysing techniques for timber structures will strengthen the competitiveness of wood against other technical materials and open up new fields of application and new markets, respectively. Among others, the Finite-Element Method (FEM) has been proven to be a powerful and versatile numerical method to predict the structural behaviour of complex systems. However, in general, commercial FE-codes can handle only deterministic quantities, but nearly all building materials used in civil engineering show a certain amount of structural variability, leading to a variability in their material properties, too.

Considering timber elements, the main variability of their effective properties is induced by uncertain density distributions and different knot groups. For example, an unfavorable located knot group can reduce the local stiffness or strength up to an order of magnitude, compared with the "undisturbed" material. Through grading processes, the variance of the effective timber properties is reduced for a certain grading class, and specified in terms of statistical information, e.g. the mean value and variance of the elasticity modulus. Current design methods are not able to take the statistical distribution of material properties into account, and thus, delivering no statistical information of the

structural response. Therefore, in recent years, effort has been made in enhancing the FE-method and implementing the ability to derive random quantities as well. These approaches are denoted as the *Stochastic-Finite-Element Method* (SFEM). Their purpose lies in the implementation of the framework of random variables, processes, and fields, which allows handling such uncertain input, implied that its statistical information, e.g. for the Gaussian assumption the mean value and the variance, is available.

In this thesis, different representations of random fields with respect to the SFEM are proposed. Furthermore, a comprehensive overview of existing SFEMs is given, and the main characteristics of each approach are briefly described. Finally, different SFE approaches are applied to a glued-laminated-timber beam, showing the performance of the different methods and giving a first idea how valuable such approaches for the understanding and improvement of wood-based products possibly can be.

1.2 Structure of the thesis

Chapter 2 gives basic insights in probability theory, while in Chapter 3 the concept of random field representation is explained. The different SFE-methods are described in Chapter 4. Finally, in Chapter 5 the application of different SFE approaches to a glued-laminated-timber beam, subjected to loading in longitudinal direction, is shown, and the obtained results are discussed. Concluding remarks are given in Chapter 6.

Chapter 2

Probability and random fields

2.1 Probability theory

The term *trial* usually describes the observation of a random phenomenon with uncertain outcome. When conducting an experiment, the actual outcome is called *realization*. The so called *sample space* Θ consists of all possible *outcomes* θ, whereas an *event* $\mathcal{A}$ is a subset of Θ, consisting of a specific set of outcomes $\theta \in \Theta$. The *probability* $P[.]$ provides a so called *probability measure* by assigning real numbers to events, thereby allowing interpretation of their probability of occurence. Since it is not always possible to assign a probability to each event $\mathcal{A} \in \Theta$, the focus will lie on the set of events $\mathcal{F}$, to which probabilities can be assigned, and which is called σ-algebra associated with Θ. The resulting so called *probability space* is denoted by $(\Theta, \mathcal{F}, P)$ [39].

The most convenient way to define the probability $P[\mathcal{A}]$ for an event $\mathcal{A}$, is to divide the number of ways event $\mathcal{A}$ can occur by the total number of outcomes Θ. This is the so called *classical definition of probability*:

$$P[\mathcal{A}] = \frac{\text{number of possibilities favorable for event } \mathcal{A}}{\text{total number of outcomes } \Theta} \tag{2.1}$$

For example when rolling the dice the number of possibilities for the number 6 to occur is 1, whereas the total number of possibilities is 6. Therefore, the probability for a perfect balanced die showing a 6 equals 1/6. For a probability of zero ($P[\mathcal{A}] = 0$), $\mathcal{A}$ is called an *impossible event*. An event is called *almost sure* if the probability equals 1. However, there exist problems, which cannot be predicted with the classical definition sufficiently, e.g. Bertrand's paradox [40].

Hence the *modern definition of probability* $P[.]$ is based on the *Kolmogorov-axioms*:

$$0 \leq P[\mathcal{A}] \leq 1, \tag{2.2}$$

$$P[\Theta] = 1, \tag{2.3}$$

$$P[\mathcal{A} \cup \mathcal{B}] = P[\mathcal{A}] + P[\mathcal{B}], \tag{2.4}$$

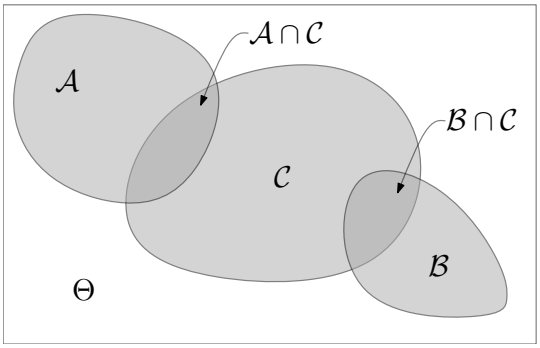

Figure 2.1: Events $\mathcal{A}$ and $\mathcal{B}$ are mutual exclusive while $\mathcal{C}$ shares an intersection area with both of them.

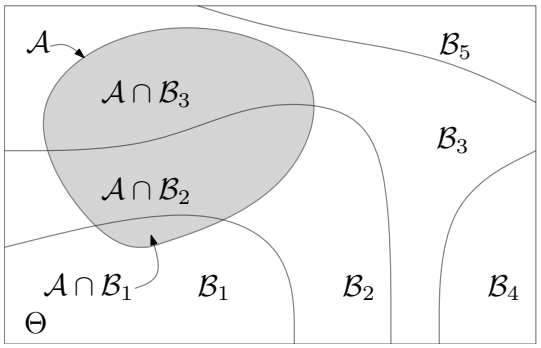

Figure 2.2: Events $\mathcal{B}_i$ are partitioning the sample space, which is shared with $\mathcal{A}$. The law of total probability provides the link between $P[\mathcal{A}]$ and the conditional probabilites $P[\mathcal{A} \mid \mathcal{B}_i]$.

where $\mathcal{A}$ and $\mathcal{B}$ are events, while Θ is the sample space consisting of all events, i.e. $\Theta = \{\mathcal{A} \cup \mathcal{B} \cup \mathcal{C} \cup \dots\}$. An event is a set of possible outcomes and thus, as stated above, the sample space is the set of all possible outcomes. Figure 2.1 shows a so called *Venn-diagram* consisting of events $\mathcal{A}, \mathcal{B}$ and $\mathcal{C}$ being embedded in sample space Θ. The probability for an event to occur ranges from 0 to 1 (see Equation (2.2)). The sum of all events in Θ equals the sample space, thus it covers every possibility. Therefore, Θ is called an *almost sure event* and its probability is equal to 1, as given in Equation (2.3). For instance, when throwing the dice, possible events are $\mathcal{A}_1 = 1, \mathcal{A}_2 = 2, \dots, \mathcal{A}_6 = 6$ with the sample space $\Theta = \{\mathcal{A}_1 \cup \dots \cup \mathcal{A}_6\} = \{1 \cup \dots \cup 6\}$. The probability $P[\Theta]$ equals the probability that the die will show any of its faces, which is obviously equal to one. The counterpart to the almost sure event is an event which covers a set of outcomes infeasible by the nature of the experiment, and is called *almost impossible event*.

The probability that different events occur, given they are *mutually exclusive* (also called mutually disjoint), equals the sum of the individual probabilities. Two mutually exclusive events are events that cannot both occur at the same time or in the same trial, in other words: They don't share an intersection area in the Venn diagram (for example, events $\mathcal{A}$ and $\mathcal{B}$ in Figure 2.1, where $\mathcal{A} \cap \mathcal{B} = \emptyset$). Two faces of a die are mutually exclusive because only one face can be up at a time. For instance, $\mathcal{A}_1 = \{1\}$ and $\mathcal{A}_2 = \{2\}$ is rolling a 1 and 2, respectively. Since they are mutually exclusive, the probability for $\mathcal{A}_1$ or $\mathcal{A}_2$ to occur is $P[\mathcal{A}_1 \cup \mathcal{A}_2] = P[\mathcal{A}_1] + P[\mathcal{A}_2] = 1/6 + 1/6 = 1/3$. Giving another example, event $\mathcal{A} = \{1 \cup 2\}$ is rolling a 1 or 2 whereas event $\mathcal{B} = \{3 \cup 4\}$ is rolling a 3 or 4. The probability of event $\mathcal{A}$ or event $\mathcal{B}$ to occur is $P[\mathcal{A} \cup \mathcal{B}] = P[\mathcal{A}] + P[\mathcal{B}] = \{1 \cup 2\} + \{3 \cup 4\} = 1/3 + 1/3 = 2/3$.

Obviously, there are events that are *not mutually exclusive*, meaning they are sharing an intersection area like events $\mathcal{A}$ and $\mathcal{C}$ in Figure 2.1. For example, event $\mathcal{A} = \{1 \cup 2\}$ is rolling a 1 or 2 whereas event $\mathcal{B} = \{2 \cup 3\}$ is rolling a 2 or 3. If the die shows a 2 then both events occur at the same time, therefore violating the mutual exclusivity. Deriving the probability $P[\mathcal{A} \cup \mathcal{B}]$ with Equation (2.4) leads to an error now, the outcome is $P[\mathcal{A} \cup \mathcal{B}] = P[\mathcal{A}] + P[\mathcal{B}] = \{1 \cup 2\} + \{2 \cup 3\} = 1/3 + 1/3 = 2/3$, which cannot be

true because number 2 is accounted twice for. The correct equation for not mutually exclusive events is

$$P[\mathcal{A} \cup \mathcal{B}] = P[\mathcal{A}] + P[\mathcal{B}] - P[\mathcal{A} \cap \mathcal{B}], \tag{2.5}$$

including the so called *joint probability* $P[\mathcal{A} \cap \mathcal{B}]$. Since we are talking about the same area in the Venn diagram, the probabilities of the so called joint events $\mathcal{A} \cap \mathcal{B}$ and $\mathcal{B} \cap \mathcal{A}$ are equal, or in other words, the events $\mathcal{A}$ and $\mathcal{B}$ can be exchanged:

$$P[\mathcal{A} \cap \mathcal{B}] = P[\mathcal{B} \cap \mathcal{A}] \tag{2.6}$$

The correct answer now is $P[\mathcal{A} \cup \mathcal{B}] = P[\mathcal{A}] + P[\mathcal{B}] - P[\mathcal{A} \cap \mathcal{B}] = P[\{1 \cup 2\}] + P[\{2 \cup 3\}] - P[\{1 \cup 2\} \cap \{2 \cup 3\}] = 1/3 + 1/3 - 1/6 = 1/2$, because $P[\{1 \cup 2\} \cap \{2 \cup 3\}] = P[\{2\}] = 1/6$.

In some cases the probability of one event given the occurence of another event is of interest. This is the so called *conditional probability*

$$P[\mathcal{A} \mid \mathcal{B}] = \frac{P[\mathcal{A} \cap \mathcal{B}]}{P[\mathcal{B}]}. \tag{2.7}$$

For instance, when looking at Figure 2.2, the relevant sample space for event $\mathcal{A}$ has changed from Θ to $\mathcal{B}_1$, since it is given the occurence of event $\mathcal{B}_1$. The space of possibilities for event $\mathcal{A}$ occuring conditional on event $\mathcal{B}_1$ is restricted to the intersection area of those two events $P[\mathcal{A} \cap \mathcal{B}_1]$. The conditional probability then equals the probability of the intersection area $P[\mathcal{A} \cap \mathcal{B}_1]$ divided by the probability of the new sample space $P[\mathcal{B}_1]$. For example event $\mathcal{A} = \{1 \cup 3 \cup 5\}$ describes the possibilities of a die showing an odd number. On the other hand event $\mathcal{B} = \{4 \cup 5 \cup 6\}$ is the roll takes a value equal or greater than 4. Then the probability of $\mathcal{A}$ conditional on $\mathcal{B}$ is $P[\mathcal{A} \mid \mathcal{B}] = P[\{1 \cup 3 \cup 5\} \cap \{4 \cup 5 \cup 6\}]/P[\{4 \cup 5 \cup 6\}] = P[\{5\}]/P[\{4 \cup 5 \cup 6\}] = (1/6)/(1/2) = 1/3$.

Two events are called *independent*, if

$$P[\mathcal{A} \mid \mathcal{B}] = P[\mathcal{A}]. \tag{2.8}$$

If two events $\mathcal{A}$ and $\mathcal{B}$ are independent, the occurrence of $\mathcal{B}$ does not affect the probability of $\mathcal{A}$ conditional on $\mathcal{B}$. Substituting Equation (2.8) into (2.7) yields

$$P[\mathcal{A} \cap \mathcal{B}] = P[\mathcal{A}] \cdot P[\mathcal{B}]. \tag{2.9}$$

Supposing two dice are rolled and the dice don't affect each other, i.e. each roll is independent. Then the probability for the first die to roll a 2 is $\mathcal{A} = \{2\} = 1/6$. The same applies for the second die, thus $\mathcal{B} = \{2\} = 1/6$. The probability for both rolls to be a 2 equals $P[\mathcal{A} \cap \mathcal{B}] = P[\mathcal{A}] \cdot P[\mathcal{B}] = (1/6) \cdot (1/6) = 1/36$.

The equations presented in this section can be generalized for more than 2 events. Equation (2.4) then becomes

$$P[\mathcal{A}_1 \cup \mathcal{A}_2 \cup \cdots \cup \mathcal{A}_N] = \sum_{i=1}^{N} P[\mathcal{A}_i]. \tag{2.10}$$

Realigning (2.7) and supposing $\mathcal{B}_i \cap \mathcal{B}_j = \emptyset, i \neq j$ are pairwise mutually exclusive events yields

$$P[\mathcal{A} \cap \mathcal{B}_i] = P[\mathcal{A} \mid \mathcal{B}_i] \cdot P[\mathcal{B}_i]. \tag{2.11}$$

Under the condition that the sum of the components $\mathcal{B}_i$ equals the sample space, i.e. $\sum_{i=1}^{N} \mathcal{B}_i = \Theta$, the probability for $\mathcal{A}$, describing any event in the same sample space Θ and thus sharing intersection areas with $\mathcal{B}_i$, can be derived with

$$P[\mathcal{A}] = \sum_{i=1}^{N} P[\mathcal{A} \cap \mathcal{B}_i] = \sum_{i=1}^{N} P[\mathcal{A} \mid \mathcal{B}_i] \cdot P[\mathcal{B}_i]. \tag{2.12}$$

Equation (2.12) is called the law of *total probability*. It is visualized in Figure 2.2. Substituting (2.11) and (2.12) into (2.6) and realigning yields the so called *Bayes' theorem*

$$P[\mathcal{B}_i \mid \mathcal{A}] = \frac{P[\mathcal{A} \mid \mathcal{B}_i] \cdot P[\mathcal{B}_i]}{P[\mathcal{A}]} = \frac{P[\mathcal{A} \mid \mathcal{B}_i] \cdot P[\mathcal{B}_i]}{\sum\limits_{i=1}^{N} P[\mathcal{A} \mid \mathcal{B}_i] \cdot P[\mathcal{B}_i]}. \tag{2.13}$$

Mathematically speaking, it provides the link between the conditional probability $P[\mathcal{B}_i \mid \mathcal{A}]$ and its inverse $P[\mathcal{A} \mid \mathcal{B}_i]$.

As an extension to (2.9) events $\mathcal{A}_1, \ldots \mathcal{A}_N$ are called independent if and only if

$$\mathrm{P}[\mathcal{A}_1 \cap \ldots \cap \mathcal{A}_N] = \mathrm{P}[\mathcal{A}_1] \cdots \mathrm{P}[\mathcal{A}_N]. \tag{2.14}$$

2.2 Random variables

A real-valued *random variable* X is a measurable function from sample space Θ to real space $\mathbb{R}$, i.e. $X : \Theta \to \mathbb{R}$. In other words, it provides a numerical description of the outcome of a trial, which is a more or less abstract term. Since any experiment with sample space Θ is considered to have random output, the corresponding real-valued number is also random [33]. For example, when throwing the dice, it can take values $\theta \in \Theta$ with sample space $\Theta = \{1, 2, 3, 4, 5, 6\}$. The most convenient way is to define the random variable X equal to the number rolled $\theta \in \Theta$. Hence X can assume values from 1 to 6. Another example for using random variables is tossing a coin. The sample space consists of $\Theta = \{\text{heads}, \text{tails}\}$, whereas the corresponding random variable X takes on values of 1 for heads and 0 for tails. In this case X represents a discrete random variable. Generally speaking, a discrete random variable can assume only a finite or countably infinite number of values. In other words, a random variable X is discrete, if indexing the feasible outcomes of X using integers $n \in \mathbb{N}$ is possible. On the contrary, continuous random variables X map the outcomes to values of an uncountable set (for example, the set of real numbers $\mathbb{R}$), in other words, indexing using integers is not possible because X can assume a continuum of values. Therefore, when estimating the strength of concrete or steel, continuous random variables are used.

2.3 Univariate probability distribution functions

For an event $\mathcal{A} = \{X < x\}$, comparing a real-valued random variable X against a deterministic real value x, there exists a probability $P[\mathcal{A}] = P[X < x]$ expressing the probability for the random variable X to exceed the deterministic value x. The magnitude of $P[X < x]$ depends on the value of x. Therefore, a new probability function is

introduced so that

$$P[X \leq x] = F_X(x). \tag{2.15}$$

$F_X(x)$ is called the *cumulative distribution function* (cdf). Since the cdf is related to one random variable, it is called an univariate distribution function.

The following properties stem from the assumption that all real-valued values x lie between the limits $-\infty$ and $+\infty$, but never reach either of them:

$$\lim_{x \to -\infty} F_X(x) = 0 \quad \text{and} \quad \lim_{x \to +\infty} F_X(x) = 1 \tag{2.16}$$

The first equation of (2.16) results from knowing that $x = -\infty$ is the smallest possible value. Thus, the probability for X assuming a value less than $x = -\infty$ is $P[x = -\infty] = 0$. The second equation stems from knowing that $x = +\infty$ is the biggest possible value and hence every value of X has to be less than $x = +\infty$ for sure, i.e. $P[x = +\infty] = 1$. Therefore, $F_X(x)$ can assume values from 0 to 1:

$$0 \leq F_X(x) \leq 1 \tag{2.17}$$

The cdf is a monotonically increasing function which can assume values between 0 and 1 for $-\infty \leq x \leq +\infty$.

For a continuous random variable X the derivative of $F_X(x)$ yields the *probability density function* (pdf)

$$f_X(x) = \frac{\mathrm{d}(F_X(x))}{\mathrm{d}x}, \tag{2.18}$$

whereas integrating the pdf returns the cdf

$$\int_{-\infty}^{x} f_X(\xi)\mathrm{d}\xi = F_X(x). \tag{2.19}$$

Integrating the pdf over the whole sample space Θ equals integrating from $-\infty$ to $+\infty$, since this covers the complete range of possibilites for X. From Equation (2.16) then follows

$$\int_{-\infty}^{+\infty} f_X(x)\mathrm{d}x = F_X(x) \mid_{x=+\infty} - F_X(x) \mid_{x=-\infty} = 1 - 0 = 1. \tag{2.20}$$

Considering Equation (2.3), the outcome of (2.20) could have been predicted in the first place. Since the cdf $F_X(x)$ is the antiderivative of the pdf $f_X(x)$, Equation (2.20) applies for every $x_1 < x_2$:

$$\int_{x_1}^{x_2} f_X(x)\mathrm{d}x = F_X(x_2) - F_X(x_1) \tag{2.21}$$

The probability for a continuous random variable X assuming a specific value x is $\int_x^x f_X(\xi)\mathrm{d}\xi = 0$ according to (2.21). The pdf provides non-zero results only for ranges of $x_1 < x_2$.

For discrete random variables the pdf becomes the *probability mass function* (pmf)

$$p_X(x) = P[X = x]. \tag{2.22}$$

The pmf expresses the finite probability of a discrete random variable X taking a specific deterministic value x by assuming values between 0 and 1. Similar to (2.20) the pmf satisfies

$$\sum_{i=1}^{N} p_X(x_i) = 1. \tag{2.23}$$

2.3.1 Expectation values of univariate pdfs

In most cases so called expected values suffice to describe a pdf completely. For a continuous random variable the expectation value E[.] is defined by

$$\mathrm{E}[X] = \int_{-\infty}^{+\infty} x f_X(x) \mathrm{d}x, \tag{2.24}$$

while for discrete random variables the definition is as follows:

$$\mathrm{E}[X] = \sum_{i=1}^{N} x p_X(x_i) \tag{2.25}$$

The first moment ($\mathrm{E}[X^n]$ with $n = 1$ in (2.24)) is called *mean* or expectation of X. It is defined by

$$\mu_X \equiv \bar{X} \equiv \mathrm{E}[X] = \int_{-\infty}^{+\infty} x f_X(x) \mathrm{d}x. \tag{2.26}$$

Deriving $\mathrm{E}[(x - \mu_X)^2]$ leads to the second central moment, also called *variance*

$$\sigma_X^2 \equiv \mathrm{Var}[X - \mu_X] = \mathrm{E}[(X - \mu_X)^2] = \int_{-\infty}^{+\infty} (x - \mu_X)^2 f_X(x) \mathrm{d}x. \tag{2.27}$$

Equation (2.27) can be simplified:

$$\begin{aligned} \sigma_X^2 &= \mathrm{E}[(X - \mu_X)^2] = \mathrm{E}[X^2 - 2\mu_X X + \mu_X^2] \\ &= \mathrm{E}[X^2] - 2\mu_X^2 + \mu_X^2 = \mathrm{E}[X^2] - \mu_X^2, \end{aligned} \tag{2.28}$$

which is equivalent to applying the Huygens-Steiner theorem. The squareroot of the variance is called *standard deviation* σ_X

$$\sigma_X = \sqrt{\sigma_X^2} = \sqrt{\mathrm{E}[X^2] - \mu_X^2}. \tag{2.29}$$

To normalize the measure of dispersion of a probability distribution the *coefficient of variation* δ_X is introduced:

$$\delta_X = \frac{\sigma_X}{\mu_X} \tag{2.30}$$

Since σ_X and μ_X have the same units, δ_X is unit-less.

The expectation E is a linear operator, thus it can be exchanged with sums and integrals

$$\mathrm{E}\left[\sum X_i\right] = \sum \mathrm{E}[X_i], \quad \mathrm{E}\left[\int X_i \mathrm{d}x\right] = \int \mathrm{E}[X_i]\mathrm{d}x. \tag{2.31}$$

Furthermore, the following rules apply:

$$\mathrm{E}[aX] = a\mathrm{E}[X], \quad a = \text{const.}, \tag{2.32}$$

$$\mathrm{E}\big[\mathrm{E}[X]\big] = \mathrm{E}[X]. \tag{2.33}$$

2.3.2 Univariate normal (Gaussian) distribution

The Gaussian or *normal distribution* is popular not only for its simplicity, its use is often justified by the *central limit theorem*. It states, that the sum of independent arbitrarily distributed random variables X_i approaches the normal distribution as the number of terms is heading to ∞. The normal probability distribution function is a continuous distribution which is completely described by the mean μ_X and the standard deviation σ_X, therefore a Gaussian random variable is commonly denoted as $\mathrm{N}(\mu_X, \sigma_X)$:

$$f_X(x) = \frac{1}{\sigma_X\sqrt{2\pi}} \exp\left[-\frac{1}{2}\left(\frac{x-\mu_X}{\sigma_X}\right)^2\right] \qquad \ldots -\infty < x < +\infty \tag{2.34}$$

Integrating yields the cdf

$$F_X(x) = \frac{1}{\sigma_X\sqrt{2\pi}} \int_{-\infty}^{x} \exp\left[-\frac{1}{2}\left(\frac{\xi-\mu_X}{\sigma_X}\right)^2\right] \mathrm{d}\xi = \Phi\left(\frac{x-\mu_X}{\sigma_X}\right). \tag{2.35}$$

Equations (2.34) and (2.35) are visualized in Figure 2.3. For the integral in Equation (2.35) no analytical solution $\Phi(.)$ exists. However, the random variable X can be transformed into a so called standard normal variable $Z = (X - \mu_X)/\sigma_X$, resulting in a random variable with zero mean and unit standard deviation, i.e. $\mathrm{N}(0, 1)$. Numerical solutions as well as tables for the cdf of this standard normal variable are widespread and can be found easily.

On the downside, one has to consider that the normal pdf can assume positive as well as negative values, what is not desirable in some situations, in particular when depicting the elastic modulus.

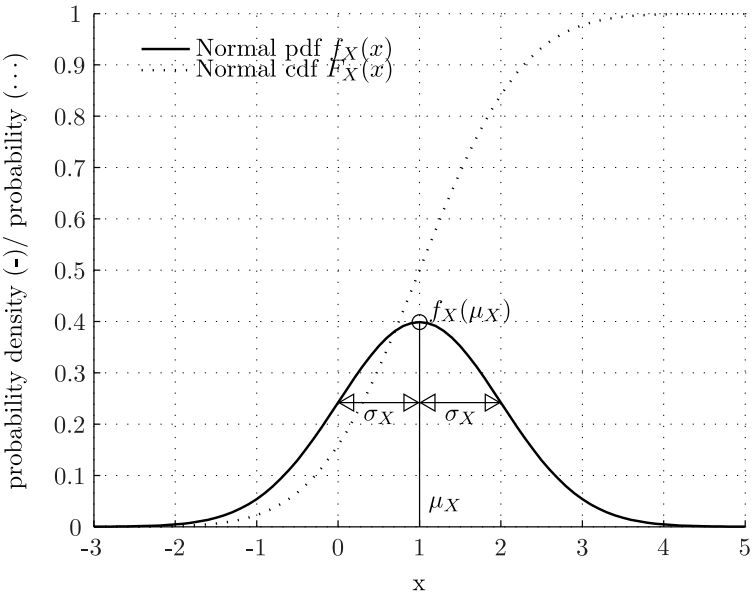

Figure 2.3: Normal pdf and cdf for N(1, 1).

2.4 Joint probability distribution functions

2.4.1 Random vectors

A *random vector* $\mathbf{X}$ is an array of random variables $X_1, \dots X_M$:

$$\mathbf{X} = [X_1, \dots X_M]^\mathsf{T} \tag{2.36}$$

Sometimes the components of $\mathbf{X}$ are mutually independent, but in many cases there exist, to varying extends, dependencies. The connection between 2 components X_i and X_j of a random vector can be described by the so called *auto-covariance*, which is

$$\begin{aligned} C_{ij} \equiv \mathrm{Cov}[X_i, X_j] &= \mathrm{E}[(X_i - \mu_{X_i})(X_j - \mu_{X_j})] \\ &= \int_{-\infty}^{+\infty}\int_{-\infty}^{+\infty} (X_i - \mu_{X_i})(X_j - \mu_{X_j}) f_{X_i,X_j}(x_i, x_j)\mathrm{d}x_i\mathrm{d}x_j. \end{aligned} \tag{2.37}$$

In (2.37) $f_{X_i,X_j}(x_i, x_j)$ denotes the so called *joint probability density function*. Its properties are similar to the univariate pdf, further details will be presented in the following sections. The quantities C_{ij} are components of the *auto-ccovariance matrix* $\mathbf{C_{XX}} = \mathrm{Cov}[\mathbf{X}, \mathbf{X}]$. For a random vector $\mathbf{X}$ containing M random variables, the covariance matrix has dimensions of $M \times M$. For the case of $i = j$ the covariance equals the variance of random variable X_i

$$C_{ii} = \mathrm{E}[(X_i - \mu_{X_i})^2] = \sigma^2_{X_i}. \tag{2.38}$$

Thus, the variance σ_X^2 can be seen as a special case of the covariance C_{ij}. The dimensionless *coefficent of correlation* is defined as [41]

$$\rho_{ij} \equiv \rho_{X_i,X_j} = \frac{\mathrm{Cov}[X_i, X_j]}{\sigma_i \sigma_j} = \frac{C_{ij}}{\sigma_i \sigma_j}. \tag{2.39}$$

The correlation coefficient assumes values in the range of $-1 \leq \rho_{ij} \leq +1$. For $\rho_{ij} = \pm 1$, random variables X_i and X_j are called *perfectly correlated*. On the contrary, for $\rho_{ij} = 0$ they are *perfectly uncorrelated*. The correlation coefficient provides a measurable quantity for the linear correlation between two random variables.

In contrast to the auto-covariance matrix $\mathbf{C_{XX}}$ the so called *cross-covariance matrix* $\mathbf{C_{XY}}$ provides information on the statistical dependencies between two different random vectors $\mathbf{X}$ and $\mathbf{Y}$. Since the indices already imply if auto-covariance or cross-covariance is used, from now on those terms will be suppressed where not absolutely necessary.

2.4.2 Bivariate probability distribution functions

The introduction of the random vector $\mathbf{X} = [X_1, X_2]^\mathsf{T}$ allows extending the concept presented in Section 2.3 for two random variables, which leads to the following definition of the so called *joint cumulative distribution function* [33, 41]

$$F_{X_1,X_2}(x_1, x_2) \equiv F(x_1, x_2) = P[\{X_1 \leq x_1\} \cap \{X_2 \leq x_2\}]. \tag{2.40}$$

The joint cdf gives the probability for the random variables X_1 and X_2 to exceed the deterministic values x_1 and x_2 respectively. Assuming the joint cdf is continuous, differentiation yields

$$f(x_1, x_2) = \frac{\partial^2 F(x_1, x_2)}{\partial x_1 \partial x_2}. \tag{2.41}$$

Integration of $f(x_1, x_2)$ returns the joint cdf $F(x_1, x_2)$

$$F(x_1, x_2) = \int_{-\infty}^{x_1} \int_{-\infty}^{x_2} f(u_1, u_2) \mathrm{d}u_1 \mathrm{d}u_2. \tag{2.42}$$

Since the assumpations stated in (2.16) still apply, setting the integration limits to $x_1 = +\infty, x_2 = +\infty$ yields

$$F(+\infty, +\infty) = \int_{-\infty}^{+\infty} \int_{-\infty}^{+\infty} f(u_1, u_2) \mathrm{d}u_1 \mathrm{d}u_2 = 1. \tag{2.43}$$

Similar to equations (2.8), (2.9) and (2.14), statements regarding the independence of random variables X_1 and X_2 can be made. For instance, two random variables X_1 and X_2 are called independent if and only if [41]

$$f(x_1, x_2) = f(x_1) f(x_2), \tag{2.44}$$

which is equal to

$$f(x_1 \mid x_2) = f(x_1). \tag{2.45}$$

2.4.3 Multivariate probability distribution functions

The concept can be expanded further for a random vector $\mathbf{X} = [X_1, \dots X_M]^\mathsf{T}$ consisting of M components. Then the joint cdf is

$$F_\mathbf{X}(\mathbf{x}) \equiv F(\mathbf{x}) \equiv F(x_1, \dots x_M) = P[\{X_1 \leq x_1\} \cap \dots \cap \{X_M \leq x_M\}]. \tag{2.46}$$

Differentiating yields the joint pdf

$$f_\mathbf{X}(\mathbf{x}) \equiv f(\mathbf{x}) = \frac{\partial^M F(\mathbf{x})}{\partial x_1 \dots \partial x_M} = \frac{\partial^M F(x_1, \dots x_M)}{\partial x_1 \dots \partial x_M}. \tag{2.47}$$

Random variables $X_1, \dots X_M$ are called independent if and only if [41]

$$f(\mathbf{x}) = f(x_1, \dots x_M) = f(x_1) \cdots f(x_M). \tag{2.48}$$

The *multi-dimensional Gaussian pdf* [6] reads

$$f_\mathbf{X}(\mathbf{x}) \equiv f(\mathbf{x}) = \frac{1}{(2\pi)^{\frac{n}{2}} \sqrt{\det \mathbf{C_{XX}}}} \exp\left[-\frac{1}{2}(\mathbf{x} - \boldsymbol{\mu}_\mathbf{X})^\mathsf{T} \mathbf{C}_\mathbf{XX}^{-1} (\mathbf{x} - \boldsymbol{\mu}_\mathbf{X})\right], \tag{2.49}$$

with $\boldsymbol{\mu}_\mathbf{X}$ and $\mathbf{C_{XX}}$ denoting the mean value vector and the covariance matrix, respectively.

2.5 Estimators

Estimators provide the ability to assess statistical properties like mean value μ or variance σ^2 for the complete population from just a finite set of samples (e.g. from observations). There exist certain conditions which have to be fulfilled by the estimators. Suppose parameter γ has to be estimated from M samples $\{X_1, \dots X_M\}$, then the estimator $\Gamma_M (= f(X_1, \dots X_M))$ is *consistent* if:

$$\lim_{M \to \infty} \mathrm{P}[|\Gamma_M - \gamma| < \epsilon] = 1, \quad \forall \epsilon > 0, \tag{2.50}$$

meaning, that the estimator Γ_M approaches the true value γ with M heading towards infinity [6]. Another requirement is called *unbiasedness*:

$$\mathrm{E}[\Gamma_M] = \gamma, \tag{2.51}$$

that is, on average the estimator equals the true value [6].

For example, it can be shown, that the *arithmetic mean* $\hat{\mu}_{X(M)}$ is a consistent and unbiased estimator for the mean value $\mathrm{E}[X] = \mu_X$

$$\hat{\mu}_{X,M} = \frac{1}{M} \sum_{i=1}^{M} X_i, \tag{2.52}$$

as is the *sample variance*

$$\hat{\sigma}^2_{X,M} = \frac{1}{M-1} \sum_{i=1}^{M} (X_i - \bar{\mu}_{X,M})^2 = \frac{1}{M-1} \sum_{i=1}^{M} X_i^2 - \bar{\mu}^2_{X,M} \tag{2.53}$$

for the variance σ^2_X.

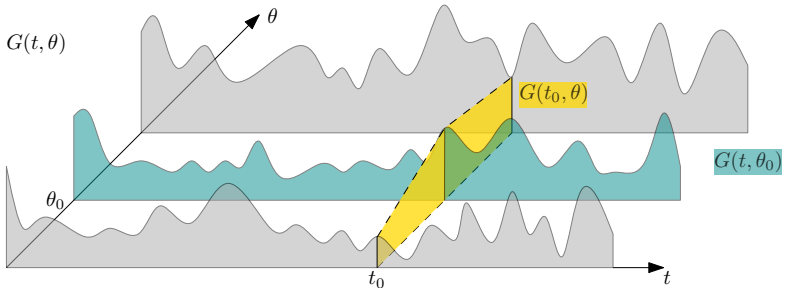

Figure 2.4: Three realizations of a random process $G(t,\theta)$.

2.6 Random processes

A *random* or stochastic *process* is defined as a set of random variables $G(t,\theta)$, with $t \in T$ usually denoting time, and the outcomes $\theta \in \Theta$ expressing the random nature of a process [17]. In other words, a random process depends on time t and chance θ [6]. For a given t_0, $G(t_0,\theta)$ is a random variable, whereas for a given θ_0, $G(t,\theta_0)$ describes a realization of the entire process for every $t \in T$, see Figure 2.4. As stated in [6], if all distribution functions of the type

$$F_G(g_1,\dots g_n) = P\left[\{G(t_1) \leq g_1\},\dots\{G(t_n) \leq g_n\}\right] \tag{2.54}$$

with arbitrary $n \in \mathbb{N}$ are multi-variate Gaussian distributions, then a random process is called Gaussian random process.

2.7 Random fields

As an extension to Subsection 2.6, a *random field* $H(\mathbf{x},\theta)$ is defined as a collection of random variables, where the coordinates $\mathbf{x} \in V \subset \mathbb{R}^d$ usually describe the spatial system geometry. For a given $\mathbf{x_0}$, $H(\mathbf{x_0},\theta)$ describes a random variable at point $\mathbf{x_0}$, whereas for a given outcome θ_0, $H(\mathbf{x},\theta_0)$ is a realization of the random field [39], as shown in Figure 2.5. Parameter θ expresses the random character of a quantity. From now on, whenever a quantity's random nature is obvious, the parameter θ will be suppressed, leading to $H(\mathbf{x},\theta) \equiv H(\mathbf{x})$. Hence, a random field $H(\mathbf{x})$ can be seen as a real-valued variable with varying statistics (e.g. mean μ or variance σ^2) depending on the coordinates $\mathbf{x}$ [6].

Usually vector $\mathbf{x}$ consists of spatial coordinates, e.g. $\mathbf{x} = [x_1,x_2,x_3]^{\mathrm{T}} = [x,y,z]^{\mathrm{T}}$ for a three-dimensional problem in $V \subset \mathbb{R}^3$. Taking the influence of time t into account "reduces" the parameter t to just another coordinate in n-dimensional space, i.e. $\mathbf{x} = [x_1,x_2,x_3,x_4]^{\mathrm{T}} = [x,y,z,t]^{\mathrm{T}}$. Thus, a random field can be seen as a generalization of a random process, which depends on an arbitrary number of parameters.

In [41] no rigorous distinction is made between random processes and random fields. However, it is noted that the term *random process* is usually reserved for processes depending on a single coordinate, e.g. time t, whereas random fields are considered to have a multi-dimensional parameter space $\mathbf{x}$.

The main focus of this work will be on spatial problems without consideration of time-dependency.

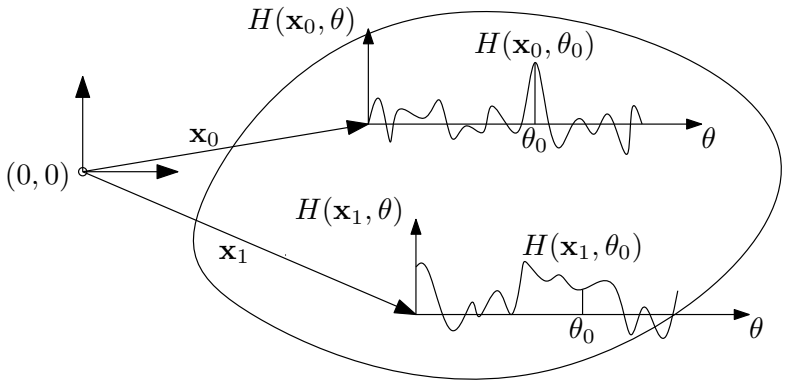

Figure 2.5: Two-dimensional random field $H(\mathbf{x}, \theta)$, showing realizations of points $\mathbf{x}_0$ and $\mathbf{x}_1$.

2.7.1 Properties of random fields

Whether the associated result of a random field at a given point $H(\mathbf{x_0})$ is a single random variable or a random vector, the random field is called univariate or multivariate, respectively. Similar to regular random variables, the *mean value function* is defined as [6]

$$\mu_H(\mathbf{x}) = \mathrm{E}[H(\mathbf{x})]. \tag{2.55}$$

In (2.55) the expectation operator E[.] denotes ensemble averaging, that is, the expectation value is to be taken at location $\mathbf{x}$ for every possible realization $\theta \in \Theta$ of $H(\mathbf{x}, \theta)$ [6]. The *auto-covariance function* can be defined similarly to (2.37) as

$$C_{ij} \equiv C_{HH}(\mathbf{x}_i, \mathbf{x}_j) = \mathrm{E}\big[(H(\mathbf{x}_i) - \mu_H(\mathbf{x}_i))(H(\mathbf{x}_j) - \mu_H(\mathbf{x}_j))\big]. \tag{2.56}$$

Similarly to (2.28), Equation (2.56) can be simplified:

$$\begin{aligned} C_{ij} &= \mathrm{E}\big[\big(H(\mathbf{x}_i) - \mu_H(\mathbf{x}_i)\big)\big(H(\mathbf{x}_j) - \mu_H(\mathbf{x}_j)\big)\big] \\ &= \mathrm{E}\big[H(\mathbf{x}_i)H(\mathbf{x}_j) - \mu_H(\mathbf{x}_i)H(\mathbf{x}_j) - H(\mathbf{x}_i)\mu_H(\mathbf{x}_j) + \mu_H(\mathbf{x}_i)\mu_H(\mathbf{x}_j)\big] \\ &= \mathrm{E}\big[H(\mathbf{x}_i)H(\mathbf{x}_j)\big] - \mu_H(\mathbf{x}_i)\mathrm{E}\big[H(\mathbf{x}_j)\big] - \mathrm{E}\big[H(\mathbf{x}_i)\big]\mu_H(\mathbf{x}_j) + \mu_H(\mathbf{x}_i)\mu_H(\mathbf{x}_j) \\ &= \mathrm{E}\big[H(\mathbf{x}_i)H(\mathbf{x}_j)\big] - 2\mu_H(\mathbf{x}_i)\mu_H(\mathbf{x}_j) + \mu_H(\mathbf{x}_i)\mu_H(\mathbf{x}_j) \\ &= \mathrm{E}\big[H(\mathbf{x}_i)H(\mathbf{x}_j)\big] - \mu_H(\mathbf{x}_i)\mu_H(\mathbf{x}_j) \end{aligned} \tag{2.57}$$

Under the condition that all quantities C_{ij} are finite (e.g. when a random field is evaluated at nodes of a lattice in space), they can be seen as components of the *auto-covariance matrix* $\mathbf{C}_{HH}$, in analogy to Subsection 2.4.1.

Further, the *auto-correlation function* is

$$\rho_{ij} \equiv \rho(\mathbf{x}_i, \mathbf{x}_j) = \frac{C_{HH}(\mathbf{x}_i, \mathbf{x}_j)}{\sigma_i \sigma_j} = \frac{C_{ij}}{\sigma_i \sigma_j}. \tag{2.58}$$

Common functions to describe the correlation of one-dimensional random fields/processes are

- the **exponential correlation**:

$$\rho_{ij} = \exp\left(-\frac{|x_j - x_i|}{l_c}\right), \tag{2.59}$$

- the **exponential square correlation**:

$$\rho_{ij} = \exp\left[-\left(\frac{x_j - x_i}{l_c}\right)^2\right], \tag{2.60}$$

- and the **sinusoidal correlation**:

$$\rho_{ij} = \sin\left(\frac{x_j - x_i}{l_c}\right)\frac{l_c}{x_j - x_i}, \tag{2.61}$$

where l_c denotes the *correlation length*.

The following properties of random fields allow classification and important simplifying assumptions:

- *Homogeneity*: Let $r = \|\boldsymbol{\xi}\|$ denote the distance between 2 points. A random field, which allows the translation of coordinates $\mathbf{x}$ without changing the joint pdf, is called *homogeneous* [41]:

$$f_{\mathbf{X}}(\mathbf{x} + \boldsymbol{\xi}) = f_{\mathbf{X}}(\mathbf{x}) \quad \forall \mathbf{x} \in V \tag{2.62}$$

  Further, a random field is called *weakly homogeneous*, if the auto-covariance function $C_{HH}(\mathbf{x}_i, \mathbf{x}_j)$ depends only on the distance vector $\boldsymbol{\xi} = \mathbf{x}_j - \mathbf{x}_i$ between two points, and if the mean value function $\mu_H(\mathbf{x})$ is constant [6]:

$$C_{HH}(\mathbf{x}, \mathbf{x} + \boldsymbol{\xi}) = C_{HH}(\boldsymbol{\xi}) \quad \forall \mathbf{x} \in V; \qquad \mu_H(\mathbf{x}) = \text{const.} \quad \forall \mathbf{x} \in V \tag{2.63}$$

  Furthermore, weakly homogeneous fields have the following properties:

$$C_{HH}(r) = C_{HH}(-r), \tag{2.64}$$

$$\max|C_{HH}(r)| = C_{HH}(0) = \sigma_H^2. \tag{2.65}$$

- *Isotropy*: If rotation of points $\mathbf{t}$ doesn't change the joint pdf, a random field is called *isotropic* [41]. In other words, a random field is isotropic if C_{HH} depends on the distance $\|\boldsymbol{\xi}\|$ only, regardless of the direction [6]:

$$C_{HH}(\mathbf{x}, \mathbf{x} + \boldsymbol{\xi}) = C_{HH}(\|\boldsymbol{\xi}\|) \quad \forall \mathbf{x} \in V \tag{2.66}$$

  For the case of an isotropic random field, the correlation length is

$$l_c = \frac{\int_0^\infty r|C_{HH}(r)|\mathrm{d}r}{\int_0^\infty |C_{HH}(r)|\mathrm{d}r}. \tag{2.67}$$

  A random field with $l_c \to \infty$ is fully correlated in the entire domain of definition V and therefore describes a single random variable. On the contrary, $l_c \to 0$ produces a random field without any spatial correlation, which is called *white noise* [6].

- *Ergodicity*: If one realization reveals all statistical information of a random field, it is called *ergodic* [41].

- *Power spectral density*: For a weakly homogeneous one-dimensional random field (which may also be called a stationary random process) the auto-power spectral density is defined as [6]

$$S_{HH}(\omega) = \frac{1}{2\pi} \int_{-\infty}^{\infty} C_{HH}(r) e^{i\omega r} \mathrm{d}r. \tag{2.68}$$

The inverse relation reads

$$C_{HH}(r) = \int_{-\infty}^{\infty} S_{HH}(\omega) e^{-i\omega r} \mathrm{d}\omega, \tag{2.69}$$

where ω denotes the frequency. Equations (2.68) and (2.69) are the so called Wiener-Khintchine relations, forming a Fourier-transform pair. Let $r = 0$, then

$$C_{HH}(0) = \sigma_H^2 = \int_{-\infty}^{\infty} S_{HH}(\omega) \mathrm{d}\omega, \tag{2.70}$$

which leads to the interpretation of the power spectral density as the distribution of the variance in the domain of frequency ω [6].

2.7.2 Gaussian random fields

A random field is called Gaussian, if $H(\mathbf{x_0}, \theta)$ is a Gaussian random variable for any given $\mathbf{x_0} \in V$. The mean value function $\mu_H(\mathbf{x})$, the variance $\sigma_H^2(\mathbf{x})$, and the auto-correlation coefficient $\rho_H(\mathbf{x}_i, \mathbf{x}_j)$ are then sufficient to completely describe a Gaussian field [1]. The central limit theorem [16, 3] is another commonly used argument justifying the use of this type of field. Furthermore, when only information about the second order moments (μ and σ^2) is available, the Gaussian field model provides the maximum entropy [37]. Thus, Gaussian fields are popular and often used.

Chapter 3

Representation of Random Fields

Similar to the spatial discretization in deterministic finite element methods, a continuous random field $H(\mathbf{x})$ can be discretized for numerical treatment and analysis. This can be explained by considering the Monte Carlo simulation, where a random field is simulated using a random number generator, which produces a finite number of random numbers. Discretization methods allow to use those random numbers for the realization of a continuous random field, thus making numerical treatment possible. The random numbers can be seen as realizations of random variables, the latter being grouped in a random vector $\boldsymbol{\chi}(\theta) \equiv \boldsymbol{\chi} = [\chi_1, \dots]^\mathsf{T}$, and yielding the approximation [39]

$$H(\mathbf{x}, \theta) \xrightarrow{\text{Discretization}} \hat{H}(\mathbf{x}, \boldsymbol{\chi}(\theta)) = \boldsymbol{\chi}(\theta)\big(\boldsymbol{\varphi}(\mathbf{x})\big)^\mathsf{T} = \sum_i^{N^{rv}} \chi_i(\theta)\varphi_i(\mathbf{x}), \tag{3.1}$$

where $\hat{H}$ denotes the discretized random field, χ_i is the i-th random variable, and φ_i denotes the corresponding interpolation function. The correlation matrix $\mathbf{C}_{\chi\chi}$ of the random vector $\boldsymbol{\chi}$ and the total number of random variables N^{rv} depend on the representation method.

It is not necessary for the discretization of the random field to match the spatial discretization of the geometry. However, in some cases they are one and the same for simplicity.

For the discretization of a random field, two parameters need to be taken into account [29]: First, the correlation length l_c (see Equation (2.67)), which describes the fluctuation (in other words: the rate of change) within the random field. Just as a conventional finite element mesh needs to depict the stress gradient in every point of the structure $\mathbf{x} \in V$ accordingly to the desired accuracy, a random field mesh needs to depict the essential features of the random field, which are strongly dependent on the correlation length l_c.

Second, the number of random variables used to discretize the random field. A higher number of random variables leads, in most cases, to exponential increase of the computational effort.

Table 3.1: Unified notation of random field representations in terms of weight functions $w(\mathbf{x})$ and coefficients $\varphi_i(\mathbf{x})$ (see Equations (3.1) and (3.2)) (${}^*N_i^{\mathrm{OLE}}(\mathbf{x})$ are optimal in a sense of minimizing the variance of the estimation error) [39].

	Midpoint	Spatial average	Shape function	Optimal linear estimation
$w(\mathbf{x})$	$\delta(\mathbf{x}-\mathbf{x}_c^e)$	$\dfrac{\delta_{V_e}(\mathbf{x})}{V_e}$	$\delta(\mathbf{x}-\mathbf{x}_i)$	$\delta(\mathbf{x}-\mathbf{x}_i)$
$\varphi_i(\mathbf{x})$	$\delta_{V_e}(\mathbf{x})$	$\delta_{V_e}(\mathbf{x})$	$N_i^e(\mathbf{x})$	$N_i^{\mathrm{OLE}}(\mathbf{x})^{*a}$

[a] $N_i^{\mathrm{OLE}}(\mathbf{x})$ are optimal in a sense of minimizing the variance of the estimation error

In the following sections, different discretization methods are described in detail. Basically, three different categories can be defined: (i) Point-discretization, (ii) average-type discretization, and (iii) series expansion methods.

Point- and average-type discretization methods seem to be the most convenient way, since, for instance the midpoint method assigns one random variable to a discrete area V of the structure, thus being particularly illustrative, see Figures 3.1 and 3.2. As shown in [39], for all point and average type discretization methods, the finite sets of random variables can be expressed as weighted integrals over the corresponding discrete domain V_e:

$$\chi_e(\theta) = \int_{V_e} H(\mathbf{x},\theta) w_e(\mathbf{x}) \mathrm{d}V, \tag{3.2}$$

where $w_e(\mathbf{x})$ are deterministic weight functions depending on the discretization method. Then the approximated random field can be formulated in a unified way as a series expansion according to (3.1). In Table 3.1 the coefficients w_e and φ_i are listed for the methods following in Sections 3.1 and 3.2.

Attention has to be paid to the fineness/accuracy of the discretization. Apart from the significant influence on computation time, the most serious drawback of using extraordinary fine meshes lies in the risk of yielding highly correlated random variables [29]. These may lead to a nearly singular correlation matrix, making further calculations difficult, not to say, impossible.

Series expansion methods avoid this problem and, in general, provide a more accurate representation of $H(\mathbf{x})$.

3.1 Point discretization methods

As stated before, point discretization methods represent a random field $H(\mathbf{x})$ by its values at one or more points $\mathbf{x}$. Advantages of point discretization methods are according to [29]:

- Straightforward computation of the covariance matrix,
- positive-definitness of the covariance matrix,
- the distribution type does not chance from the original to the discretized case, thus (theoretically) no restriction to Gaussian fields.

In the following, let

$$\delta_{V_e}(\mathbf{x}) = \begin{cases} 1 & \mathbf{x} \in V_e \\ 0 & \mathbf{x} \notin V_e \end{cases} \tag{3.3}$$

and

$$\delta(\mathbf{x} - \mathbf{x}_c) = \begin{cases} 1 & \mathbf{x} = \mathbf{x}_c \\ 0 & \mathbf{x} \neq \mathbf{x}_c \end{cases}. \tag{3.4}$$

3.1.1 Midpoint method

The midpoint method, introduced by [11] represents a random field $H(\mathbf{x})$ as follows:

$$\hat{H}\big(\mathbf{x}, \boldsymbol{\chi}(\theta)\big) = \sum_{e=1}^{N^{rf}} \chi_e(\theta)\delta_{V_e}(\mathbf{x}), \tag{3.5}$$

where N^{rf} is the total number of random field elements, and

$$\chi_e(\theta) = \int_V H(\mathbf{x}, \theta)\delta(\mathbf{x} - \mathbf{x}_c^e)\mathrm{d}V = H(\mathbf{x}_c^e, \theta), \tag{3.6}$$

with $\mathbf{x}_c^e$ denoting the center point of the random field element e, reading

$$\mathbf{x}_c^e = \frac{1}{n}\sum_{i=1}^{n} \mathbf{x}_i. \tag{3.7}$$

Within one element, the random field is represented by one random variable χ_e, with the same mean μ, variance σ^2, and marginal pdf as the random field at point $\mathbf{x}_c^e$. The covariance between two random variables χ_i and χ_j can be obtained from the covariance function of the original random field, computed at the points $\mathbf{x}_c^i$ and $\mathbf{x}_c^j$

$$\mathrm{Cov}(\chi_i, \chi_j) = C_{ij} \equiv C_{HH}(\mathbf{x}_c^i, \mathbf{x}_c^j). \tag{3.8}$$

All realizations of $\hat{H}$ are piecewise constant, with discontinuities at the element boundaries. This is illustrated in Figure 3.1 for square elements. This method appears to be the only one over-estimating the variability of the random field, and thus, representing an upper bound [11].

3.1.2 Nodal point method

Similar to the midpoint method, the nodal point method represents the random field by random variables χ_i at each of the nodal points $\mathbf{x}_i$, where

$$\chi_i(\theta) = \int_V H(\mathbf{x}, \theta)\delta(\mathbf{x} - \mathbf{x}_i)\mathrm{d}V = H(\mathbf{x}_i, \theta). \tag{3.9}$$

Again, each realization is piecewise constant (see Figure 3.2). In analogy to the midpoint method, the entire random field is represented by the random vector $\boldsymbol{\chi} = [\chi_1, \dots \chi_{N^{rv}}]^\mathsf{T}$, where the number of random variables N^{rv} equals the total number of nodal points N^{rf} of the discretized random field. Statistical quantities like mean μ, variance σ^2 and covariance function $\mathrm{Cov}(\chi_i, \chi_j)$ are be obtained in the same way as in the midpoint method.

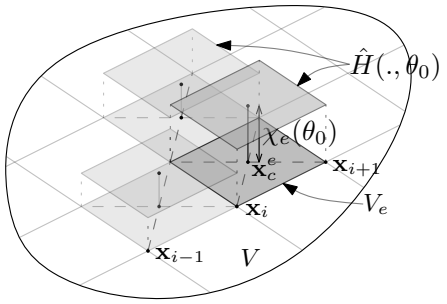

Figure 3.1: When using midpoint method, each realization of the random field is piecewise constant. Each element e is represented by one value $\chi_e(\theta_0)$, computed at the center point $\mathbf{x}_c^e$.

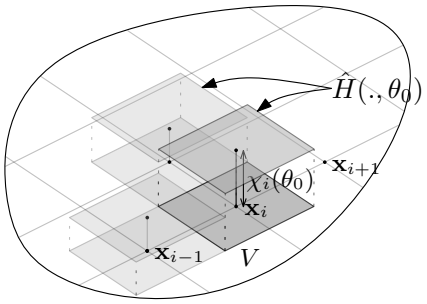

Figure 3.2: Each realization of a random field represented by the nodal point method is piecewise constant by means of the values $\chi_i(\theta_0)$, being computed at global nodes $\mathbf{x}_i$.

3.1.3 Integration point method

The integration point method, as stated in [6], represents a random field with a random variable χ_{e*} at each integration point $\mathbf{x}^{e*}$ of the mechanical finite-element mesh.

Since most finite element packages provide integration rules for the construction of the element matrices, implementation of the integration point method is straightforward compared to other methods. Further references regarding the nodal- and integration point method can be found in [29].

3.1.4 Shape function/Interpolation method

The shape function method represents a random field $H(\mathbf{x})$ with random variables $\chi_i = H(\mathbf{x}_i)$ at nodal points $\mathbf{x}_i$, which define the stochastic finite element nodes, see Equation (3.9). In analogy to the conventional FE method, the random field is approximated within each stochastic finite element e, using shape functions $N_i(\mathbf{x})$ as follows:

$$\hat{H}(\mathbf{x},\boldsymbol{\chi}) = \sum_{e=1}^{N_e^{rf}} \left(\delta_{V_e}(\mathbf{x}) \sum_{i=1}^{n} \chi_i N_i(\mathbf{x}) \right) = \sum_{e=1}^{N_e^{rf}} \sum_{i=1}^{n} \chi_i \underbrace{N_i(\mathbf{x})\delta_{V_e}(\mathbf{x})}_{N_i^e(\mathbf{x})}$$
$$= \sum_{i=1}^{N^{rf}} \chi_i N_i^e(\mathbf{x}), \tag{3.10}$$

where N_e^{rf} and n denote the total number of elements of the random field discretization and the number of nodes of one random field element e, respectively. The shape functions $N_i^e(\mathbf{x})$ assume non-zero values only for $\mathbf{x} \in V_e$, that is, they are non-zero only for the random field element e corresponding to vector $\mathbf{x}$. Hence, one summation over $i = 1, \dots N^{rf}$, where N^{rf} is the total number of nodal points, is sufficient. Since the shape function method assigns one random variable χ_i to each node i, it requires as many random variables for representation as the nodal point method. Therefore, the

random vector $\boldsymbol{\chi} = [\chi_1, \dots \chi_{N^{rf}}]^\mathsf{T} = [H(\mathbf{x}_1), \dots H(\mathbf{x}_{N^{rf}})]^\mathsf{T}$ has the same dimension as for the nodal point method. Its advantage over the midpoint and nodal point method, however, is the fact, that each realization $\hat{H}(\mathbf{x}, \theta_0)$ is a continuous function over V [39] (see Figure 3.3). The mean value function $\mu_{\hat{H}}(\mathbf{x})$ of the approximated field is

$$\mu_{\hat{H}}(\mathbf{x}) = \mathrm{E}[\hat{H}(\mathbf{x})] = \mathrm{E}\left[\sum_{i=1}^{N^{rf}} \chi_i(\mathbf{x}) N_i^e(\mathbf{x})\right] = \sum_{i=1}^{N^{rf}} \mathrm{E}[\chi_i] N_i^e(\mathbf{x})$$
$$= \sum_{i=1}^{N^{rf}} \mu_{\chi_i} N_i^e(\mathbf{x}) = \sum_{i=1}^{N^{rf}} \mu_H(\mathbf{x}_i) N_i^e(\mathbf{x}), \quad (3.11)$$

where μ_{χ_i} denotes the mean value of random variable χ_i at nodal point i, which is equal to the mean value function evaluated at point $\mathbf{x}_i$. Therefore, the mean value function of the approximated random field is an interpolation of the corresponding random variables. Substituting (3.10) and (3.11) into (2.57) yields

$$\begin{aligned} C_{\hat{H}\hat{H}}(\mathbf{x}_k, \mathbf{x}_l) &= \mathrm{E}[\hat{H}(\mathbf{x}_k)\hat{H}(\mathbf{x}_l)] - \mu_{\hat{H}}(\mathbf{x}_k)\mu_{\hat{H}}(\mathbf{x}_l) \\ &= \mathrm{E}\left[\sum_{i=1}^{N^{rf}}\sum_{j=1}^{N^{rf}} N_i^e(\mathbf{x}_k) N_j^e(\mathbf{x}_l) \chi_i \chi_j\right] - \sum_{i=1}^{N^{rf}}\sum_{j=1}^{N^{rf}} N_i^e(\mathbf{x}_k) N_j^e(\mathbf{x}_l) \mu_{\chi_i}\mu_{\chi_j} \\ &= \sum_{i=1}^{N^{rf}}\sum_{j=1}^{N^{rf}} N_i^e(\mathbf{x}_k) N_j^e(\mathbf{x}_l) \mathrm{E}\left[\chi_i \chi_j\right] - \sum_{i=1}^{N^{rf}}\sum_{j=1}^{N^{rf}} N_i^e(\mathbf{x}_k) N_j^e(\mathbf{x}_l) \mu_{\chi_i}\mu_{\chi_j} \\ &= \sum_{i=1}^{N^{rf}}\sum_{j=1}^{N^{rf}} N_i^e(\mathbf{x}_k) N_j^e(\mathbf{x}_l) \left(\mathrm{E}\left[\chi_i \chi_j\right] - \mu_{\chi_i}\mu_{\chi_j}\right). \end{aligned} \quad (3.12)$$

Moreover, substituting (2.57) into the equation above, the result is the covariance of the approximated field

$$C_{\hat{H}\hat{H}}(\mathbf{x}_k, \mathbf{x}_l) = \sum_{i=1}^{N^{rf}}\sum_{j=1}^{N^{rf}} N_i^e(\mathbf{x}_k) N_j^e(\mathbf{x}_l) \mathrm{Cov}(\chi_i, \chi_j), \quad (3.13)$$

where $\mathrm{Cov}(\chi_i, \chi_j) = C_{ij} \equiv C_{HH}(\mathbf{x}_i, \mathbf{x}_j)$ (see Equation (3.8)). As stated in [29], depending on the proper choice of shape functions, this method provides accurate results even for coarse discretizations.

3.1.5 Optimum linear estimation (OLE) method

Also known as the *Kriging method*, the optimal linear estimation method is a special type of shape function method. The approximation $\hat{H}$ is defined as a linear function of random variables $\boldsymbol{\chi} = [\chi_1, \dots \chi_N]^\mathsf{T} = [H(\mathbf{x}_1), \dots H(\mathbf{x}_N)]^\mathsf{T}$ located at nodal points $\mathbf{x}_i$ [28, 39]:

$$\hat{H}(\mathbf{x}, \boldsymbol{\chi}) = a(\mathbf{x}) + \sum_{i=1}^{N^{rf}} b_i(\mathbf{x}) \chi_i = a(\mathbf{x}) + \mathbf{b}^\mathsf{T}(\mathbf{x}) \cdot \boldsymbol{\chi}, \quad (3.14)$$

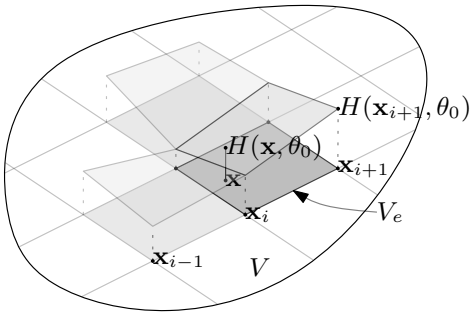

Figure 3.3: Illustration of the shapefunction method, which provides continuous realizations $H(\mathbf{x}, \theta_0)$.

with N^{rf} denoting the total number of points used for the representation. The functions $a(\mathbf{x})$ and $\mathbf{b}^\mathsf{T}(\mathbf{x})$ are optimal with respect to the variance of the error $\epsilon = H(\mathbf{x}) - \hat{H}(\mathbf{x})$, reading

$$\min \left(\mathrm{Var} \left[H(\mathbf{x}) - \hat{H}(\mathbf{x}) \right] \right), \quad \forall \mathbf{x} \in V. \tag{3.15}$$

As stated in [6] and [39], the estimator $\hat{H}(\mathbf{x})$ is called unbiased, if

$$\mathrm{E} \left[H(\mathbf{x}) - \hat{H}(\mathbf{x}) \right] = 0, \quad \forall \mathbf{x} \in V, \tag{3.16}$$

meaning that the estimator is expected to be equal to the value of the random field $H(\mathbf{x})$ on average.

The functions $a(\mathbf{x})$ and $b(\mathbf{x})$ are determined as

$$\begin{aligned} a(\mathbf{x}) &= \mu(\mathbf{x}) - \mathbf{b}^\mathsf{T}(\mathbf{x}) \cdot \boldsymbol{\mu}_\chi, \\ \mathbf{b}(\mathbf{x}) &= \mathbf{C}_{\chi\chi}^{-1} \mathbf{c}_{\chi(x),\chi}, \end{aligned} \tag{3.17}$$

with $\mu(\mathbf{x})$ and $\boldsymbol{\mu}_\chi$ being the mean value function of the original random field and the vector of the random vector $\boldsymbol{\chi}$, respectively. Furthermore, $\mathbf{C}_{\chi\chi}$ denotes the auto-covariance matrix of $\boldsymbol{\chi}$, and $\mathbf{c}_{\chi(x),\chi}$ the components of the covariances of a random variable $\chi(\mathbf{x})$ located at point $\mathbf{x}$ with all components of random vector $\boldsymbol{\chi}$, thus

$$\begin{aligned} \mathbf{c}_{\chi(x),\chi} &= \left[\mathrm{Cov}[\chi(\mathbf{x}), \chi_1], \ldots \mathrm{Cov}[\chi(\mathbf{x}), \chi_N] \right]^\mathsf{T} \\ &\equiv \left[\mathrm{Cov}[H(\mathbf{x}), H(\mathbf{x}_1)], \ldots \mathrm{Cov}[H(\mathbf{x}), H(\mathbf{x}_N)] \right]^\mathsf{T}. \end{aligned} \tag{3.18}$$

Substituting the two equations (3.17) into (3.14) finally yields the optimal linear estimation

$$\begin{aligned} \hat{H}(\mathbf{x}, \boldsymbol{\chi}) &= \overbrace{\mu(\mathbf{x}) - \mathbf{b}^\mathsf{T}(\mathbf{x}) \cdot \boldsymbol{\chi}}^{a(\mathbf{x})} + \mathbf{b}^\mathsf{T}(\mathbf{x}) \cdot \boldsymbol{\mu}_\chi = \mu(\mathbf{x}) + \mathbf{b}^\mathsf{T}(\mathbf{x}) \cdot (\boldsymbol{\chi} - \boldsymbol{\mu}_\chi) \\ &= \mu(\mathbf{x}) + \mathbf{c}_{\chi(x),\chi}^\mathsf{T} \mathbf{C}_{\chi\chi}^{-1} \cdot (\boldsymbol{\chi} - \boldsymbol{\mu}_\chi). \end{aligned} \tag{3.19}$$

Finally, the variance of error yields

$$\mathrm{Var}[H(\mathbf{x}) - \hat{H}(\mathbf{x})] = \sigma_H^2 - \sigma_{\hat{H}}^2, \tag{3.20}$$

and is always positive, thus

$$\sigma_H^2 > \sigma_{\hat{H}}^2. \tag{3.21}$$

In other words, $\hat{H}(\mathbf{x})$ always underestimates the variance of the original random field [39]. For further references, see [29]. It is mentioned, that the OLE method is particularly suitable for interpolating random field samples where certain values are known.

3.2 Average-type discretization methods

3.2.1 Local averaging method

Introduced by [41], and also known as the spatial average method (when only functions of space are being used), this method represents a random field $H(\mathbf{x})$ in each element e with one random variable, computed as follows:

$$\chi_e(\theta) = \frac{1}{V_e} \int_V H(\mathbf{x}, \theta) \delta_{V_e}(\mathbf{x}) \mathrm{d}V, \tag{3.22}$$

where V_e denotes the volume or surface area of element e. The entire random field is represented by the random vector $\boldsymbol{\chi} = [\chi_1, \dots \chi_{N_e^{rf}}]$, reading

$$\hat{H}(\mathbf{x}, \boldsymbol{\chi}(\theta)) = \sum_e^{N_e^{rf}} \chi_e(\theta) \delta_{V_e}(\mathbf{x}), \tag{3.23}$$

with N_e^{rf} as the total number of elements. The mean vector $\boldsymbol{\mu}_\chi$ and the covariance matrix $\mathbf{C}_{\chi\chi}$ are obtained by integration over the domain V_e. In [41] solutions for this integral are presented.

As stated in [29], the two major disadvantages are:

- The use of non rectangular elements may lead to a non-positive definite covariance matrix.
- The pdf of each random variable χ_i can be obtained for Gaussian fields only, otherwise its computation is almost impossible.

However, [29] refer to [11], where it is shown that the local averaging method appears to give accurate results even for coarse meshes. Furthermore, this method tends to under-represent the variability, thus, providing a lower bound. In combination with the midpoint method (with the same discretization) upper and lower bounds of the variability can be given.

3.2.2 Weighted integral method

Within finite element methods, the element stiffness matrix $\mathbf{k}^e$ can be expressed as

$$\mathbf{k}^e = \int_{V_e} \mathbf{B}^\mathsf{T}\mathbf{D}\mathbf{B}\mathrm{d}V, \tag{3.24}$$

with $\mathbf{D}$ denoting the so called element elasticity matrix and $\mathbf{B}$ linking the node displacements to element strains. The weighted integral method proposes the use of a deterministic elasticity matrix multiplied by a random field value (for example, the modulus of elasticity), that is

$$\mathbf{D}(\mathbf{x},\theta) = \mathbf{D}_0 \cdot (1 + I(\mathbf{x},\theta)), \tag{3.25}$$

where $\mathbf{D}_0$ denotes the mean value elasticity matrix and $I(\mathbf{x},\theta)$ is an univariate random field with zero mean. Substituting (3.25) into (3.24) yields

$$\mathbf{k}^e = \underbrace{\int_{V_e} \mathbf{B}^\mathsf{T}\bar{\mathbf{D}}\mathbf{B}\mathrm{d}V}_{\bar{\mathbf{k}}^e} + \underbrace{\int_{V_e} H(\mathbf{x},\theta)\mathbf{B}^\mathsf{T}\bar{\mathbf{D}}\mathbf{B}\mathrm{d}V}_{\Delta\mathbf{k}^e(\theta)} = \bar{\mathbf{k}}^e + \Delta\mathbf{k}^e(\theta). \tag{3.26}$$

The weighted integral method turns out to be a special case of the shape function method and shares its advantages. However, since the representation of the random field depends on the discretization of the deterministic problem, the quality of results may vary [39].

3.3 Series expansion methods

In contrast to all methods presented in Sections 3.1 and 3.2, series expansion methods deal with an infinite number of coefficients $\varphi_i(\mathbf{x})$. This allows theoretically an exact representation of a random field. The approximation is obtained by truncation of the series [39]. Furthermore, the methods presented in the following sections provide solutions for non-Gaussian random fields as well as for unknown covariance functions.

3.3.1 Orthogonal functions

Since the approaches presented in the following sections involve orthogonal functions, a short mathematical overview will be given first. In Section 2.1 the probability space $(\Theta, \mathcal{F}, P)$ was introduced. All real-valued random variables X with a finite second moment $\mathrm{E}[X^2] < \infty$ form a vectorial space $\mathcal{L}^2(\Theta, \mathcal{F}, P)$. The term $\mathcal{L}^2$ emphazises the fact that a *Lebesgue space* of square-integrable functions is involved. A random field $H(\mathbf{x},\theta)$ can be defined as a curve in $\mathcal{L}^2(\Theta, \mathcal{F}, P)$, which can be shown to be a *Hilbert space* [39]. A Hilbert space is a vector space with an *inner product* $\langle f, g\rangle$ allowing to measure length and angle in analogy to the inner product $f \cdot g$. In analogy to vector algebra, two functions $f(x)$ and $g(x)$ are called orthogonal if their inner product $\langle f, g\rangle$ is zero [42]. A common definition of the inner product is given by

$$\langle f, g\rangle = \int_V f(\mathbf{x})g(\mathbf{x})\mathrm{d}V. \tag{3.27}$$

For instance, the functions $f(x) = \cos(x)$ and $g(x) = \sin(x)$ are orthogonal with respect to the range of real values $0 \leq x \leq 2\pi$, since

$$\langle \cos(x), \sin(x) \rangle = \int_0^{2\pi} \cos(x) \sin(x) \mathrm{d}x = 0. \tag{3.28}$$

Other examples for orthogonal coefficients are *Hermite polynomials* or *Legendre Polynomials*. The one-dimensional Hermite polynomials read

$$\Psi_i(x) = (-1)^i \frac{\mathrm{d}^i}{\mathrm{d}x^i} \left[e^{(-\frac{1}{2}x^2)} \right] e^{(-\frac{1}{2}x^2)}, \tag{3.29}$$

whereas the Legendre polynomials can be obtained using *Rodrigues' formula* [22]:

$$P_i(x) = \frac{1}{2^i i!} \frac{\mathrm{d}^i}{\mathrm{d}x^i} (x^2 - 1)^i. \tag{3.30}$$

The functions are called orthonormal, if

$$\langle f, f \rangle = \int_V [f(\mathbf{x})]^2 \mathrm{d}V = 1. \tag{3.31}$$

Thus, for an orthonormal set of functions $\mathbf{f} = \{f_1, \dots f_n\}$ the inner product reads

$$\langle f_i, f_j \rangle = \delta_{ij}, \tag{3.32}$$

where δ_{ij} denotes the Kronecker-delta. Choosing the deterministic coefficients $\varphi_i(\mathbf{x})$ in Equation (3.1) to be mutually orthogonal or even orthonormal yields several advantages which will be showed in the following sections. In addition, orthogonality or orthonormality between random variables can be interpreted as independency.

In probability theory, the expectation value $\mathrm{E}[X]$ allows another important definition of the inner product [39] as well as the relating norm

$$\langle X, Y \rangle = \mathrm{E}[XY], \tag{3.33}$$

$$\|X\| = \sqrt{\mathrm{E}[X^2]}. \tag{3.34}$$

Obviously, the angle between two functions depends on the definition of the inner product.

3.3.2 Karhunen-Loève expansion

The Karhunen-Loève expansion, introduced by [18] (in fact, it was introduced by Ghanem and Spanos 1991, 2003 a new edition was released) and also known as *kernel expansion method*, is based on the *spectral decomposition* of the autocovariance function $C_{HH}(\mathbf{x}_i, \mathbf{x}_j)$

$$C_{HH}(\mathbf{x}_i, \mathbf{x}_j) = \sum_{k=0}^{\infty} \lambda_k f_k(\mathbf{x}_i) f_k(\mathbf{x}_j), \tag{3.35}$$

with λ_k and $f_k(\mathbf{x})$ denoting the eigenvalue and the eigenvector, respectively, to the following eigenvalue problem

$$\int_V C_{HH}(\mathbf{x}_i, \mathbf{x}_j) f_k(\mathbf{x}) \mathrm{d}x_i = \lambda_k f_k(\mathbf{x}_j). \tag{3.36}$$

Equation (3.36) describes a Fredholm integral equation. Since the covariance kernel C_{HH} is symmetric and positive-definite, the eigenfunctions $f_i(\mathbf{x})$ are orthogonal and form a complete set. Moreover, they can be normalized, thus being orthonormal and fulfilling Equation (3.32). The random field then can be written as follows:

$$H(\mathbf{x}, \boldsymbol{\chi}(\theta)) = \mu_H(\mathbf{x}) + \sum_{i=0}^{\infty} \chi_i(\theta) \sqrt{\lambda_i} f_i(\mathbf{x}), \tag{3.37}$$

with $\mu_H(\mathbf{x})$ as the mean value function and the second term denoting a zero mean random process, with random variables $\chi_i(\theta)$, deterministic eigenvalues $\lambda_i(\mathbf{x})$ and eigenfunctions $f_i(\mathbf{x})$, respectively. While (3.37) is still exact, approximation is accomplished by truncating the series after N terms

$$H(\mathbf{x}, \boldsymbol{\chi}(\theta)) = \mu_H(\mathbf{x}) + \sum_{i=0}^{N} \chi_i(\theta) \sqrt{\lambda_i} f_i(\mathbf{x}). \tag{3.38}$$

The approximation is optimal in the Fourier sense, i.e. the mean square error resulting from truncation of the series is minimized [18].

The random variables χ_i are a set of orthonormal variables according to (3.33), and therefore, mutually independent, reading

$$\langle \chi_i, \chi_j \rangle = \mathrm{E}[\chi_i \chi_j] = \delta_{ij}. \tag{3.39}$$

The orthogonal property of the eigenfunctions $f_i(\mathbf{x})$ allows a closed form solution for each of the random variables $\chi_i(\mathbf{x})$ [39], given as

$$\chi_i(\theta) = \frac{1}{\lambda_i} \int_V \left[H(\mathbf{x}, \theta) - \mu_H(\mathbf{x}) \right] f_i(\mathbf{x}) \mathrm{d}V. \tag{3.40}$$

It can be seen that when $H(\mathbf{x}, \theta)$ is a Gaussian random field, the random variables χ_i are Gaussian as well. In addition, as noted in Subsection 3.3.1, the orthonormality of the random variables χ_i leads to the conclusion that they are mutually independent. Thus, for the represention of a Gaussian random field the random variables form a set of independent standard normal variables [39].

In [18] analytical solutions are presented for a few special - yet important - cases of covariance functions C_{HH}. Furthermore, a Galerkin type numerical procedure is presented, allowing approximation of the eigenvalue problem for arbitrary covariance kernels.

The eigenvalues, reflecting the importance of the corresponding random variables and arranged in descending order, quickly converge to zero. Hence, truncation of the series after just a few terms already yields very good approximations. For instance, as summarized in [37], the KL-expansion yields good results with $N \approx 4$ terms, given that the correlation length is large enough.

However, the requirement to solve the eigenvalue problem is a major disadvantage. Moreover, the Karhunen-Loève expansion requires knowing the covariance function C_{HH}. Altough it can be used for a known random excitation or random material property, the method cannot be used to represent the yet unknown random solution process.

As stated in [39], the KL-expansion always under-represents the variability of the random field.

3.3.3 Orthogonal series expansion

The orthogonal series expansion method involves a set of orthogonal functions $h_i(\mathbf{x})$, which, in contrast to the Karhunen-Loève expansion method, are not evaluated by solving an eigenvalue problem. The functions $h_i(\mathbf{x})$ are chosen right from the beginning, circumventing the time consuming solution of the eigenvalue problem, see [44]. Any complete set of orthogonal functions, for instance, Legendre polynomials or Hermite polynomials, can be used.

A random field $H(\mathbf{x}, \theta)$ with mean value function $\mu_H(\mathbf{x})$ and covariance function C_{HH} is then represented by expanding it by means of the known orthogonal functions $h_i(\mathbf{x})$:

$$H\left(\mathbf{x}, \boldsymbol{\chi}(\theta)\right) = \mu_H(\mathbf{x}) + \sum_{i=1}^{\infty} \chi_i(\theta) h_i(\mathbf{x}), \tag{3.41}$$

with $\chi_i(\theta)$ denoting the random variables. Truncation of the series after the N-th term yields the approximation. In analogy to the Karhunen-Loève expansion, exploiting the orthogonality, a closed form solution for the random variables can be derived:

$$\chi_i(\theta) = \int_V [H(\mathbf{x}, \theta) - \mu_H(\mathbf{x})] h_i(\mathbf{x}) \mathrm{d}V, \tag{3.42}$$

Equation (3.42) reveals that when representing a zero-mean Gaussian random field $H(\mathbf{x}, \theta)$, the random variables $\chi_i(\theta)$ are Gaussian with zero-mean as well.

Furthermore, it can be shown that

$$\langle \chi_i, \chi_j \rangle = \mathrm{E}[\chi_i \chi_j] = \int_V \int_V C_{HH}(\mathbf{x}_k, \mathbf{x}_l) h_i(\mathbf{x}_k) h_j(\mathbf{x}_l) \mathrm{d}V_{\mathbf{x}_k} \mathrm{d}V_{\mathbf{x}_l}. \tag{3.43}$$

Thus, the random variables χ_i are not necessarily uncorrelated. Nevertheless, the covariance function of the random variables χ_i, keeping in mind that they have zero-mean, is given by

$$C_{\chi\chi}(\chi_i, \chi_j) = \mathrm{E}\big[(\chi_i - \mu_{\chi_i})(\chi_j - \mu_{\chi_j})\big] = \mathrm{E}[\chi_i \chi_j] = \langle \chi_i, \chi_j \rangle, \tag{3.44}$$

showing that the inner product equals the covariance function of the random variables, which can be orthogonalized using spectral decomposition. As shown in [44] the spectral decomposition leads to independent random variables and finally to the same result as the Karhunen-Loève expansion. Likewise, this method requires the covariance function C_{HH} to be known.

3.3.4 Polynomial Chaos expansion

For the Polynomial Chaos expansion method [18], the covariance C_{HH} is not required in advance. This method expands the random field as follows:

$$\begin{aligned}\hat{H}(\mathbf{x},\boldsymbol{\chi}(\theta)) = a_0(\mathbf{x})\Gamma_0 &\\ + \sum_{i_1=1}^{\infty} a_{i_1}\Gamma_1(\mathbf{x})(\chi_{i_1}(\theta)) &\\ + \sum_{i_1=1}^{\infty}\sum_{i_2=1}^{\infty} a_{i_1 i_2}(\mathbf{x})\Gamma_2(\chi_{i_1}(\theta),\chi_{i_2}(\theta)) &\\ + \sum_{i_1=1}^{\infty}\sum_{i_2=1}^{\infty}\sum_{i_3=1}^{\infty} a_{i_1 i_2 i_3}(\mathbf{x})\Gamma_3(\chi_{i_1}(\theta),\chi_{i_2}(\theta),\chi_{i_3}(\theta))\ldots, &\end{aligned} \tag{3.45}$$

where $\Gamma_i(.)$ denotes the Homogeneous Chaos of i-th order and $a_i(\mathbf{x})$ are deterministic coefficients. For a Gaussian random field, the Homogeneous Chaoses Γ_i equal the corresponding multidimensional Hermite polynomials Ψ_i mentioned in Subsection 3.3.1. Equation (3.45) can also be written as

$$\hat{H}(\mathbf{x},\boldsymbol{\chi}(\theta)) = \sum_{i=0}^{\infty} a_i(\mathbf{x})\Psi_i(\theta), \tag{3.46}$$

with $\Psi_i(\theta)$ denoting the set of Hermite polynomials. Forming a complete set of orthogonal random variables, they provide the following properties [39]:

$$\Psi_0 = 1, \tag{3.47}$$

$$\mathrm{E}\left[\Psi_i\right] = 0, \qquad i > 0, \tag{3.48}$$

and [18]

$$\mathrm{E}\left[\Psi_i\Psi_j\right] = \delta_{ij}\mathrm{E}\left[\Psi_i^2\right]. \tag{3.49}$$

In [18] a list of the Polynomial Chaoses is given. Furthermore, [39] present an algorithm to compute the Polynomial Chaoses. Since this method does not require the covariance C_{HH}, it is suitable for the representation of the resulting displacements, e.g. in the SSFEM method or the response surface method. Moreover, the Polynomial Chaos is also suitable for representing non-Gaussian random fields ([18], [29]). For instance, in [10] the Polynomial Chaos is employed to represent the random input as well as the response, allowing to investigate non-Gaussian random field problems. In addition, instead of the Hermite polynomials, any type of orthogonal polynomials can be used. In [10], a list of appropriate choices for a number of distribution function types is given.

3.3.5 Expansion optimum linear estimation (EOLE) method

This method combines the OLE-concept (see Subsection 3.1.5) with a spectral decomposition of the covariance matrix $\mathbf{C}_{\chi\chi}$. The OLE method represents H as a linear combination of random variables $\boldsymbol{\chi} = [\chi_1,\ldots\chi_{N^{rf}}]^{\mathsf{T}} = [H(\mathbf{x}_1),\ldots H(\mathbf{x}_{N^{rf}})]^{\mathsf{T}}$ located at

nodal points $\mathbf{x}_i$ (see Equation (3.14)). The random vector $\boldsymbol{\chi}$ is characterized by mean value $\boldsymbol{\mu}_\chi$ and covariance matrix $\mathbf{C}_{\chi\chi}$. Using the EOLE method, the latter is decomposed into Eigenvalues λ_i and Eigenvectors $\boldsymbol{\phi}_i$ by solving the eigenvalue problem

$$\mathbf{C}_{\chi\chi}\boldsymbol{\phi}_i = \lambda_i\boldsymbol{\phi}_i. \tag{3.50}$$

Then the random vector $\boldsymbol{\chi}$ can be written in analogy to the random field H in Equation (3.38):

$$\boldsymbol{\chi}(\theta) = \boldsymbol{\mu}_\chi + \sum_{i=0}^{N^{rf}} \zeta_i(\theta)\sqrt{\lambda_i}\boldsymbol{\phi}_i, \tag{3.51}$$

where ζ_i denotes independent standard normal variables, and λ_i and $\boldsymbol{\phi}_i$ the corresponding eigenvalues and eigenvectors, respectively. Substituting (3.51) into (3.14) and solving the OLE-problem yields [44]

$$\hat{H}(\mathbf{x},\theta) = \mu_H(\mathbf{x}) + \sum_{i=1}^{N^{rf}} \frac{\zeta_i(\theta)}{\sqrt{\lambda_i}}\boldsymbol{\phi}_i^{\mathsf{T}}\mathbf{c}_{\chi(\mathbf{x}),\chi}. \tag{3.52}$$

Truncating the series after r terms yields the approximated solution similarly to the Karhunen-Loève expansion. Thus, the EOLE approximates a random field on two levels:

- **Grid size**: The grid size defines the dimension $M \times M$ of $\mathbf{C}_{\chi\chi}$ and, thus, the size of the eigenvalue problem. The more terms are retained, the more accurate the representation.
- **Number of random variables**: In analogy to the Karhunen-Loève expansion, the series can be truncated after r terms, thus reducing the expansion to the r most important random variables $\zeta_i(\theta)$.

3.4 Summary

Except for the Polynomial Chaos, the presented methods are almost exclusively suitable for Gaussian random fields, as stated in [37], where methods for the representation of non-Gaussian fields are summarized.

In [38] it is stated, that, mathematically speaking, the Midpoint- and Average-type discretization methods expand the random field on a finite, incomplete set of deterministic functions $\varphi_i(\mathbf{x})$ using the coordinates $\chi_i(\theta)$ as shown in Equation (3.1). Furthermore, it can be seen that these methods are *linear methods*, i.e. the discretization parameters are linear functionals of the random field [29].

Series expansion methods, on the other hand, provide a complete set of basis functions, thus, allowing theoretically an exact representation of the random field.

The representation methods shown in this chapter allow using simulation methods as well as further analytical treatment. However, a great number of representation methods is devoted exclusively to simulation methods. Such methods are e.g. the turning bands method (TBM), the autoregressive (AR) and moving average (MA) as well as their combination (ARMA). Furthermore, the autoregressive integral moving average (ARIMA) is worth mentioning.

Chapter 4

The Stochastic-Finite-Element method (SFEM)

In structural mechanics, the system equilibrium equation for static loading used within Finite elements methods reads

$$\mathbf{K}\mathbf{u} = \mathbf{f}, \tag{4.1}$$

where $\mathbf{f}$ and $\mathbf{u}$ denote the excitation and the response vector, respectively, and $\mathbf{K}$ denotes the system stiffness matrix. Some tasks in structural engineering involve a random excitation $\mathbf{f} = \mathbf{f}(\theta)$, whereas some problems involve a random system stiffness $\mathbf{K} = \mathbf{K}(\theta)$, which may stem from a random elastic modulus $E = E(\mathbf{x}, \theta)$ or Poisson's ratio $\nu = \nu(\mathbf{x}, \theta)$, with both of them being expressed as random fields. However, if at least one of the quantities in Equation (4.1) is random, the structural response is assumed to be random as well [18]. In this work, the randomness of the system stiffness matrix $\mathbf{K}(\theta)$ is of interest, and the excitation remains to be deterministic, hence

$$\mathbf{K}(\theta)\mathbf{u}(\theta) = \mathbf{f}. \tag{4.2}$$

4.1 Discretization of the stochastic global stiffness matrix

Under the assumption that the random variation of the elastic modulus E can be represented using a homogeneous random field and that the material behaviour is isotropic, the following applies:

$$E(\mathbf{x}, \theta) = \mu_E \cdot \big(1 + I(\mathbf{x}, \theta)\big), \tag{4.3}$$

where $I(\mathbf{x}, \theta)$ is a homogeneous random field with zero mean and autocovariance C_{EE}. It can be shown that the global stiffness matrix $\mathbf{K}$ can be divided into the mean $\bar{\mathbf{K}}$ and

the deviatoric (random) part $\mathbf{\Delta K}$ [31]. In deterministic finite elements, the e-th element stiffness matrix reads

$$\mathbf{k}^{(e)} = \int_{V_e} \mathbf{B}^{\mathsf{T}}\mathbf{D}\mathbf{B}\mathrm{d}V_e, \tag{4.4}$$

where $\mathbf{B}$ and $\mathbf{D}$ are the strain-displacement matrix and the elasticity matrix, respectively. Provided the material behaviour is isotropic, the elasticity matrix for stochastic finite elements is

$$\mathbf{D}\big(E(\mathbf{x},\theta)\big) = \bar{\mathbf{D}} \cdot \big(1 + I(\mathbf{x},\theta)\big), \tag{4.5}$$

where $\bar{\mathbf{D}}$ is a constant matrix. Thus, in stochastic finite elements, the element stiffness matrix reads

$$\begin{aligned}\mathbf{k}^{(e)}(\theta) &= \int_{V_e} \big(1 + I(\mathbf{x},\theta)\big)\mathbf{B}^{\mathsf{T}}\bar{\mathbf{D}}\mathbf{B}\mathrm{d}V_e \\ &= \underbrace{\int_{V_e} \mathbf{B}^{\mathsf{T}}\bar{\mathbf{D}}\mathbf{B}\mathrm{d}V_e}_{\bar{\mathbf{k}}^{(e)}} + \underbrace{\int_{V_e} I(\mathbf{x},\theta)\mathbf{B}^{\mathsf{T}}\bar{\mathbf{D}}\mathbf{B}\mathrm{d}V_e}_{\mathbf{\Delta k}^{(e)}(\theta)}.\end{aligned} \tag{4.6}$$

Assembling the elements matrices $\mathbf{k}^{(e)}$ yields the global stiffness matrix

$$\begin{aligned}\mathbf{K} = \sum_{e=1}^{N_e} \mathbf{k}^{(e)}(\theta) &= \sum_{e=1}^{N_e} \big(\bar{\mathbf{k}}^{(e)} + \mathbf{\Delta k}^{(e)}(\theta)\big) \\ &= \sum_{e=1}^{N_e} \bar{\mathbf{k}}^{(e)} + \sum_{e=1}^{N_e} \mathbf{\Delta k}^{(e)}(\theta) = \bar{\mathbf{K}} + \mathbf{\Delta K}(\theta),\end{aligned} \tag{4.7}$$

where N_e is the number of finite elements, $\bar{\mathbf{k}}^{(e)}$ is the e-th element mean value stiffness matrix, and θ is denoting the random character of $\mathbf{\Delta K}$. The random field $I(\mathbf{x},\theta)$ is discretized by a finite number of random variables $\chi_i(\theta)$, using one of the methods shown in Chapter 3. Thus, the global stiffness matrix reads

$$\mathbf{K} = \bar{\mathbf{K}} + \mathbf{\Delta K}(\theta) \xrightarrow{\text{Discretization}} \mathbf{K}\left(\boldsymbol{\chi}\right) = \bar{\mathbf{K}} + \mathbf{\Delta K}\left(\boldsymbol{\chi}\right) \equiv \bar{\mathbf{K}} + \mathbf{\Delta K}, \tag{4.8}$$

with $\boldsymbol{\chi} = [\chi_1(\theta), \chi_2(\theta), \dots]^{\mathsf{T}}$, and $\bar{\mathbf{K}}$ and $\mathbf{\Delta K}$ denoting the mean value stiffness matrix and the deviatoric (random) stiffness matrix, respectively.

The k-th realization of the random field $I(\mathbf{x},\theta_k)$ leads to

$$\mathbf{K}^{(k)} = \bar{\mathbf{K}} + \mathbf{\Delta K}(\theta_k) \xrightarrow{\text{Discretization}} \mathbf{K}\left(\boldsymbol{\chi}^{(k)}\right) = \bar{\mathbf{K}} + \mathbf{\Delta K}\left(\boldsymbol{\chi}^{(k)}\right) \equiv \bar{\mathbf{K}} + \mathbf{\Delta K}^{(k)}, \tag{4.9}$$

with the k-th realization of random variables $\boldsymbol{\chi}^{(k)} = [\chi_1(\theta_k), \chi_2(\theta_k), \dots]^{\mathsf{T}}, k = 1, \dots m$, and $\bar{\mathbf{K}}$ and $\mathbf{\Delta K}^{(k)}$ denoting the mean value stiffness matrix and the k-th deviatoric (random) stiffness matrix, respectively.

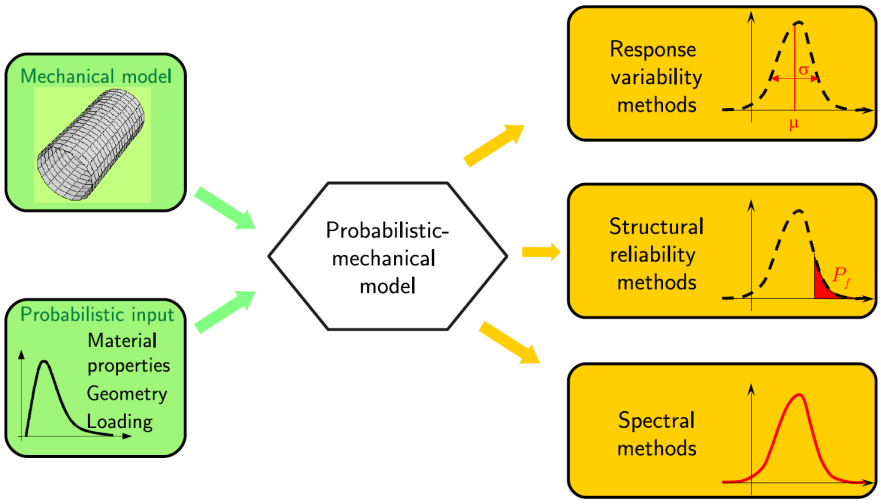

Figure 4.1: Basic structure of an uncertainty analysis, figure from [38].

4.2 Overview

The term SFEM covers several approaches capable of solving the problem at hand, which can be divided into three groups, as suggested in the overview given in 4.1 [38]:

- **Reliability assessment methods** are suitable for dealing with small probabilities (e.g. the probability of failure).
- **Second moment methods** are efficient, but only appropriate for obtaining the response variability, meaning that the mean value and variance of the response are derived, but, except for MCS, no statement about the pdf can be given. Furthermore, most of these approaches are, except for MCS, subject to severe limitations regarding the random input.
- **Spectral methods** use complete sets of functions to represent the involved random fields, thus, providing an unified (and theoretically exact) framework of uncertainty assessment. These methods represent the complete random response in terms of a series expansion, which can be used to obtain the second order moments as well as moments of higher order.

4.3 Monte Carlo simulation (MCS)

The Monte Carlo simulation is the most illustrative and simple - yet, most stable and generally applicable - method. Thanks to its simplicity, this method is used frequently. The general approach is illustrated in Figure 4.2.

4.3.1 Direct MCS

The stochastic global stiffness matrix is assumed to be assembled as shown in Section 4.1. Therefore, the randomness is no longer expressed in terms of a random field $H(\mathbf{x}, \theta)$

but random variables χ_i. The basic concept, as described in [6], consists of generating m random samples/realizations $\mathbf{X}^{(k)} = \boldsymbol{\chi}^{(k)} = [\chi_1(\theta_k), \chi_2(\theta_k), \dots]^\mathsf{T}, k = 1, 2, \dots m$, using a quasi-random number generator. The samples are required to comply with the given distribution parameters, and to be statistically independent from each other, see [6]. Therefore, the use of a reliable random number generator is necessary. Then the given problem is solved for each of the samples, giving a set of structural responses $\mathbf{R}^{(k)} = \mathbf{u}^{(k)}$. Using the Finite element method, according to Equation (4.1) the problem for each realization reads

$$\mathbf{K}\left(\boldsymbol{\chi}^{(k)}\right)\mathbf{u}^{(k)} = \mathbf{f}, \qquad k = 1, \dots m. \tag{4.10}$$

Multiplying by $\left(\mathbf{K}\left(\boldsymbol{\chi}^{(k)}\right)\right)^{-1}$ yields

$$\mathbf{u}^{(k)} = \left(\mathbf{K}\left(\boldsymbol{\chi}^{(k)}\right)\right)^{-1}\mathbf{f} = \left(\bar{\mathbf{K}} + \boldsymbol{\Delta}\mathbf{K}^{(k)}\right)^{-1}\mathbf{f}, \qquad k = 1, \dots m. \tag{4.11}$$

Finally, the statistical information/variability of the structural answer $\mathbf{u}$ can be obtained using estimators. The estimated mean value $\hat{\mu}_\mathbf{u}$ and the variance $\hat{\sigma}^2_\mathbf{u}$, respectively, of the structural response are

$$\hat{\mu}_{\mathbf{u},m} = \frac{1}{m}\sum_{k=1}^{m}\mathbf{u}^{(k)} \tag{4.12}$$

and

$$\hat{\sigma}^2_{\mathbf{u},m} = \frac{1}{m-1}\sum_{k=1}^{m}\left(\mathbf{u}^{(k)} - \hat{\mu}_{\mathbf{u},m}\right)^2. \tag{4.13}$$

The estimator $\hat{\mu}$ is consistent, unbiased and asymptotically normal distributed with a variance of

$$\begin{aligned}\sigma^2_{\hat{\mu}_{\mathbf{u},m}} = \frac{\sigma^2_{\mathbf{u},m}}{m} \approx \frac{\hat{\sigma}^2_{\mathbf{u},m}}{m} &= \frac{1}{m}\left(\frac{1}{m-1}\sum_{k=1}^{m}\left(\mathbf{u}^{(k)} - \hat{\mu}_{\mathbf{u},m}\right)^2\right) \\ &= \frac{1}{m}\frac{1}{m-1}\left(\sum_{k=1}^{m}\left(\mathbf{u}^{(k)}\right)^2 - \hat{\mu}^2_{\mathbf{u},m}\right).\end{aligned} \tag{4.14}$$

MCS can also be employed for reliability assessment. Then the estimated failure probability is

$$\hat{p}_F = P[F] = \frac{1}{m}\sum_{k=1}^{m} I_{F,(k)}, \tag{4.15}$$

where F is the event of failure and $I_{F,(k)}$ denotes the indicator function

$$I_{F,(k)} = \begin{cases} 1 & \text{if system collapses} \\ 0 & \text{otherwise.} \end{cases} \tag{4.16}$$

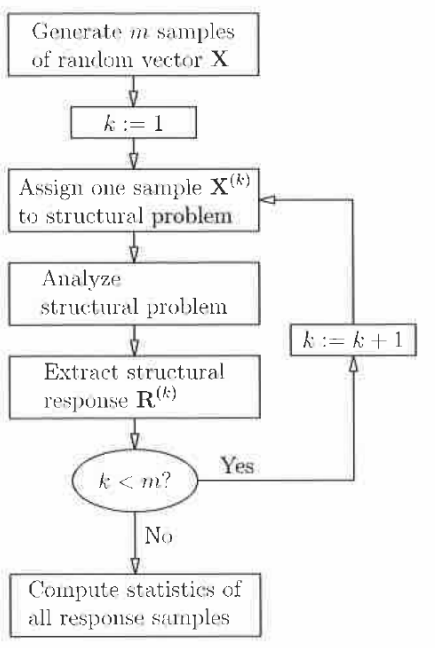

Figure 4.2: Flow-chart for Monte Carlo stochastic analysis, $\mathbf{X}^{(k)} = \boldsymbol{\chi}^{(k)}, \mathbf{R}^{(k)} = \mathbf{u}^{(k)}$, figure taken from [6]

The variance of the estimator is [6]

$$\sigma^2_{\hat{p}_F} = \frac{p_F}{m} - \frac{p_F^2}{m} \Rightarrow \sigma_{\hat{p}_F} \approx \sqrt{\frac{p_F}{m}}. \tag{4.17}$$

Thus, for reliability assessment, the accuracy of the estimation depends not only on the sample size m, but also on the failure probability. According to [34], a sample size of $m = 30$ to 100 is sufficient for estimating μ and σ^2 with acceptable accuracy, whereas a sample size of $m \approx 500$ provides enough information to estimate the cdf [37]. However, since failure is supposed to be a rare event and, thus, only few realizations induce failure, reliability computation requires a relatively big number - proportional to $1/p_F$ - of samples, see Equation (4.17). For this reason, deriving the failure probability using direct MCS is time-consuming and inefficient. To overcome this major disadvantage, numerous approaches like Latin Hypercube sampling, importance sampling, as well as line sampling, directional sampling, and subset sampling have been proposed. Their main goal is to reduce the number of samples m. Since the main focus of this work is the structural response variability, reliability assessment methods will be presented only superficially.

4.3.2 Importance sampling

The basic idea of importance sampling is to produce samples particularly in an important domain of the sample space. This is accomplished by choosing the probability distribution parameters accordingly, e.g. the distribution function for the important domain is $f_X^{IS}(\mathbf{x})$, whereas the original distribution function is $f_X(\mathbf{x})$. In reliability assessment,

the important domain denotes the area close and within the failure domain, usually it is chosen around the most probable point. The latter can be computed using FORM (see Section 4.4.1), which in turn is just an approximation and prone to error. In case of FORM giving appropriate results, more realizations are situated in the failure region, thus, reducing the required sample size and the variance error. The failure probability is then obtained by modifying Equation (4.15)

$$\hat{p}_F = \frac{1}{m} \sum_{k=1}^{m} \frac{f_X(\mathbf{x})}{f_X^{IS}(\mathbf{x})} I_{F,(k)}. \tag{4.18}$$

As stated in [37], importance sampling is efficient for static linear and nonlinear systems, which are depending on a small number of random variables. In high stochastic dimensions, however, finding a appropriate distribution function $f_X^{IS}(\mathbf{x})$ may become difficult.

4.3.3 Latin hypercube sampling

Latin hypercube sampling is employed to decrease the variance of the estimator and, thus, reducing the required number of samples.

Suppose, a problem depends on 2 random variables X_1 and X_2, then the sample space is two-dimensional, with each realization being a point with coordinates $\big(X_1(\theta_0), X_2(\theta_0)\big)$. A square grid over the sample space is called Latin square grid if (and only if) there is only one realization $\big(X_1(\theta_0), X_2(\theta_0)\big)$ in each row and each column of the grid.

The generalization of this concept for n random variables, denoting a point $(X_1, \dots X_n)$ in n-dimensionial sample space, is called Latin hypercube. As stated in [6], Latin hypercube sampling provides a good coverage of the sample space and, hence, when estimating the coefficient of correlation δ, the method may reduce the required sample size by a factor of more than 10. However, with increasing dimensionality n, the computation time grows exponentially. Thus, the Latin hypercube sampling method is very sensitive to problems with high stochastic dimensionality.

4.3.4 Line Sampling

A method, suitable for problems with high stochastic dimensionality, is line sampling, proposed by [27]. Instead of a most probable point, a so called important direction $\boldsymbol{\alpha}$ can be used. The estimator for the failure probability $\hat{p}_F$ writes

$$\hat{p}_F = \frac{1}{N} \sum_{i=1}^{m} p_F^{(i)}, \tag{4.19}$$

with conditional probabilities, which can be computed quasi-exactly according to the normal cdf

$$p_F^{(i)} = \int_{-\infty}^{+\infty} I_F\left(\mathbf{x}^{(i)}\right) \frac{1}{\sqrt{2\pi}} \exp\left(-\frac{\left(\mathbf{x}_1^{(i)}\right)^2}{2}\right) = \Phi\left(\beta_1^{(i)}\right) + \Phi\left(-\beta_u^{(i)}\right), \tag{4.20}$$

where the safe region is denoted by $[\beta_1^{(i)}, \beta_u^{(i)}]$. The variance of the line sampling estimator is always smaller than the variance of direct MCS [27].

4.3.5 Neumann expansion

When performing Monte Carlo simulation, for each realization k the inverse of the system stiffness matrix $\mathbf{K}$ has to be built, which is a time consuming process. Applying the Neumann expansion method, the computation time for this inversion can be reduced significantly. The method, introduced by [43], is based on the series expansion of a square and non-singular matrix $\mathbf{P}$

$$(\mathbf{I}-\mathbf{P})^{-1}=\sum_{i=0}^{\infty}\mathbf{P}^i=\mathbf{I}+\mathbf{P}+\mathbf{P}^2+\dots \tag{4.21}$$

It converges only for $\|\mathbf{P}\|<1$, or if all Eigenvalues λ_i of $\mathbf{P}$ fulfil $\|\lambda_i\|<1$. Thus, for this approach the random field $I(\mathbf{x},\theta)$ according to (4.3) needs to comply with $-1<I(\mathbf{x},\theta)<1$. Substituting (4.8) into (4.10) yields

$$\mathbf{K}\left(\boldsymbol{\chi}^{(k)}\right)\mathbf{u}^{(k)}=\left[\bar{\mathbf{K}}+\boldsymbol{\Delta}\mathbf{K}^{(k)}\right]\mathbf{u}^{(k)}=\mathbf{f}. \tag{4.22}$$

Multiplied by $\bar{\mathbf{K}}^{-1}$ gives

$$\Big[\mathbf{I}+\underbrace{\bar{\mathbf{K}}^{-1}\boldsymbol{\Delta}\mathbf{K}^{(k)}}_{-\mathbf{P}^{(k)}}\Big]\mathbf{u}^{(k)}=\bar{\mathbf{K}}^{-1}\mathbf{f}, \tag{4.23}$$

and further

$$\mathbf{u}^{(k)}=\left[\mathbf{I}-\mathbf{P}^{(k)}\right]^{-1}\bar{\mathbf{K}}^{-1}\mathbf{f}. \tag{4.24}$$

Applying the Neumann series expansion leads to

$$\mathbf{u}^{(k)}=\left(\sum_{i=0}^{\infty}\left(\mathbf{P}^{(k)}\right)^i\right)\bar{\mathbf{K}}^{-1}\mathbf{f}=\left[\sum_{i=0}^{\infty}(-1)^i\left(\bar{\mathbf{K}}^{-1}\boldsymbol{\Delta}\mathbf{K}^{(k)}\right)^i\right]\bar{\mathbf{K}}^{-1}\mathbf{f}. \tag{4.25}$$

Truncating the series after N terms yields the approximation

$$\mathbf{u}^{(k)}=\left[\sum_{i=0}^{N}(-1)^i\left(\bar{\mathbf{K}}^{-1}\boldsymbol{\Delta}\mathbf{K}^{(k)}\right)^i\right]\bar{\mathbf{K}}^{-1}\mathbf{f}. \tag{4.26}$$

Finally, in analogy to the direct MCS the response statistics are obtained using Equations (4.12) and (4.13).

The major advantage of (4.26) over (4.11) is the fact that only the deterministic part $\bar{\mathbf{K}}$ needs to be inverted. Since $\bar{\mathbf{K}}$ is constant for all samples, only one inversion has to be done for the entire simulation process, which reduces the computation time significantly.

Although any distribution type can be assigned to $I(\mathbf{x},\theta)$, the Neumann expansion approach only allows to compute the solution characteristics up to the second moments, i.e. mean and variance. Another drawback is that the random variables are required to remain in the range of $-1<I(\mathbf{x},\theta)<1$, thus, each realization with values exceeding this range has to be excluded from the Monte Carlo simulation, biasing the result.

4.3.6 Subset simulation

The subset simulation method was proposed by [2], providing a method which is not influenced by the dimension of the stochastic problem. The basic idea of subset simulation is to replace the failure event F by a sequence of supersets F_i, denoting intermediate failure events of greater probability. This is accomplished by defining the supersets as $F_1 \supset F_2 \supset \ldots \supset F_m = F$ with $F_k = \bigcap_{i=1}^{k} F_i, k = 1, \ldots, m$. Then, considering Equation (2.7), the failure probability writes

$$\begin{aligned} p_F &= \mathrm{P}[F] = \mathrm{P}[F_1 \cap F_2 \cap \ldots \cap F_{m-1} \cap F_m] = \mathrm{P}[F_{m-1} \cap F_m] \\ &= P[F_m \cap F_{m-1}] = P[F_m \mid F_{m-1}]P[F_{m-1}]. \end{aligned} \tag{4.27}$$

Repeating the steps for $\mathrm{P}[F_{m-1}]$ gives

$$P[F_{m-1}] = P[F_{m-1} \mid F_{m-2}]P[F_{m-2}], \tag{4.28}$$

which, substituted into (4.27), yields

$$p_F = P[F_m \mid F_{m-1}]P[F_{m-1} \mid F_{m-2}]P[F_{m-2}], \tag{4.29}$$

and so forth. The general equation finally reads

$$p_F = \mathrm{P}[F_1] \prod_{i=1}^{m-1} \mathrm{P}[F_{i+1} \mid F_i]. \tag{4.30}$$

With properly chosen intermediate failure events F_i, the subset simulation method is very efficient. For example, the failure probability of a certain system is assumed to be $p_F \leq 10^{-4}$. Verification via direct MCS is in most cases inefficient (depending on the complexity of the system). However, using subset simulation, 4 intermediate failure events with conditional failure probability $\mathrm{P}[F_{i+1} \mid F_i] \approx 0.1$ are chosen. Those conditional probabilities can be efficiently computed using direct MCS, providing the same solution quality as the direct MCS. Nevertheless, [2] use a Markov chain MCS simulation method, based on the Metropolis algorithm, to further increase the efficiency.

A major advantage of subset simulation is the fact, that the efficiency is not depending on the stochastic dimensionality of the problem. However, the convergence rate depends on the choice of intermediate failure events [37].

4.4 Reliability assessment

The response $\mathbf{X}$ of a structural system (e.g. a bridge), subject to random parameters $\boldsymbol{\chi}$, is random as well. For every system, desired (safe) and undesired (unsafe) states are defined. Usually, the so called *limit state function* $g(\mathbf{X})$ defines the border between safe and unsafe region. For instance, the unsafe region can be defined as points of structural failure, undesired deformation states, or when cracking starts. In general, structural responses located in the unsafe region $g(\mathbf{X}) \leq 0$ are considered as failure.

Obviously, the probability of failure is demanded to be small, depending on the type of structural problem. It can be written as

$$\mathrm{P}[g(\mathbf{X}) \leq 0] = \int_{g(\mathbf{X}) \leq 0} \cdots \int f_X(\mathbf{x}) \mathrm{d}\mathbf{x}, \tag{4.31}$$

where $f_X(\mathbf{x})$ denotes the joint probability. In general, when analysing complex structures, numerical methods like FEM are applied. Thus, the limit state function is not available explicitly. Another issue is the joint pdf $f_X(\mathbf{x})$, which is usually not known. Hence, the integral in (4.31) cannot be solved analytically. In the following, some approaches to numerically solve the integral, and compute the probability of failure $\mathrm{P}[g(\mathbf{X}) \leq 0]$, are summarized.

4.4.1 First-/second order reliability method (FORM/SORM)

This method requires the transformation from non-Gaussian random variables $\mathbf{X}$ into standard normal random variables $\mathbf{U}$ with zero mean. Furthermore, correlated random variables are transformed into uncorrelated variables (see e.g. [39]).

The First order reliability method is used to obtain the so called design- or *most probable point*, which is the point $\mathbf{u}^*$ on the limit state function $g(\mathbf{u})$ with minimal distance $\beta = \|\mathbf{u}\|$, also called *reliability index*, to the origin:

$$\mathbf{u}^* = \min \big(\|\mathbf{u}\| \;\big|\; g(\mathbf{u}) = 0 \big). \tag{4.32}$$

For this purpose, the Rackwitz-Fiessler algorithm can be applied [13]. Then the limit state function is linearized at the design point and the probability of failure is estimated as

$$p_F \approx \Phi(-\beta). \tag{4.33}$$

As stated in [39], accurate results are obtained only for the tails of the pdf, i.e. a large reliability index is required. When using SORM, the second order term is added to the linearization of $g(\mathbf{u})|_{\mathbf{u}=\mathbf{u}^*}$. This increases the computational cost significantly while hardly improving the results.

FORM is a method easy to implement and, thus, widely used. However, it cannot be guaranteed that the global minimum of β is found. Furthermore, in some cases the algorithm does not converge. Therefore numerous improvements and new methods were developed, e.g. the Sequential quadratic programming (SQP), see [26].

4.4.2 Monte Carlo simulation

Using direct Monte Carlo simulation, the probability of failure can be estimated, according to Section 4.3, as

$$\bar{p}_F = P[F] = \frac{1}{m} \sum_{k=1}^{m} I_{F,(k)}. \tag{4.34}$$

Furthermore, methods improving the direct MCS, such as Importance sampling, Line sampling, and Subset sampling, have been presented.

4.4.3 Response surface method

The response surface method aims at using an approximated limit state surface for the reliability analysis. The approximated limit state surface $\hat{g}(\mathbf{X})$ can be expanded as

quadratic function [39]

$$\hat{g}(\mathbf{x}) = \hat{g}(x_1, x_2, \dots) = a_0 + \sum_{i=1}^{N} a_i x_i + \sum_{i=1}^{N}\sum_{j=1}^{N} a_{ij} x_i x_j. \tag{4.35}$$

The coefficients $\mathbf{a} = \{a_0, a_1, \dots a_{NN}\}$ are obtained by either regression or interpolation [6], evaluating the problem at hand at a number of grid points $\mathbf{x}^{(k)}, k = 1, \dots M$ (e.g. using the Finite element method). For instance, using the least-square regression method, the error writes

$$\epsilon(\mathbf{a}) = \sum_{k=1}^{M} \left(g(\mathbf{x}) - \hat{g}(\mathbf{x})\right)^2, \tag{4.36}$$

with $N \leq M$. Finally, by minimizing ϵ the coefficients $\mathbf{a}$ can be computed

$$\min\left[\epsilon(\mathbf{a})\right] \Rightarrow \frac{\mathrm{d}\epsilon(\mathbf{a})}{\mathrm{d}\mathbf{a}} = 0. \tag{4.37}$$

The resulting response surface may be analyzed using the methods presented above, for example FORM or Importance sampling.

As stated in [7], since the limit state function depicts the mechanical behaviour, the approximation $\hat{g}(\mathbf{X})$ is made in a mechanical context, thus, being open to engineering judgement. Meanwhile, approximations or assumptions regarding the random variables/statistics (like FORM) are more or less infeasible to verify (apart from MCS, which is computationally expensive).

4.5 Second moment methods

The basic idea of second moment methods is to obtain the second order statistics, i.e. mean μ (first moment) and variance σ^2 (second central moment), of the system response, due to varying input parameters. The latter being expressed by nothing more than their mean value and variance. No statement is made regarding the higher order moments nor the probability distribution type.

4.5.1 Monte Carlo simulation

As stated in Subsection 4.3.1, the Monte Carlo simulation can be used to obtain estimates of mean and variance, requiring approximately 100 samples for sufficient accuracy. In particular, direct Monte Carlo simulation, Latin hypercube sampling, and Neumann expansion are of interest in this regard. However, the MCS is not limited to second moment analysis.

4.5.2 Neumann expansion method

When coupled with the Spectral Stochastic Finite-Element Method (which is presented in Section 4.6), the Neumann expansion method is a second order method. However, since it is often coupled with MCS, it is explained in Subsection 4.3.5.

4.5.3 Perturbation method

The Perturbation method aims at giving the second order statistics of the response vector $\mathbf{u}$. It is based on Taylor series expansions of the three quantities found in Equation (4.1), namely the global stiffness matrix $\mathbf{K}$, the displacement vector $\mathbf{u}$, and the excitation vector $\mathbf{f}$. The Perturbation method can be combined with the discretization techniques presented in Sections 3.1 and 3.2, a list of combinations accomplished is found in [39]. After the random field representing the elastic modulus is discretized, the global stiffness matrix writes, in analogy to Equation (4.8),

$$\mathbf{K} = \bar{\mathbf{K}} + \mathbf{\Delta K}(\boldsymbol{\chi}), \tag{4.38}$$

where $\bar{\mathbf{K}}$ is the corresponding mean value stiffness matrix $\bar{\mathbf{K}} = f(\boldsymbol{\mu}_E)$ and $\mathbf{\Delta K}(\boldsymbol{\chi})$ denotes the random deviatoric part, being a function of the random vector $\boldsymbol{\chi} = [\chi_1, \chi_2, \dots]^\mathsf{T}$. The excitation vector $\mathbf{f}$ and the response vector $\mathbf{u}$ are operated on in the same manner:

$$\mathbf{f} = \bar{\mathbf{f}} + \mathbf{\Delta f}(\boldsymbol{\chi}), \tag{4.39}$$

$$\mathbf{u} = \bar{\mathbf{u}} + \mathbf{\Delta u}(\boldsymbol{\chi}). \tag{4.40}$$

The Taylor series expansion is applied on the deviatoric parts, resulting in

$$\mathbf{K} = \bar{\mathbf{K}} + \sum_{i=1}^{N} \frac{\partial \mathbf{K}}{\partial \chi_i}\Big|_{\boldsymbol{\chi}=\mathbf{0}} \chi_i + \frac{1}{2}\sum_{i=1}^{N}\sum_{j=1}^{N} \frac{\partial^2 \mathbf{K}}{\partial \chi_i \partial \chi_j}\Big|_{\boldsymbol{\chi}=\mathbf{0}} \chi_i \chi_j + \dots, \tag{4.41}$$

$$\mathbf{u} = \bar{\mathbf{u}} + \sum_{i=1}^{N} \frac{\partial \mathbf{u}}{\partial \chi_i}\Big|_{\boldsymbol{\chi}=\mathbf{0}} \chi_i + \frac{1}{2}\sum_{i=1}^{N}\sum_{j=1}^{N} \frac{\partial^2 \mathbf{u}}{\partial \chi_i \partial \chi_j}\Big|_{\boldsymbol{\chi}=\mathbf{0}} \chi_i \chi_j + \dots, \tag{4.42}$$

$$\mathbf{f} = \bar{\mathbf{f}} + \sum_{i=1}^{N} \frac{\partial \mathbf{f}}{\partial \chi_i}\Big|_{\boldsymbol{\chi}=\mathbf{0}} \chi_i + \frac{1}{2}\sum_{i=1}^{N}\sum_{j=1}^{N} \frac{\partial^2 \mathbf{f}}{\partial \chi_i \partial \chi_j}\Big|_{\boldsymbol{\chi}=\mathbf{0}} \chi_i \chi_j + \dots. \tag{4.43}$$

Since obtaining the derivatives of higher order than 2 is increasing the computation time substantially, without improving the results significantly, the Taylor series is truncated after the second order term. The derivation of $\mathbf{K}$ is made preferably on the element stiffness matrix level, either analytically or using the finite difference method. Substituting (4.41), (4.42), and (4.43) into (4.1) and comparing coefficients gives

$$\bar{\mathbf{u}} = \bar{\mathbf{K}}^{-1}\bar{\mathbf{f}}, \tag{4.44}$$

$$\frac{\partial \mathbf{u}}{\partial \chi_i} = \bar{\mathbf{K}}^{-1}\left(\frac{\partial \mathbf{f}}{\partial \chi_i} - \frac{\partial \mathbf{K}}{\partial \chi_i}\bar{\mathbf{u}}\right), \tag{4.45}$$

and

$$\frac{\partial^2 \mathbf{u}}{\partial \chi_i \partial \chi_j} = \bar{\mathbf{K}}^{-1}\left(\frac{\partial^2 \mathbf{f}}{\partial \chi_i \partial \chi_j} - \frac{\partial \mathbf{K}}{\partial \chi_i}\frac{\partial \mathbf{u}}{\partial \chi_j} - \frac{\partial \mathbf{K}}{\partial \chi_j}\frac{\partial \mathbf{u}}{\partial \chi_i} - \frac{\partial^2 \mathbf{K}}{\partial \chi_i \partial \chi_j}\bar{\mathbf{u}}\right), \tag{4.46}$$

showing that the response vector $\mathbf{u}$ can be readily computed up to the second order term. In case of a deterministic excitation vector $\mathbf{f}$, the first and second derivatives are zero, while $\mathbf{f}$ represents the mean.

Finally, in [37], a first order estimation is provided, the mean being

$$\bar{\boldsymbol{\mu}}_{\mathbf{u}}^{\mathrm{I}} = \bar{\mathbf{u}}, \tag{4.47}$$

whereas the covariance matrix reads

$$\mathbf{C}_{\mathbf{uu}}^{\mathrm{I}} = \sum_{i=1}^{N}\sum_{i=1}^{N} \frac{\partial \mathbf{u}}{\partial \chi_i}\left(\frac{\partial \mathbf{u}}{\partial \chi_j}\right)^{\mathsf{T}} \mathrm{Cov}[\chi_i, \chi_j]. \tag{4.48}$$

The second order approximation of the mean is given in [39] as

$$\bar{\boldsymbol{\mu}}_{\mathbf{u}}^{\mathrm{II}} = \bar{\mathbf{u}} + \frac{1}{2}\sum_{i=1}^{N}\sum_{j=1}^{N} \frac{\partial^2 \mathbf{u}}{\partial \chi_i \partial \chi_j}\mathrm{Cov}[\chi_i, \chi_j]. \tag{4.49}$$

It is stated that the second order estimation of the covariance can be derived, but terms of fourth order are involved and computation is possible only for the case of a Gaussian random field.

The major advantage of this method is its high efficiency. In contrast to the Neumann expansion method, only one structural analysis needs to be performed. Furthermore, the accuracy is high for Gaussian random variables and linear problems, see [19].

However, since this method involves a linearization at the mean value, it is limited to small coefficients of variation with values $\delta < 0.1$. To overcome this drawback, the method has been improved in [15]. In [24] further improvements regarding the efficiency and the a priori quantification of the estimation accuracy are developed. Furthermore, this method has been applied in elasto-statics [23], as well as in elastic stability problems [25].

4.5.4 Quadrature method

The quadrature method approximates moments of i-th order by applying a weighted summation. As can be seen in previous sections, the system response can be expressed as a functional of the random vector $\mathbf{u} = f(\boldsymbol{\chi})$. The i-th moment writes

$$\mathrm{E}\left[\mathbf{u}(\chi_1, \chi_2, \dots \chi_N)\right] = \int_{-\infty}^{+\infty} \cdots \int_{-\infty}^{+\infty} \big(\mathbf{u}(\chi_1, \chi_2, \dots \chi_N)\big)^i f(\chi_1) f(\chi_2) \cdots f(\chi_N) \mathrm{d}\chi_1 \cdots \mathrm{d}\chi_N, \tag{4.50}$$

where $f(\chi_i)$ is the standard normal pdf. The approximation reads

$$\mathrm{E}\left[\mathbf{u}(\chi_1, \chi_2, \dots \chi_N)\right] \approx \sum_{k_1=1}^{M} \cdots \sum_{k_N=1}^{M} w_{k_1} \cdots w_{k_N} \left[\mathbf{u}(\chi_{k_1}, \dots \chi_{k_N})\right]^i, \tag{4.51}$$

with w_{k_j} denoting the weights. A major disadvantage is the exponential increase of computations with the number of random variables.

4.6 Spectral-Stochastic-Finite-Element method (SSFEM)

This method, developed by [18], is based on a series expansion of the global stiffness matrix as well as the response vector. A summary of the procedure is given in [39]. The global stiffness matrix $\mathbf{K}$ and the response vector $\mathbf{u}$ are represented using the Karhunen-Loève series expansion and the Polynomial Chaos expansion, respectively. As shown in Section 3.3.2, the Karhunen-Loève expansion of a Gaussian homogeneous random field $E(\mathbf{x},\theta)$ reads

$$E(\mathbf{x},\theta) = \mu_E(\mathbf{x}) + \sum_{i=1}^{\infty} \chi_i(\theta)\sqrt{\lambda_i} f_i(\mathbf{x}), \tag{4.52}$$

where $\mu_E(\mathbf{x})$ is the mean value function, $\chi_i(\theta)$ are mutually independent normal distributed random variables, and λ_i and $f_i(\mathbf{x})$ are the Eigenvalues and Eigenfunctions, respectively. Provided the material behaviour is isotropic, the elasticity matrix writes

$$\mathbf{D} \equiv \mathbf{D}\big(E(\mathbf{x},\theta)\big) = E(\mathbf{x},\theta)\mathbf{D}_0 = \left(\mu_E(\mathbf{x}) + \sum_{i=1}^{\infty} \chi_i(\theta)\sqrt{\lambda_i} f_i(\mathbf{x})\right)\mathbf{D}_0, \tag{4.53}$$

with $\mathbf{D}_0$ denoting a constant matrix. Substituting (4.53) into (4.4) yields the element stiffness matrix

$$\begin{aligned}
\mathbf{k}^{(e)}(\theta) &= \int_{V_e} \mathbf{B}^{\mathsf{T}}\mathbf{D}\big(E(\mathbf{x},\theta)\big)\mathbf{B}\mathrm{d}V_e \\
&= \underbrace{\int_{V_e} \mu_E(\mathbf{x})\mathbf{B}^{\mathsf{T}}\mathbf{D}_0\mathbf{B}\mathrm{d}V_e}_{\mathbf{k}_0^{(e)}} + \sum_{i=1}^{\infty} \chi_i(\theta)\underbrace{\sqrt{\lambda_i}\int_{V_e} \mathbf{B}^{\mathsf{T}}\mathbf{D}_0\mathbf{B} f_i(\mathbf{x})\mathrm{d}V_e}_{\mathbf{k}_i^{(e)}} \\
&= \mathbf{k}_0^{(e)} + \sum_{i=1}^{\infty} \chi_i(\theta)\mathbf{k}_i^{(e)}.
\end{aligned} \tag{4.54}$$

Assembling the element stiffness matrices gives the global stiffness matrix, which can be expressed in the same manner

$$\begin{aligned}
\mathbf{K}(\theta) &= \sum_{e=1}^{N_e} \mathbf{k}^{(e)}(\theta) = \sum_{e=1}^{N_e} \mathbf{k}_0^{(e)} + \sum_{e=1}^{N_e}\sum_{i=1}^{\infty} \chi_i(\theta)\mathbf{k}_i^{(e)} = \underbrace{\sum_{e=1}^{N_e} \mathbf{k}_0^{(e)}}_{\mathbf{K}_0} + \sum_{i=1}^{\infty} \chi_i(\theta)\underbrace{\sum_{e=1}^{N_e} \mathbf{k}_i^{(e)}}_{\mathbf{K}_i} \\
&= \mathbf{K}_0 + \sum_{i=1}^{\infty} \chi_i(\theta)\mathbf{K}_i.
\end{aligned} \tag{4.55}$$

with N_e denoting the number of finite elements and $\mathbf{K}_i$ being deterministic matrices. Substituting (4.55) into (4.2) gives the stochastic equilibrium equation

$$\mathbf{K}(\theta)\mathbf{u}(\theta) = \left(\mathbf{K}_0 + \sum_{i=1}^{\infty} \chi_i(\theta)\mathbf{K}_i\right)\mathbf{u}(\theta) = \mathbf{f}. \tag{4.56}$$

4.6.1 Improved Neumann series expansion

Originally, in [18] the Neumann series expansion method was applied to Equation (4.56) similar to Subsection 4.3.5, being called *improved Neumann series expansion*

$$\begin{aligned}\mathbf{u}(\theta) &= \left[\sum_{r=1}^{\infty}(-1)^r\left(\sum_{i_1\dots i_r=1}^{\infty}\dots\sum^{\infty}\chi_{i_r}\mathbf{K}_0^{-1}\mathbf{K}_{i_r}\right)^r\right]\mathbf{K}_0^{-1}\mathbf{f}\\ &= \left(\mathbf{I}-\sum_{i_1=1}^{\infty}\chi_{i_1}\mathbf{K}_0^{-1}\mathbf{K}_{i_1}+\sum_{i_1=1}^{\infty}\sum_{i_2=1}^{\infty}\chi_{i_1}\chi_{i_2}\mathbf{K}_0^{-1}\mathbf{K}_{i_1}\mathbf{K}_0^{-1}\mathbf{K}_{i_2}-\dots\right)\mathbf{K}_0^{-1}\mathbf{f}. \qquad (4.57)\end{aligned}$$

Truncating the Neumann series (with index r) and the Karhunen-Loève (with index i_r) after M and N terms, respectively, gives the approximation

$$\begin{aligned}\mathbf{u} &= \left[\sum_{r=1}^{M}(-1)^r\left(\sum_{i_1\dots i_r=1}^{N}\dots\sum^{N}\chi_{i_r}\mathbf{K}_0^{-1}\mathbf{K}_{i_r}\right)^r\right]\mathbf{K}_0^{-1}\mathbf{f}\\ &= \left(\mathbf{I}-\sum_{i_1=1}^{N}\chi_{i_1}\mathbf{K}_0^{-1}\mathbf{K}_{i_1}+\dots+\sum_{i_1=1}^{N}\dots\sum_{i_M=1}^{N}\chi_{i_1}\cdots\chi_{i_M}\mathbf{K}_0^{-1}\mathbf{K}_{i_1}\cdots\mathbf{K}_0^{-1}\mathbf{K}_{i_M}\right)\mathbf{K}_0^{-1}\mathbf{f}.\end{aligned} \qquad (4.58)$$

In contrast to the Neumann series expansion coupled with Monte Carlo simulation (see Subsection 4.3.5), no MCS is required here. However, the number of computational tasks grows exponentially with the number of terms r retained in the Neumann series expansion. Another drawback is the requirement of

$$\left\|\sum\chi_i\mathbf{K}_0^{-1}\mathbf{K}_i\right\|<1, \qquad (4.59)$$

with $\|.\|$ denoting the norm, as discussed in Subsection 4.3.5.

4.6.2 Polynomial Chaos expansion

In [18], the Polynomial Chaos expansion is applied to overcome the disadvantages of the Neumann series expansion. By definition, the spectral stochastic finite element method (SSFEM) is the combination of Karhunen-Loève- with Polynomial Chaos expansion.

Expanding the response vector $\mathbf{u}$ subject to the Polynomial Chaos writes

$$\mathbf{u}(\theta)=\sum_{j=0}^{\infty}\mathbf{u}_j\Psi_j(\theta), \qquad (4.60)$$

where $\mathbf{u}_j$ are yet unknown deterministic coefficients. Substituting (4.60) into (4.56) gives

$$\left(\mathbf{K}_0+\sum_{i=1}^{\infty}\chi_i(\theta)\mathbf{K}_i\right)\sum_{j=0}^{\infty}\mathbf{u}_j\Psi_j(\theta)=\mathbf{f}, \qquad (4.61)$$

which can be reformulated to

$$\sum_{i=0}^{\infty}\chi_i(\theta)\mathbf{K}_i\sum_{j=0}^{\infty}\mathbf{u}_j\Psi_j(\theta)=\sum_{i=0}^{\infty}\sum_{j=0}^{\infty}\chi_i(\theta)\Psi_j(\theta)\mathbf{K}_i\mathbf{u}_j=\mathbf{f}, \qquad (4.62)$$

with $\chi_0(\theta) \equiv 1$. Truncation of the Karhunen-Loève expansion and the Polynomial Chaos expansion after $i = M$ and $j = P$ terms, respectively, gives the approximation

$$\sum_{i=0}^{M}\sum_{j=0}^{P} \chi_i(\theta)\Psi_j(\theta)\mathbf{K}_i\mathbf{u}_j \approx \mathbf{f}. \tag{4.63}$$

Usually, the Karhunen-Loève expansion is truncated after $M \approx 4$ terms, implied the correlation length is sufficiently large. From now on, reference to the random parameter θ will be withhold for simplicity, thus $\chi_i(\theta) \equiv \chi_i, \Psi_i(\theta) \equiv \Psi_i$. Multiplying (4.63) by Ψ_k and taking the expectation value leads to a minimum of the error made by truncation [39], hence

$$\begin{aligned}
\sum_{i=0}^{M}\sum_{j=0}^{P} \underbrace{\mathrm{E}\left[\chi_i\Psi_j\Psi_k\right]}_{c_{ijk}}\mathbf{K}_i\mathbf{u}_j &= \underbrace{\mathrm{E}\left[\Psi_k\mathbf{f}\right]}_{\mathbf{f}_k} \\
&= \sum_{j=0}^{P}\underbrace{\sum_{i=0}^{M} c_{ijk}\mathbf{K}_i}_{\mathbf{K}_{jk}}\mathbf{u}_j = \mathbf{f}_k \\
&= \sum_{j=0}^{P}\mathbf{K}_{jk}\mathbf{u}_j = \mathbf{f}_k, \qquad k = 0,\dots P
\end{aligned} \tag{4.64}$$

with

$$\mathbf{f}_k = \begin{cases} \mathbf{f} & k = 0 \\ \mathbf{0} & k > 0 \end{cases}, \tag{4.65}$$

since $\mathrm{E}[\Psi_0\mathbf{f}] = \mathrm{E}[\Psi_0]\mathbf{f} = \mathbf{f}$ (see Eq. (3.48)). Furthermore, each matrix $\mathbf{K}_{jk}$ is a linear combination of $M+1$ matrices $\mathbf{K}_i$. Equation (4.64) can be rewritten as

$$\underbrace{\left[\begin{array}{c|c|c|c} \mathbf{K}_{00} & \mathbf{K}_{10} & \dots & \mathbf{K}_{P0} \\ \hline \mathbf{K}_{01} & \mathbf{K}_{11} & & \vdots \\ \hline \vdots & & \ddots & \\ \hline \mathbf{K}_{0P} & \dots & & \mathbf{K}_{PP} \end{array}\right]}_{\mathcal{K}} \cdot \underbrace{\left[\begin{array}{c} \mathbf{u}_0 \\ \hline \mathbf{u}_1 \\ \hline \vdots \\ \hline \mathbf{u}_P \end{array}\right]}_{\mathcal{U}} = \underbrace{\left[\begin{array}{c} \mathbf{f}_0 \\ \hline \mathbf{f}_1 \\ \hline \vdots \\ \hline \mathbf{f}_P \end{array}\right]}_{\mathcal{F}}, \tag{4.66}$$

which can be solved for $\mathcal{U}$

$$\mathcal{U} = \mathcal{K}^{-1}\mathcal{F}. \tag{4.67}$$

Thus, the coefficients $\mathbf{u}_j, j = 0,\dots P$ are obtained, fully describing the response vector $\mathbf{u}$ in terms of Equation (4.60). Considering (3.48) and (3.49), the mean vector writes

$$\boldsymbol{\mu}_{\mathbf{u}} = \mathrm{E}[\mathbf{u}] = \mathrm{E}\left[\sum_{j=0}^{P}\mathbf{u}_j\Psi_j\right] = \sum_{j=0}^{P}\mathbf{u}_j\mathrm{E}\left[\Psi_j\right] = \mathbf{u}_0, \tag{4.68}$$

whereas the covariance matrix is

$$\mathbf{C_{uu}} = \sum_{j=0}^{P} \mathrm{E}\left[\Psi_j^2\right] \mathbf{u}_j \mathbf{u}_j^{\mathsf{T}}. \tag{4.69}$$

Each coefficient $\mathbf{u}_j$ in (4.60) is a vector with N terms, where N is denoting the number of degrees of freedom (d.o.f.). Since vector $\mathcal{U}$ consists of $P+1$ vectors $\mathbf{u}_j$, the vectors $\mathcal{U}$ and $\mathcal{F}$ have $N(P+1)$ rows, while the matrix $\mathcal{K}$ is of dimensions $N(P+1) \times N(P+1)$. As stated in [39], for practical application P usually equals 15 to 35, therefore, increasing the dimensionality and the computational cost significantly compared to the corresponding deterministic FE analysis. However, because most of the coefficients c_{ijk} are zero, $\mathcal{K}$ forms a relatively sparse matrix already being subdivided into submatrices $\mathbf{K}_{jk}$. In [32], an iterative algorithm is employed to efficiently solve the linear equation system.

For non-Gaussian random fields, a Polynomial Chaos representation not only for the response, but also for the input random field is suggested, see [9, 10]. As stated in [39], the input random field can also be represented using orthogonal series expansion or EOLE.

The SSFEM provides a unified framework for uncertainty analysis, which, in theory, is exact for an infinite number of terms in the according series expansions. However, although in [18] the applicability to second moment statistics as well as reliability analysis is emphasized, in [39] the accuracy for reliability assessment is doubted. Furthermore, the method is limited to linear material behaviour and geometrical linearity [39].

Chapter 5

Application of SFEM

In this chapter, different SFE approaches are applied to GLT beams, giving the mean value and variance of the effective elasticity modulus E_{eff}. The performance of the different approaches is compared and the obtained results are discussed. To gain understanding of the basic response of a GLT beam with varying stiffness, at first, one lamination is investigated. Then, compound structures of up to four laminations are analysed.

5.1 Problem description

The stiffness distribution in *glued-laminated timber* (GLT) layers (*laminations*) is subject to uncertainty, thus, the effective stiffness of the compound structure is assumed random as well, see Figure 5.1. It is assumed that the stiffness of each lamination only varies in longitudinal direction (along the x-axis).

The mechanical behaviour of GLT beams is mainly determined by the combined load transfer of laminations. It is influenced by varying properties due to knots or global strain deviation and the natural variability of wood. The main challenge in their mechanical description is to determine the influence of this variability on the variability of the resulting effective properties. The involved effects are commonly summarized under the term "laminating effects" .

Research on the mechanical behaviour of glued-laminated timber has mainly been performed experimentally so far. In general, comprehensive test series were carried out and the results analysed statistically in order to identify the relation between the distribution of mechanical properties of the laminations and corresponding characteristics of GLT beams (see [5] and references therein). Following this approach, no separation of mechanical and stochastic effects is possible. Moreover, the derived relations are only valid for an investigated sample and the specific testing conditions must be taken into account. This limits the comparability of results and universality of the derived relations.

In order to obtain enhanced insight, the experimental approaches were complemented

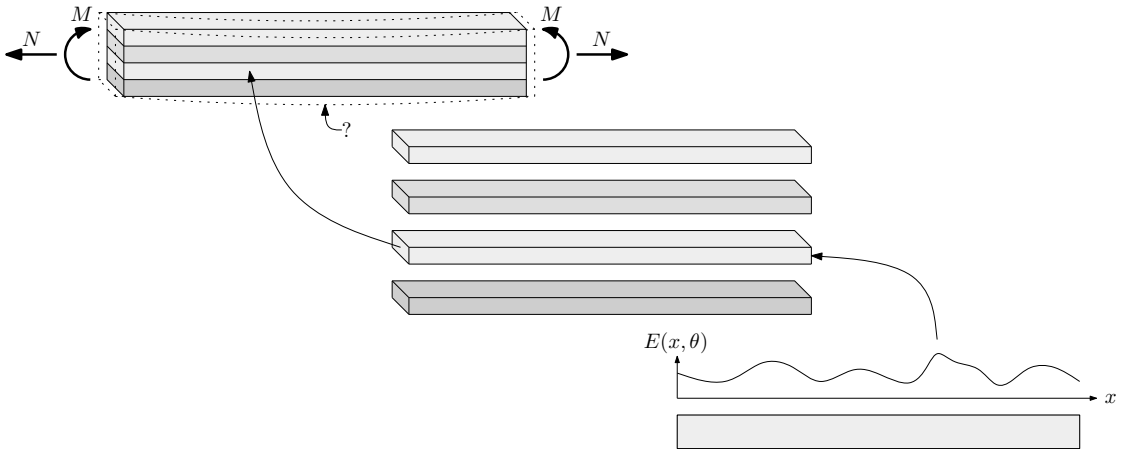

Figure 5.1: Illustration of the stiffness variation within a GLT beam.

by analytical or numerical investigations. The former are mainly based on application of stochastic concepts to mixed parallel-serial systems (e.g. [21], [12], [4, 5]). Numerical approaches mostly use the finite element method to study the internal load transfer within GLT beams. The most elaborate model in this context is the KAREM model, which was developed at TU Karlsruhe [14], where a simulation program mimics the grading process and derives statistical distribution functions of mass densities and knots in the laminations and corresponding mechanical properties. These data serve as input for a MCS simulation, which is coupled with a two-dimensional finite element program. Similar approaches were proposed by [20] and [35]. A summary can be found in [36]. However, the high computational effort of these stochastic schemes is a serious drawback. Extending the SSFEM, [8] developed a model for laminated composite plates, which is adapted for the application to GLT beams in this thesis.

5.2 Applied methods

Since the mean value and the covariance of the system response are of particular interest, methods capable of efficiently obtaining the second moments are considered. A literature study (e.g. [29], [37], [34]) has revealed the Perturbation method (for its high efficiency), the Spectral stochastic Finite-element method (for its unified framework and its versatility regarding the computation effort), and the Monte Carlo simulation as the most promising ones in this context. The MCS is also applied for comparison purposes, since it is the least complex and most investigated approach.

Regarding the random field representation, the Karhunen-Loève expansion is applied, which can be coupled with MCS as well as SSFEM. Furthermore, from a data acquisition point of view, each lamination is divided into sections with constant stiffness according to the grading method (e.g. by means of knothole clusters). Obviously, the midpoint method seems most suitable for this kind of purpose. Furthermore, the midpoint method and the Karhunen-Loève expansion describe upper and lower bounds of the variability representation of random fields. Thus, the true solution can be expected to lie within those bounds. To sum up, the following methods are applied:

- The **direct Monte Carlo simulation** (MCS) using the **midpoint method** (MP), as well as the **Karhunen-Loève expansion** (KL) for the discretization of the random field,
- the **Perturbation method** (PERT) with the MP method for the random field discretization, and
- the **spectral stochastic finite element method** (SSFEM) with the KL expansion and the Polynomial Chaos (PC) expansion to represent the input and the response random field, respectively.

All methods, including the underlying finite element code, are implemented in MATLAB. The GLT beam is discretized using two-dimensional 4-node finite elements with bilinear interpolation functions, and isotropic material behaviour is assigned.

In the following, after the input parameters are specified, the FE code is verified by a deterministic calculation, where the results are compared to the analytical solution (Section 5.4). Then, in Section 5.5 the application of the SFEM is discussed in detail considering a single lamination. Afterwards, an extension to multiple laminations (GLT beams) is carried out and results are presented for up to four laminations (Section 5.6). Finally, to gain understanding of how the statistical input parameters influence the resulting effective modulus of elasticity E_{eff}, a parameter study where the number of laminations and the probabilistic parameters are varied (according to Tables 5.1 and 5.2) is proposed in Section 5.7.

5.3 Input parameters

The elastic modulus E is assumed random, whereas Poisson's ratio ν, geometry (L_x, L_y, L_z), and loading (F_x, F_y) are deterministic values, see Table 5.1. Further, the spatial variability is represented using the exponential correlation function (see Eq. 2.59):

$$\rho_{ij} = \exp\left(-\frac{|x_j - x_i|}{l_x}\right). \tag{5.1}$$

Multiplied by σ_E^2 it yields the covariance function

$$C_{ij} = \rho_{ij}\sigma_E^2, \tag{5.2}$$

which is illustrated in Figure 5.2. The mean value μ_E and coefficient of variation (COV) δ_E are given in Table 5.2.

5.4 Deterministic investigation of one lamination

At first, to verify the underlying FE-code one lamination is analysed, where the elasticity modulus E is set to $1100\,\text{kN/cm}^2$ as deterministic input. The static system and the finite element discretization are illustrated in Figures 5.3 and 5.4, respectively. The resulting displacement u_x at node 146 (located at the rightmost border of the structure) is 0.272 cm, which is equal to the analytical solution, reading

$$u_x \equiv \Delta l = \frac{F_x L_x}{\mu_E A} = \frac{30 \cdot 400}{1100 \cdot 40} = 0.272\,\text{cm}, \tag{5.3}$$

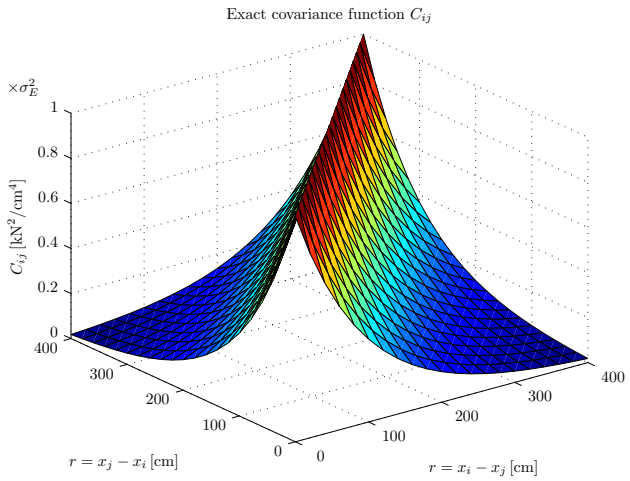

Figure 5.2: Illustration of the exponential covariance function C_{ij} with $l_x = 100\,\text{cm}$.

Table 5.1: Deterministic properties of GLT beam model

Number of laminations	1	2	3	4
Length L_x [cm]	400			
Height L_y [cm]	4	8	12	16
Width L_z [cm]	10			
Loading F_x [kN]	30	60	90	120
Boundary Conditions acc. to	Fig. 5.4			
Poisson's ratio ν [-]	0.03			

Table 5.2: Properties of the random field representing the elastic modulus E

exp. correlation ρ_{ij} [-]	$= \exp\left(-\left\lvert\frac{x_i - x_j}{l_x}\right\rvert\right)$			
mean μ_E [kN/cm^2]	1100			
Varied parameters:				
COV δ_E [-]	0.1	0.15	0.20	0.25
standard deviation σ_E [kN/cm^2]	110	165	220	275
correlation length l_x [cm]	100	200	400	

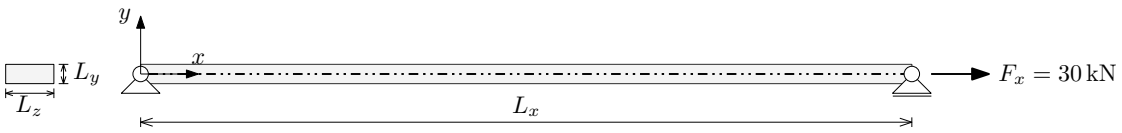

Figure 5.3: Illustration of the static system of one lamination.

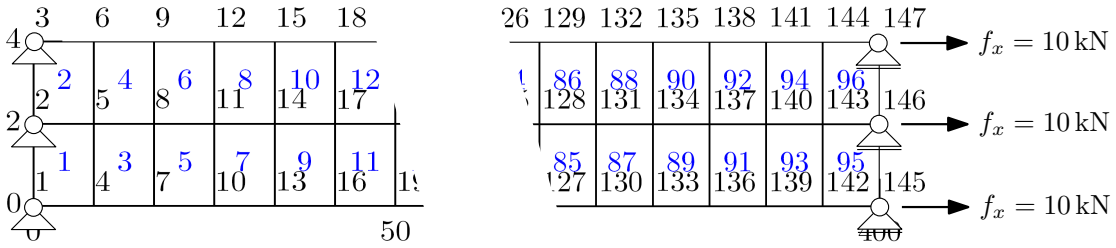

Figure 5.4: Finite element discretization of one lamination.

where $A = L_y L_z = 40\,\mathrm{cm}^2$.

5.5 Probabilistic investigation of one lamination

Assuming that the elastic modulus is varying only along the x-axis, the random field reduces to one dimension and, thus, may be called a random process. In the following, the procedure and results for one lamination are presented. The coefficient of variation of the elastic modulus is specified with $\delta_E = 0.1$ and the correlation length with $l_x = 100\,\mathrm{cm}$.

5.5.1 Midpoint discretization of the random field

First, the random field is discretized using the MP method for the implementation in the PERT approach. To investigate the accuracy of the PERT estimation, the MP method is also applied in combination with the MCS. To correctly depict the fluctuations of the approximated random field, the random field element size in x-direction $s_x^{(e)}$ is derived according to the following criterion [29]:

$$s_x^{(e)} \leq \frac{1}{2} l_x. \tag{5.4}$$

For a correlation length l_x of 100 cm (which is the smallest value for l_x considered in this thesis), Eq. (5.4) yields a maximum random field element size $s_x^{(e)}$ of 50 cm. Since for further research an investigation of correlation lengths smaller than 100 cm could be of interest, 25 cm are chosen as the random field element size, so that comparison with future results is straightforward.

To every finite element the probabilistic quantities of the corresponding random field element are assigned . Each realization of the elastic modulus E is piecewise constant, thus, the element stiffness matrix reads

$$\mathbf{k}^{(e)} = \bar{\mathbf{k}}^{(e)} + \boldsymbol{\Delta}\mathbf{k}^{(e)} \tag{5.5}$$

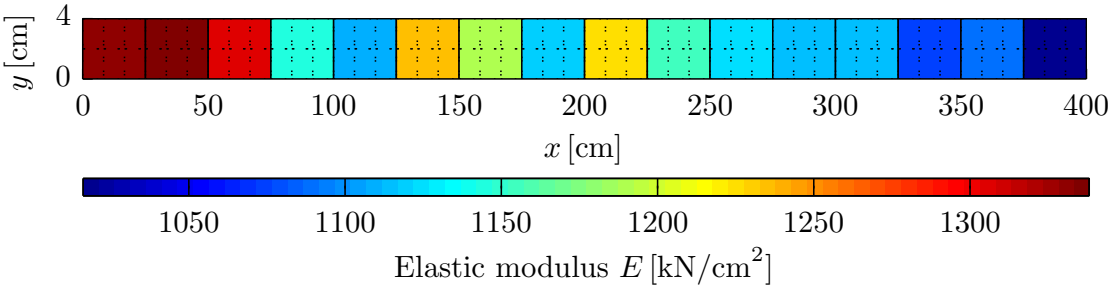

Figure 5.5: One realization of the random field using the MP method with $\delta_E = 0.1$ and $l_x = 100$. The solid and dotted lines depict the random field discretization and the deterministic finite element discretization, respectively.

with

$$\bar{\mathbf{k}}^{(e)} = \mu_E \int_{V_e} \mathbf{B}^\mathsf{T}\mathbf{D}_0\mathbf{B}\mathrm{d}V \quad \text{and} \quad \boldsymbol{\Delta}\mathbf{k}^{(e)} = \hat{E}(\mathbf{x}, \boldsymbol{\chi}) \int_{V_e} \mathbf{B}^\mathsf{T}\mathbf{D}_0\mathbf{B}\mathrm{d}V, \tag{5.6}$$

where

$$\mathbf{D}_0 = \frac{1}{1-\nu^2}\begin{bmatrix} 1 & \nu & 0 \\ \nu & 1 & 0 \\ 0 & 0 & \frac{1-\nu}{2} \end{bmatrix}. \tag{5.7}$$

$\hat{E}(\mathbf{x}, \boldsymbol{\chi})$ denotes the discretized zero-mean random field, obtained with the MP method. As shown in Subsection 3.1.1, it represents the random field by means of a random vector $\boldsymbol{\chi}$, thus

$$\boldsymbol{\Delta}\mathbf{k}^{(e)} = \boldsymbol{\chi} \int_{V_e} \mathbf{B}^\mathsf{T}\mathbf{D}_0\mathbf{B}\mathrm{d}V. \tag{5.8}$$

In Figure 5.5, one realization of the random field is shown. The solid and dotted lines depict the random field elements and the finite elements, respectively. The corresponding covariance matrix $\mathbf{C}_{ij} \equiv \mathbf{C}_{\chi\chi}$, obtained according to Equation (3.8), is illustrated in Figure 5.6.

5.5.2 Karhunen-Loève expansion of the random field

For the SSFEM the random field is discretized using the Karhunen-Loève expansion. In addition, to evaluate the accuracy of the SSFEM, the KL-expansion will be used in combination with the MCS. In [18] two transcendental equations for the case of the exponential correlation kernel ρ_{ij} and rectangular domain are given

$$\frac{1}{l_x} - \omega_i \tan(\omega_i a) = 0, \quad \text{and} \quad \omega_i^* + \frac{1}{l_x}\tan(\omega_i^* a) = 0, \tag{5.9}$$

where $a = L_x/2$. The i-th solutions ω_i and ω_i^* lead to the corresponding Eigenvalues λ_i and λ_i^*, reading

$$\lambda_i = \frac{2l_x}{1+\omega_i^2 l_x^2} \quad \text{and} \quad \lambda_i^* = \frac{2l_x}{1+(\omega_i^*)^2 l_x^2}. \tag{5.10}$$

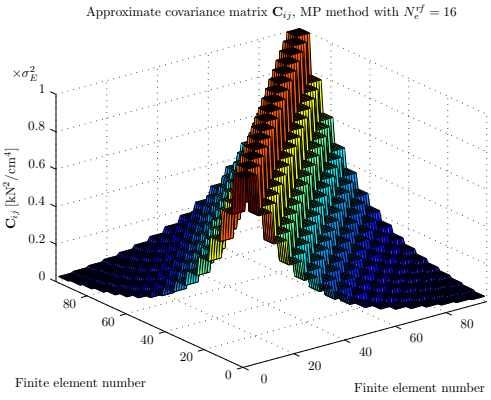

Figure 5.6: Covariance matrix $\mathbf{C}_{ij} \equiv \mathbf{C}_{\chi\chi}$ for the discretized random field (16 random field elements and 96 finite elements).

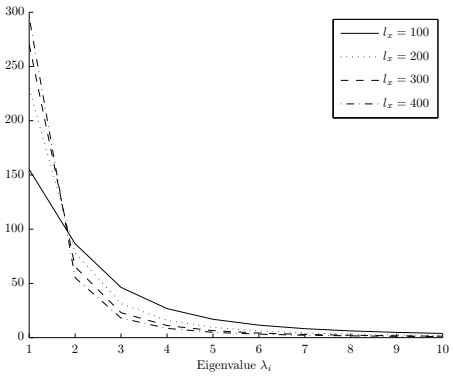

Figure 5.7: Illustration of the first 10 Eigenvalues λ_i of the random field, represented by the KL expansion.

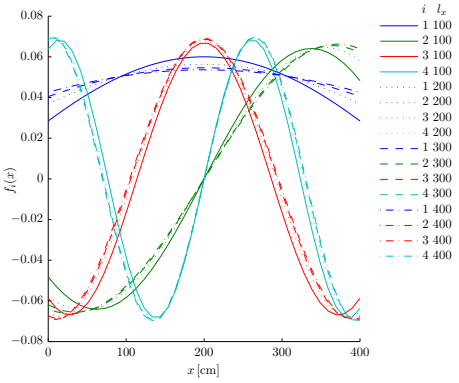

Figure 5.8: First 4 Eigenfunctions $f_i(x)$ of the random field represented by a KL expansion, for different correlation lengths l_x.

The corresponding Eigenfunctions f_i and f_i^* are

$$f_i(x) = \cos(\omega_i x)\left(a + \frac{\sin(2\omega_i a)}{2\omega_i}\right)^{-\frac{1}{2}} \quad \text{and} \quad f_i^*(x) = \sin(\omega_i^* x)\left(a - \frac{\sin(2\omega_i^* a)}{2\omega_i^*}\right)^{-\frac{1}{2}}. \tag{5.11}$$

As it can be seen in Figure 5.7, the Eigenvalues λ_i decay faster with increasing correlation length l_x. Therefore, with increasing l_x, the first few random variables become more important (see Eq. (3.38)), and thus, the KL-expansion represents the random field more accurately for a certain number of terms in the series expansion. Figure 5.8 illustrates the first four eigenfunctions of the random field for various correlation lengths l_x. It can be seen, that a change in correlation length l_x does not have great impact on the eigenfunctions.

The element stiffness matrix is computed according to Equation (4.55), where the

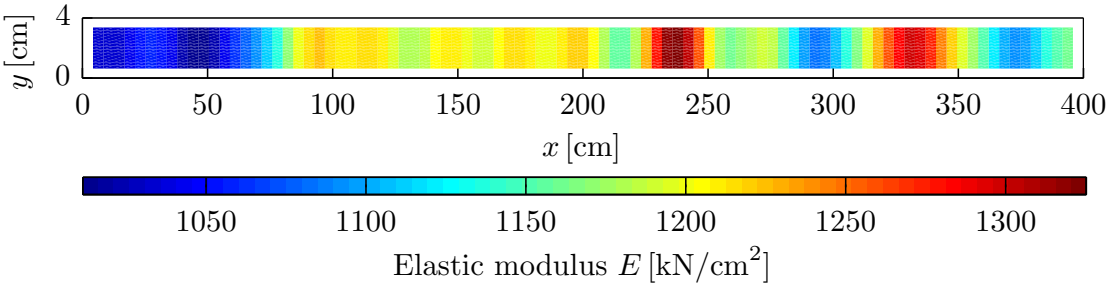

Figure 5.9: One realization of the random field using the KL expansion with $\delta_E = 0.1$ and $l_x = 100\,\text{cm}$.

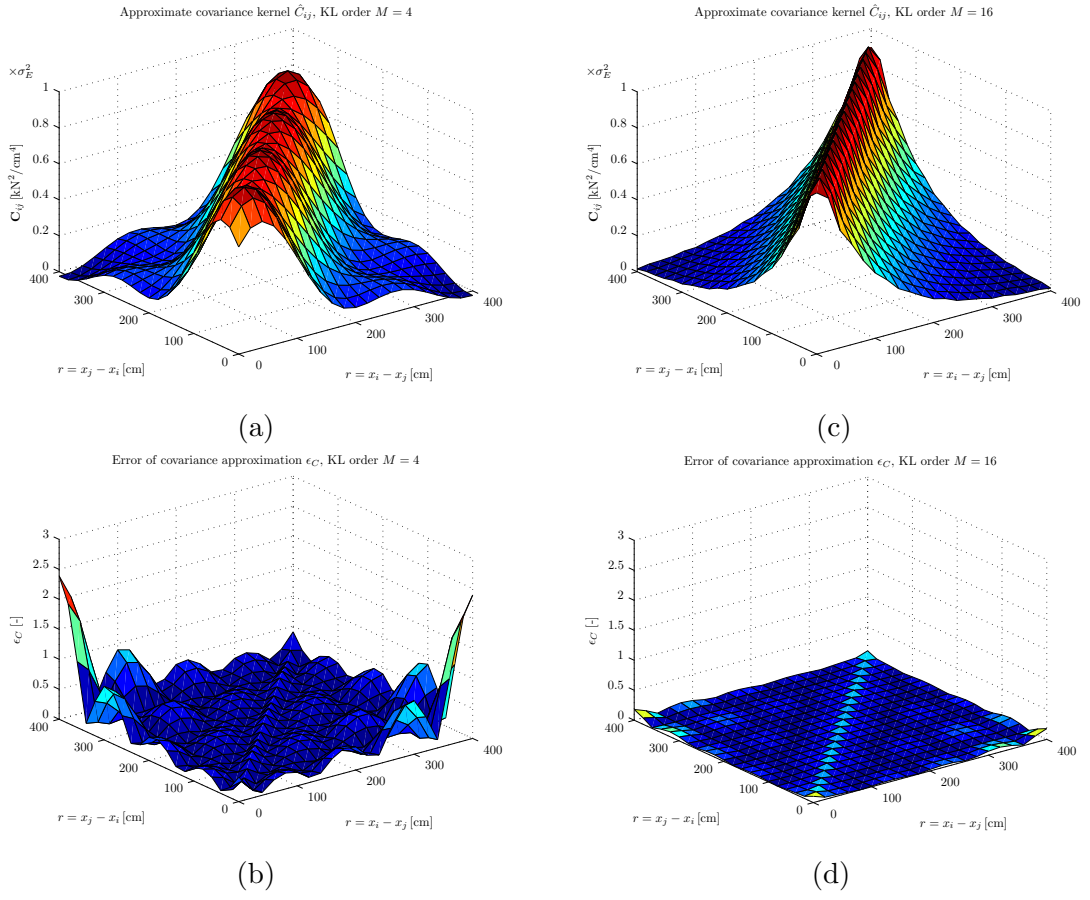

Figure 5.10: Illustration of the (a) 4-th and (c) 16-th order approximation of the covariance kernel C_{ij} and the corresponding approximation error (b) and (d), respectively.

first term $\mathbf{k}_0^{(e)}$ is equivalent to the first term $\bar{\mathbf{k}}^{(e)}$ in (5.6) and $\mathbf{k}_i^{(e)}$ is obtained from Equation (4.54). Using a four-point Gaussian integration scheme, where the eigenfunctions are evaluated directly at the Gauss integration points, yields the solution of the integral in (4.54). After assemblation of the global stiffness matrix as described in Section 4.6, each realization can be generated according to Equation (4.55), where χ_i are independent standard normal random variables. In Figure 5.9, one realization of the random field is illustrated. Since the dimension of the stochastic global stiffness matrix increases drastically with the number of terms considered in the KL expansion, the series is truncated after $M = 4$ terms. On the contrary, the computational effort of the MCS is insensible to the number of terms considered in the KL expansion. Therefore, for the MCS method the KL series is truncated after $M = 16$ terms. In Figure 5.10, the 4-th and 16-th order approximated covariance $\hat{C}_{ij}$ (according to (3.35)) are illustrated. In addition, the approximation error compared to the exact covariance function C_{ij} is shown. Obviously, the 16-th order expansion seems by far more accurate than the 4-th order expansion.

The MP method and the KL-expansion method require the generation of $m \cdot N_e^{rf}$ and $m \cdot M$ random numbers, respectively. In our case, the number of random variables was chosen to be equal, giving $N_e^{rf} = M = 16$. The Gaussian random numbers for the MP method are produced my a random number generator using the covariance matrix $\mathbf{C}_{ij}$ illustrated in Figure 5.6, whereas the Karhunen-Loève expansion is based on independent standard normal Gaussian distributed random numbers. Using a random number generator, 10000 samples of the random vector $\boldsymbol{\chi}$ (with zero mean) are produced. Each sample k is denoted by $\boldsymbol{\chi}^{(k)}$ with $k = 1, \dots m$.

The PERT method is based on the Taylor-series expansion of the stiffness matrix. Since in this thesis, it is coupled with the MP discretization, $\mathbf{K}$ is derived with respect to the random variables $\chi_i, i = 1, \dots N_e^{rf}$, representing the random field elements. For the mean value, the second order solution μ^{II} is given. The covariance is computed using the first order Taylor-series approximation.

The SSFEM is applied using a 4-th order ($M = 4$) KL-expansion of the random field $E(\mathbf{x}, \theta)$ coupled with a 3-rd order ($N = 3$) Polynomial Chaos (PC) expansion of the displacements $\mathbf{u}$, resulting in a series expansion with a total number of 35 basis polynomials, which are computed using an algorithm proposed in [39].

5.5.3 Results

In Figure 5.11 the displacement of the rightmost part of the lamella is shown. In the following, the results are compared by means of the displacement u_x in x-direction of node 146, which is the rightmost node at height $L_y/2$, see Figure 5.4.

First, in order to compare the MP method to the KL expansion, the results of the MCS are presented in numerical form in Table 5.3 for $100, 1000$, and 10000 samples, and in graphical form in Figure 5.12. After 10000 samples, the results for μ and σ of the MP method and KL expansion are almost identical, therefore both representation techniques can be assumed to appropriately describe the present input random field. It should be noted, that the convergence of the MCS results is stronlgy influenced by the input coefficient of variation. In the present case, with $\delta_E = 0.1$, a reasonable accuracy is achieved after approximately 1000 samples.

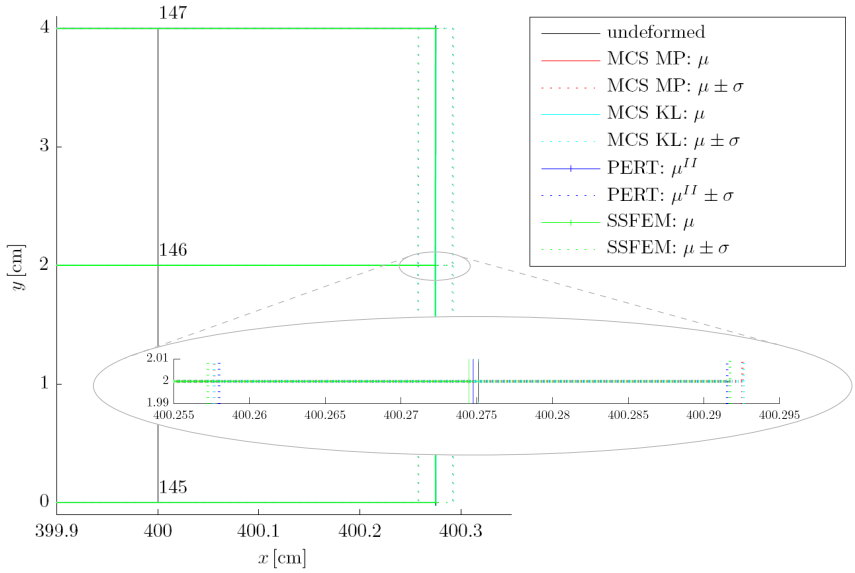

Figure 5.11: Illustration of the displacements of the rightmost border of the lamella (nodes 145-147).

Table 5.3: MCS results for the displacement u_x^{146} of node 146 with $N_e^{rf} = M = 16$.

	MP method			KL-expansion		
samples m	100	1000	10000	100	1000	10000
μ [cm]	0.2745	0.2749	0.2751	0.2731	0.2753	0.2751
σ [cm]	0.0196	0.0178	0.0174	0.0180	0.0173	0.0175
δ [-]	0.0715	0.0638	0.0634	0.0659	0.0638	0.0636

As mentioned in Subsections 3.1.1 and 3.3.2, respectively, the MP method tends to over-represent, whereas the KL expansion always under-represents the variability of a random field. Hence, the results of these two methods represent give lower and upper bounds of the true random field, and as they converge, the "real" solution can be narrowed well.

The results of PERT and SSFEM are compared with those of MCS in Table 5.4 and in Figure 5.12, respectively. It can be seen, that the mean value μ^{II} obtained with PERT agrees well with the corresponding result of MCS (MP). The relative error of the standard deviation σ is less than 4%. SSFEM provides results for both the mean value μ and standard deviation σ, which are very close to those of MCS (KL). The relative error between SSFEM results and MCS (KL) results is less than 1.5%. The computed covariance matrix $\mathbf{C}_{uu}$ for the displacements is displayed in Figures 5.13 and 5.14, respectively. Comparison with the MCS shows, that the covariances obtained with the PERT method and the SSFEM are accurate for all nodes.

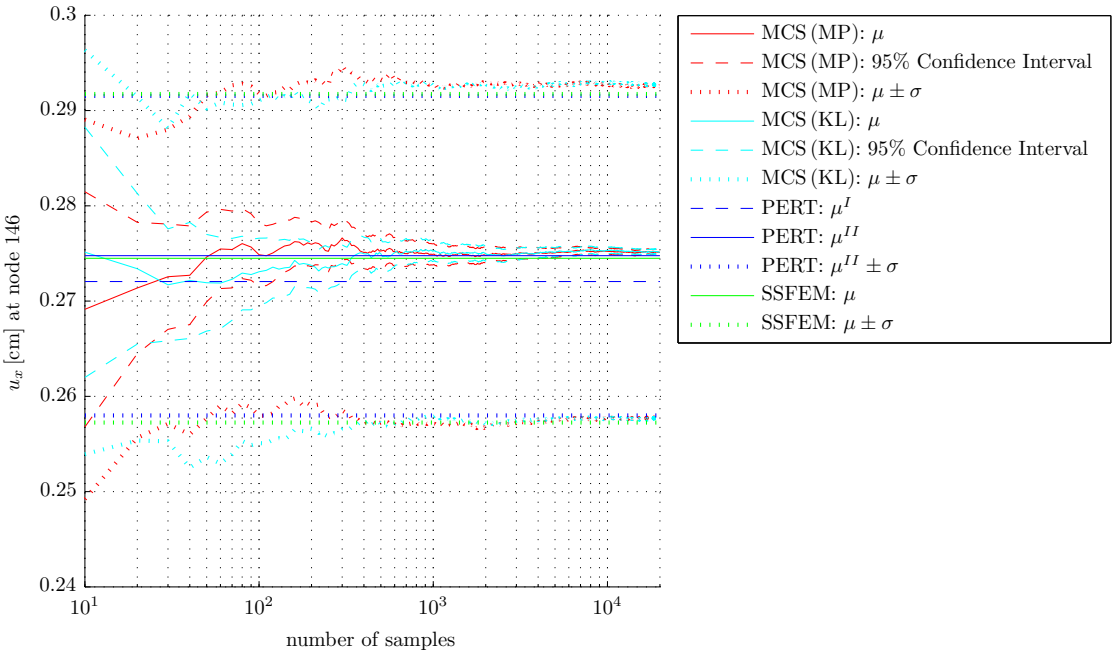

Figure 5.12: Convergence behaviour of different SFE methods, shown by means of the displacement u_x^{146} as a function of considered samples (realizations).

Table 5.4: Comparison of mean and standard deviation of displacement u_x^{146} obtained with: MCS (MP, $N_e^{rf} = 16$, 10000 samples) and MCS (KL, $M = 16$, 10000 samples), PERT (MP, $N_e^{rf} = 16$) and SSFEM (KL order $M = 4$ and PC order $N = 3$). Error relative to MCS values.

	MP method			KL-expansion		
	MCS	PERT	ϵ_{PERT}	MCS	SSFEM	ϵ_{SSFEM}
μ [cm]	0.2751	0.2748	0.0013	0.2751	0.2745	0.0023
σ [cm]	0.0174	0.0168	0.0383	0.0175	0.0172	0.0141
δ [-]	0.0634	0.0610	0.0371	0.0636	0.0628	0.0118

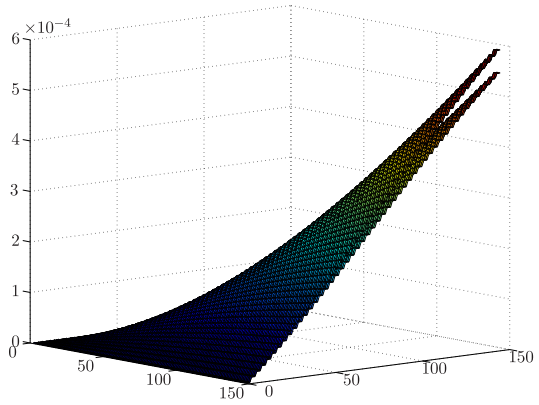

Figure 5.13: Illustration of the covariance matrix $\mathbf{C}_{uu}$ for displacements $\mathbf{u}_x = [u_1, \dots u_{147}]^\mathsf{T}$ obtained with MCS (MP) and PERT.

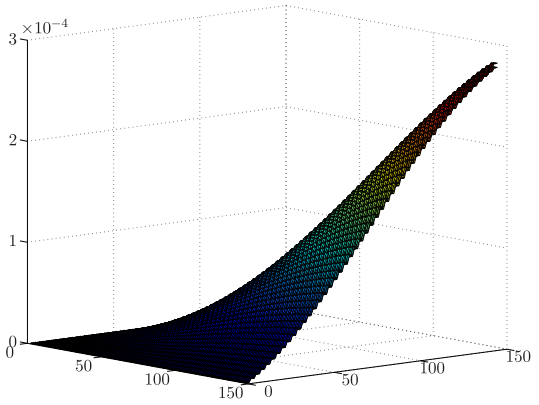

Figure 5.14: Illustration of the covariance matrix $\mathbf{C}_{uu}$ for displacements $\mathbf{u}_x = [u_1, \dots u_{147}]^\mathsf{T}$ obtained with MCS (KL) and SSFEM.

In summary, all methods correspond surprisingly well. Both the PERT and SSFEM method provide reasonably accurate results for one lamination. However, the accuracy of the SSFEM result is particularly interesting, considering that the random field discretization for MCS (KL) is carried out using a $M = 16$-th order expansion, in contrast to the KL expansion for SSFEM, which is already truncated after $M = 4$ terms. Thus, the seemingly rough approximation of the correlation kernel, shown in Figure 5.10, is of no significant consequence.

5.6 Probabilistic investigation of GLT beams

The GLT-beam is subjected to a tensile force in axial direction in such a way, that the tension stresses are equal for all configurations, see Table 5.1. As it can be seen in Figure 5.15, each lamination is discretized using two layers of finite elements. The boundary conditions are specified in analogy to the single lamella (see Figure 5.4).

5.6.1 Midpoint discretization of the random field

The extension of the midpoint method for multiple laminations is straightforward. Each lamination is represented by a row of random field elements. Since the random field is now two-dimensional, in theory, a two-dimensional correlation function ρ_{ij} is required. However, considering the structure and production process of GLT beams, the laminations can be assumed as mutually independent. Thus, there is no correlation in y-direction, and the one-dimensional exponential correlation function given in Eq. (5.1) remains valid.

5.6.2 Karhunen-Loève expansion of the random field

In [8], the extension of the KL-expansion method to multiple laminations is introduced. The basic idea is to assemble the stiffness matrix for each lamination m according to

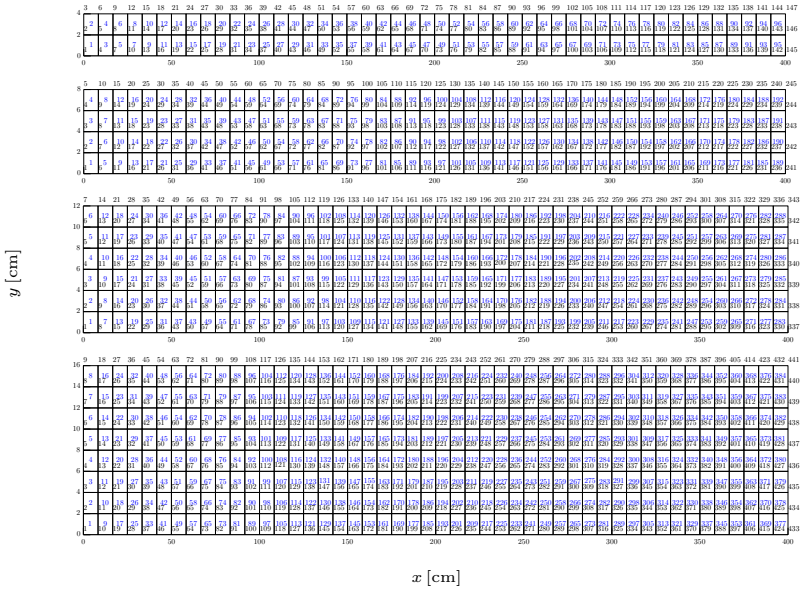

Figure 5.15: Illustration of the deterministic FE discretization for $1, 2, 3$, and 4 laminations. Each lamination is discretized with two elements in thickness direction. Blue and black numbers denote the element and the node numbers, respectively.

Subsection 5.5.2:

$$\mathbf{K}_m = \mathbf{K}_m^0 + \sum_{i=1}^{M} \chi_{mi}(\theta)\mathbf{K}_{mi} \quad \text{with} \quad m = 1, \dots NL, \tag{5.12}$$

where NL denotes the total number of laminations, and M is the number of terms retained in the KL-expansion. The global stiffness matrix of the compound structure is then given by

$$\begin{aligned} \mathbf{K} = \sum_{m=1}^{NL} \mathbf{K}_m &= \sum_{m=1}^{NL} \left(\mathbf{K}_m^0 + \sum_{i=1}^{M} \chi_{mi}(\theta)\mathbf{K}_{mi} \right) \\ &= \sum_{m=1}^{NL} \mathbf{K}_m^0 + \sum_{m=1}^{NL} \sum_{i=1}^{M} \chi_{mi}(\theta)\mathbf{K}_{mi}. \end{aligned} \tag{5.13}$$

With $j = (m-1) \cdot NL + i$ the second term can be rewritten such that

$$\mathbf{K} = \underbrace{\sum_{m=1}^{NL} \mathbf{K}_m^0}_{\mathbf{K}_0} + \sum_{j=1}^{NL \cdot M} \chi_j(\theta)\mathbf{K}_j. \tag{5.14}$$

Equation (5.14) has the same form as (4.55), thus, the following proceedings are similar to those shown in Subsection 4.6.2.

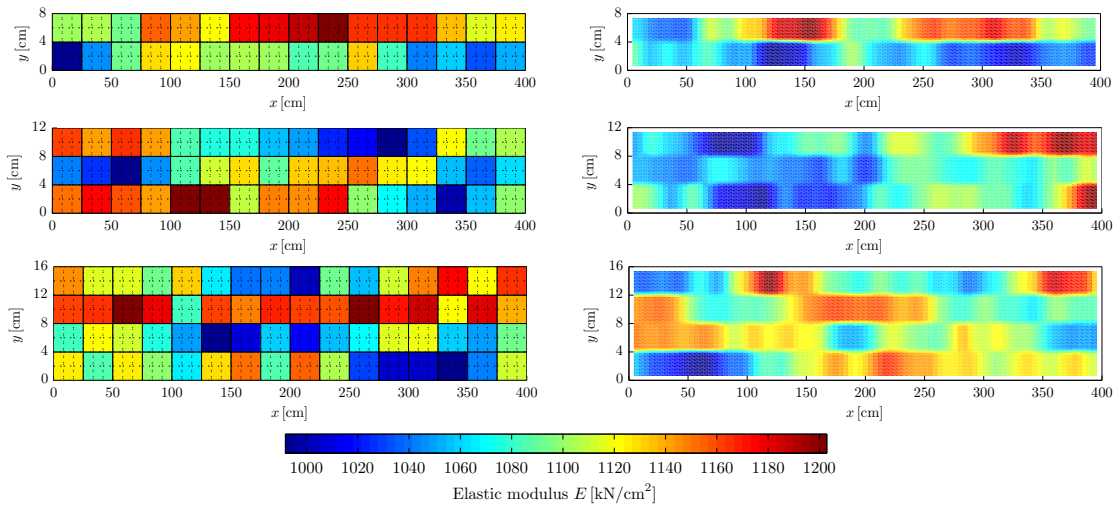

Figure 5.16: Realizations of GLT beam with $2, 3$, and 4 laminations, using MP-discretization (left-hand side) with $N_e^{rf} = 16$ for each lamination and KL-expansion (right-hand side) of order $M = 16$, COV $\delta_E = 0.1$ and $l_x = 100$.

5.6.3 Results

Figure 5.16 shows realizations of the discretized random fields of the MP and KL method. It can be seen that the KL expansion provides continuous realizations, whereas the MP method is piecewise constant, and furthermore, that for both methods the elasticity modulus is correlated only within each lamination.

The resulting displacement u_x of the rightmost node halfway up for 1 to 4 laminations is given in Table 5.5. Both MCS approaches and the PERT method provide similar results for multiple laminations. Regarding the PERT method, the maximum error for the mean value and the COV is approximately 0.1 % and 5 %, respectively. The maximal difference between MCS (MP) and the PERT method appears for one lamination. On the contrary, the SSFEM provides accurate results for one lamination, but for multiple laminations a large difference is obtained compared to the corresponding MCS (KL) results, which can not be explained by the author at this moment.

Summarizing, the mean value μ_u shows no significant difference for different numbers of laminations. In contrast, it can be seen that, as a consequence of the lamination effect, δ_u decreases with increasing number of laminations, which is explained further in Subsection 5.7.2.

In Table 5.6, the computational effort of each method is shown. Using MCS, the computation time is directly related to the number of samples m [30], whereas the computational effort of the Perturbation approach strongly depends on the number of random variables (i.e. the stochastic dimensionality). The computational cost of the SSFEM is mainly influenced by the KL- and PC-expansion order. Since the KL-expansion contains random variables, the SSFEM is strongly influenced by the stochastic dimensionality, too.

Table 5.5: Comparison of mean value and standard deviation of the displacement u_x of the rightmost border, obtained with: MCS (MP, $N_e^{rf} = 16$, 20000 samples) and MCS (KL, $M = 16$, 10000 samples), PERT (MP, $N_e^{rf} = 16$), and SSFEM (KL order $M = 4$ and PC order $N = 2$). Error relative to MCS values.

		MP method			KL-expansion		
Laminations		MCS	PERT	ϵ_{PERT}	MCS	SSFEM	ϵ_{SSFEM}
1 (node 146)	μ [cm]	0.2751	0.2748	0.0013	0.2751	0.2745	0.0023
	σ [cm]	0.0174	0.0168	0.0383	0.0175	0.0172	0.0141
	δ [-]	0.0634	0.0610	0.0371	0.0636	0.0628	0.0118
2 (node 243)	μ [cm]	0.2735	0.2733	0.0007	0.2735	0.2744	0.0034
	σ [cm]	0.0122	0.0119	0.0244	0.0119	0.0172	0.4471
	δ [-]	0.0444	0.0434	0.0237	0.0435	0.0628	0.4422
3 (node 340)	μ [cm]	0.2732	0.2729	0.0011	0.2731	0.2743	0.0046
	σ [cm]	0.0098	0.0097	0.0120	0.0097	0.0172	0.7710
	δ [-]	0.0359	0.0355	0.0109	0.0356	0.0628	0.7628
4 (node 437)	μ [cm]	0.2729	0.2726	0.0009	0.2728	0.2743	0.0054
	σ [cm]	0.0085	0.0084	0.0187	0.0084	0.0172	1.0550
	δ [-]	0.0313	0.0307	0.0178	0.0307	0.0628	1.0440

Table 5.6: Problem dimension and computational effort of considered SFE methods. For all GLT-beams each lamination is represented using KL order $M = 4$ or $N_e^{rf} = 16$ random field elements (MP). Note that the global stochastic stiffness matrix for SSFEM is sparse and, in spite of its dimensions, easily handled when using a suitable solution algorithm.

Lam.	size($\mathbf{K}_{\text{det.}}$)	number of terms			size($\mathbf{K}_{\text{stoch.}}$)		
		MP	KL	PC	MCS	PERT	SSFEM
1	$[294 \times 294]$	16	4	2	size($\mathbf{K}_{\text{det.}}$)	size($\mathbf{K}_{\text{det.}}$)	$[4410 \times 4410]$
2	$[490 \times 490]$	32	8	2			$[22050 \times 22050]$
3	$[686 \times 686]$	48	12	2			$[62426 \times 62426]$
4	$[882 \times 882]$	64	16	2			$[134946 \times 134946]$
number of solutions of $\mathbf{Ku} = \mathbf{f}$					10000	1	-
further computations					-	$\frac{\partial \mathbf{K}}{\partial \chi}, \frac{\partial^2 \mathbf{K}}{\partial \chi \partial \chi}$	$\mathcal{K}\mathcal{U} = \mathcal{F}$

5.7 Parameter studies

In this section, the structural sensitivity with respect to material variability and, furthermore, the application limits of the different methods are investigated. Therefore, the influence of the coefficient of variation and the correlation length of the raw material on the structural response is determined. These parameters are varied in the range of $\delta_E = \{0.10, 0.15, 0.20, 0.25\}$ and $l_x = \{100, 200, 400\}$, as specified in Table 5.2. Furthermore, the number of laminations is varied from 1 to 4 (see Table 5.1).

The deterministic Finite element discretization is chosen with 48 and 2 subdivisions in horizontal and vertical direction, respectively. Using midpoint discretization, each lamination is represented by $N_e^{rf} = 16$ random field elements in longitudinal direction. The KL-expansion is truncated after 16 terms. Therefore, both discretization methods are based on a series expansion using 16 random variables per lamination.

The MCS (MP) and MCS (KL) results are based on 20000 samples, and can therefore be seen as reliable reference for comparison. For values $\delta_E \geq 0.25$, some realizations give negative values for the elastic modulus E. In order to circumvent numerical issues, those samples are replaced by new realizations with $E > 0$. The PERT results are the second order mean value μ^{II} and first order standard deviation σ^{I}, according to Equations (4.49) and (4.48). The SSFEM results are obtained with KL expansion order $M = 4$ for each random field and a Polynomial Chaos expansion order of $N = 2$.

5.7.1 Effective elastic modulus

For practical purposes, the so called effective elastic modulus E_{eff}, defined as

$$E_{\mathrm{eff}} = \frac{N}{A}\frac{l}{\Delta l}, \tag{5.15}$$

is of particular interest, since it describes the "overall" stiffness of the GLT beam, which may be used for classification in grading industry. However, the computation of E_{eff} is based on the displacements obtained with SFEM. Thus, in the following, the Taylor series expansion is applied to approximate the moments of a function

$$Y = f(X), \tag{5.16}$$

where X denotes one random variable. Basically, this approach is the univariate case of the perturbation approach, presented in Section 4.5.3. Considering Equation (4.49), the first and second order mean value of the displacement read

$$\hat{\mu}_Y^{\mathrm{I}} = f(\mu_X) \tag{5.17}$$

and

$$\hat{\mu}_Y^{\mathrm{II}} = f(\mu_X) + \frac{1}{2} f''(x)\big|_{x=\mu_X} \sigma_X^2, \tag{5.18}$$

respectively. In analogy to (4.48), the variance is approximated by

$$\hat{\sigma}_Y^2 = \left(f'(x)\big|_{x=\mu_X} \right)^2 \sigma_X^2. \tag{5.19}$$

As it can be seen, f needs to be differentiable and the moments of X are required to be finite. In Equation (5.15), let $\Delta l = u_x$, length $l = L_x$, longitudinal force $N = F_x$, and cross section area $A = L_y L_z$, as listed in Table 5.1, then the problem at hand is described by

$$u_x = f(E_{\text{eff}}) = \underbrace{\frac{F_x L_x}{L_y L_z}}_{c} \frac{1}{E_{\text{eff}}}, \tag{5.20}$$

with the random variable E_{eff} determined by mean value $\mu_{E_{\text{eff}}}$ and variance $\sigma^2_{E_{\text{eff}}}$. Substituting Equation (5.20) into (5.18) and (5.19) yields the mean value

$$\begin{aligned} \hat{\mu}^{\text{II}}_{u_x} &= f(\mu_{E_{\text{eff}}}) + \frac{1}{2} f''(\mu_{E_{\text{eff}}}) \sigma^2_{E_{\text{eff}}} \\ &= \frac{c}{\mu_{E_{\text{eff}}}} + \frac{1}{2} \left(\frac{2c}{\mu^3_{E_{\text{eff}}}} \right) \sigma^2_{E_{\text{eff}}} \\ &= \left(\frac{1}{\mu_{E_{\text{eff}}}} + \frac{\sigma^2_{E_{\text{eff}}}}{\mu^3_{E_{\text{eff}}}} \right) c \end{aligned} \tag{5.21}$$

and the variance

$$\begin{aligned} \hat{\sigma}^2_{u_x} &= \left(f'(\mu_{E_{\text{eff}}}) \right)^2 \sigma^2_{E_{\text{eff}}} \\ &= \left(-\frac{c}{\mu^2_{E_{\text{eff}}}} \right)^2 \sigma^2_{E_{\text{eff}}} \\ &= \frac{c^2}{\mu^4_{E_{\text{eff}}}} \sigma^2_{E_{\text{eff}}}, \end{aligned} \tag{5.22}$$

where

$$c = \frac{F_x L_x}{L_y L_z}. \tag{5.23}$$

In analogy, the mean and variance of the effective elastic modulus

$$E_{\text{eff}} = f(u_x) = c \frac{1}{u_x} \tag{5.24}$$

are computed as

$$\hat{\mu}_{E_{\text{eff}}} = \left(\frac{1}{\mu_{u_x}} + \frac{\sigma^2_{u_x}}{\mu^3_{u_x}} \right) c \tag{5.25}$$

and

$$\hat{\sigma}^2_{E_{\text{eff}}} = \frac{c^2}{\mu^4_{u_x}} \sigma^2_{u_x}. \tag{5.26}$$

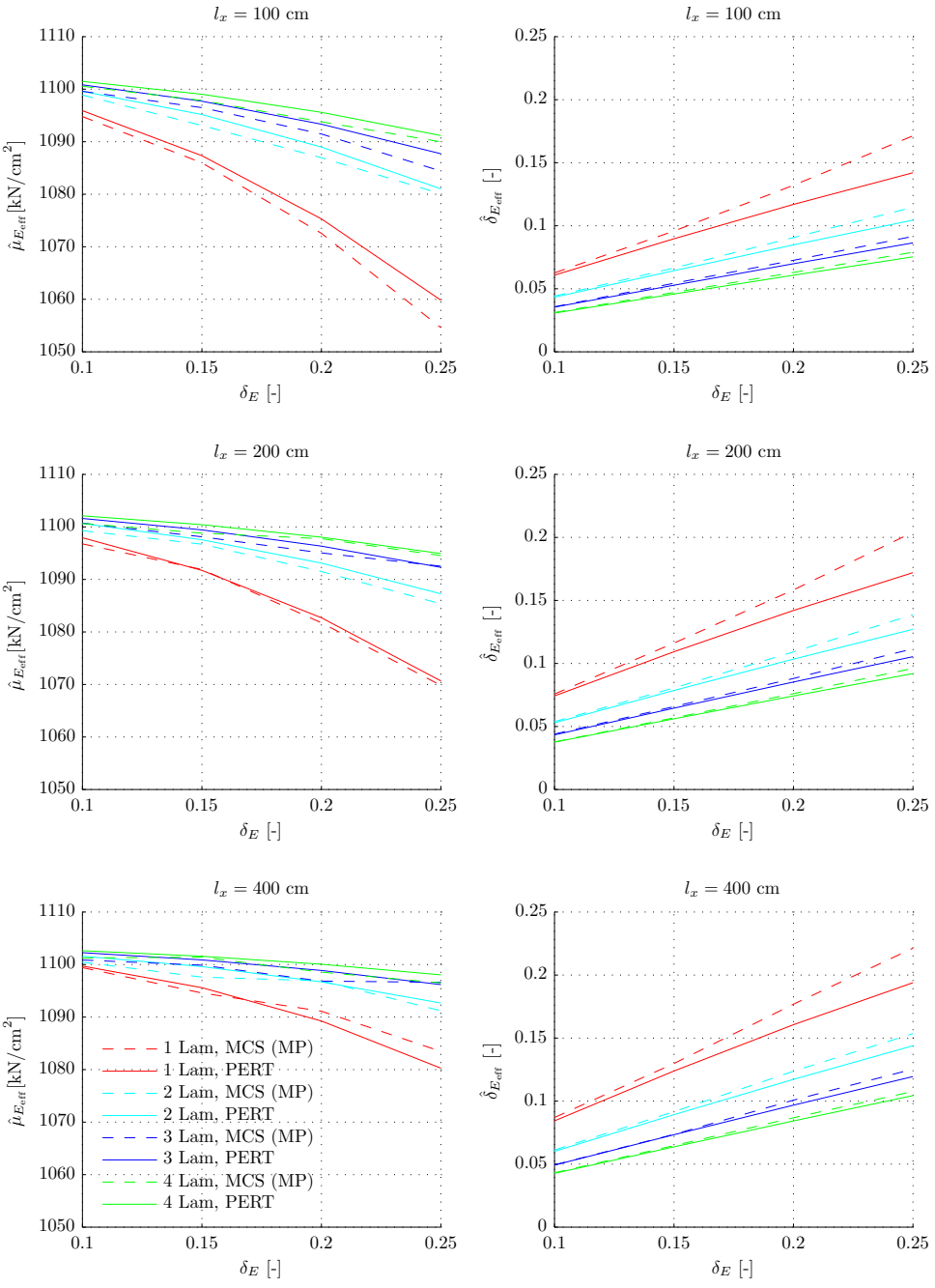

Figure 5.17: Mean and COV of the effective elastic modulus E_{eff} as a function of the COV δ_E of the "raw" material and for three different correlation lengths l_x, for up to four laminations, and for two SFE methods (MCS (MP) with 20000 samples and PERT method).

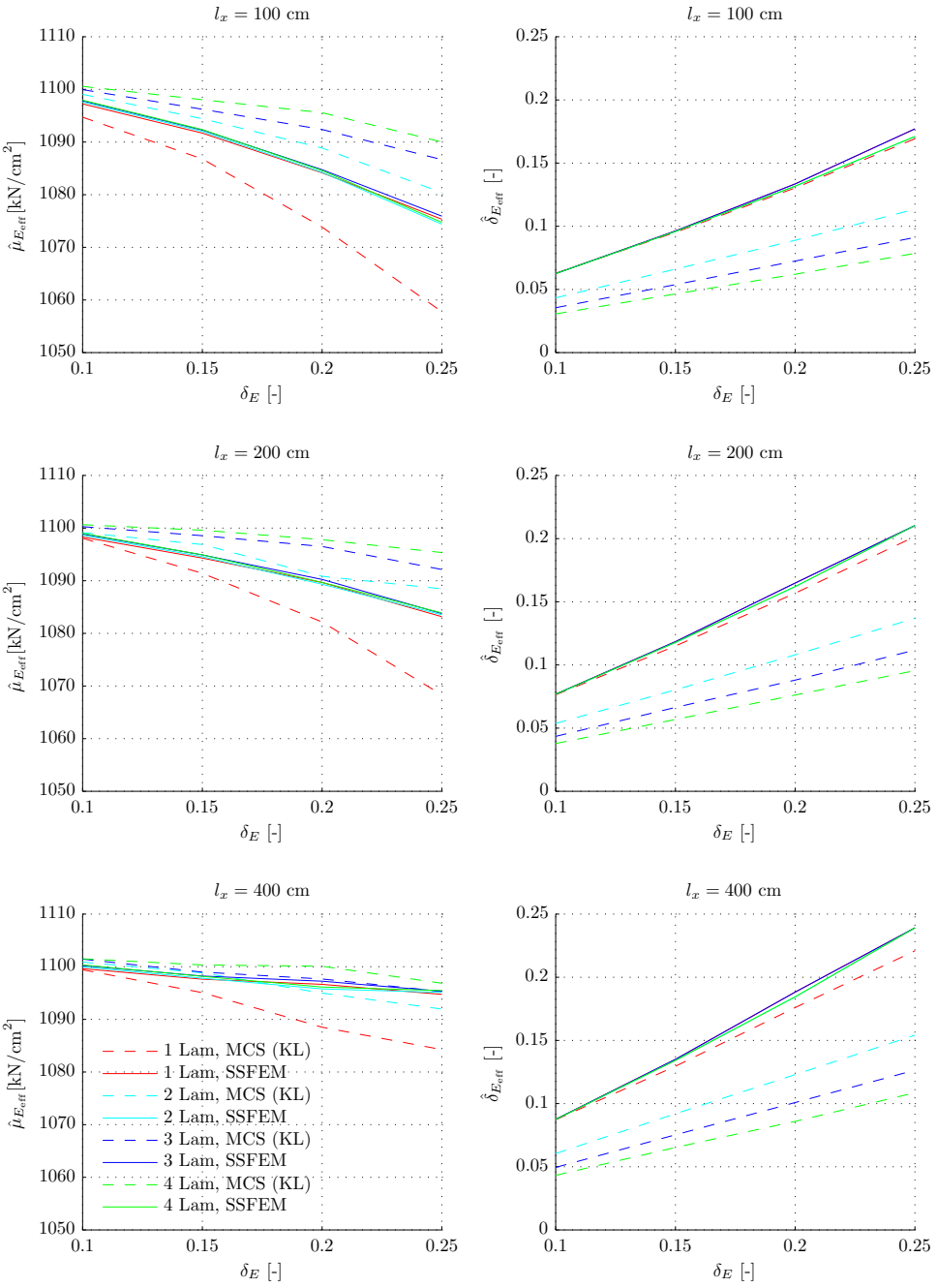

Figure 5.18: Mean and COV of the effective elastic modulus E_{eff} as a function of the COV δ_E of the "raw" material and for three different correlation lengths l_x, for up to four laminations, and for two SFE methods (MCS (KL) with 20000 samples and SSFEM).

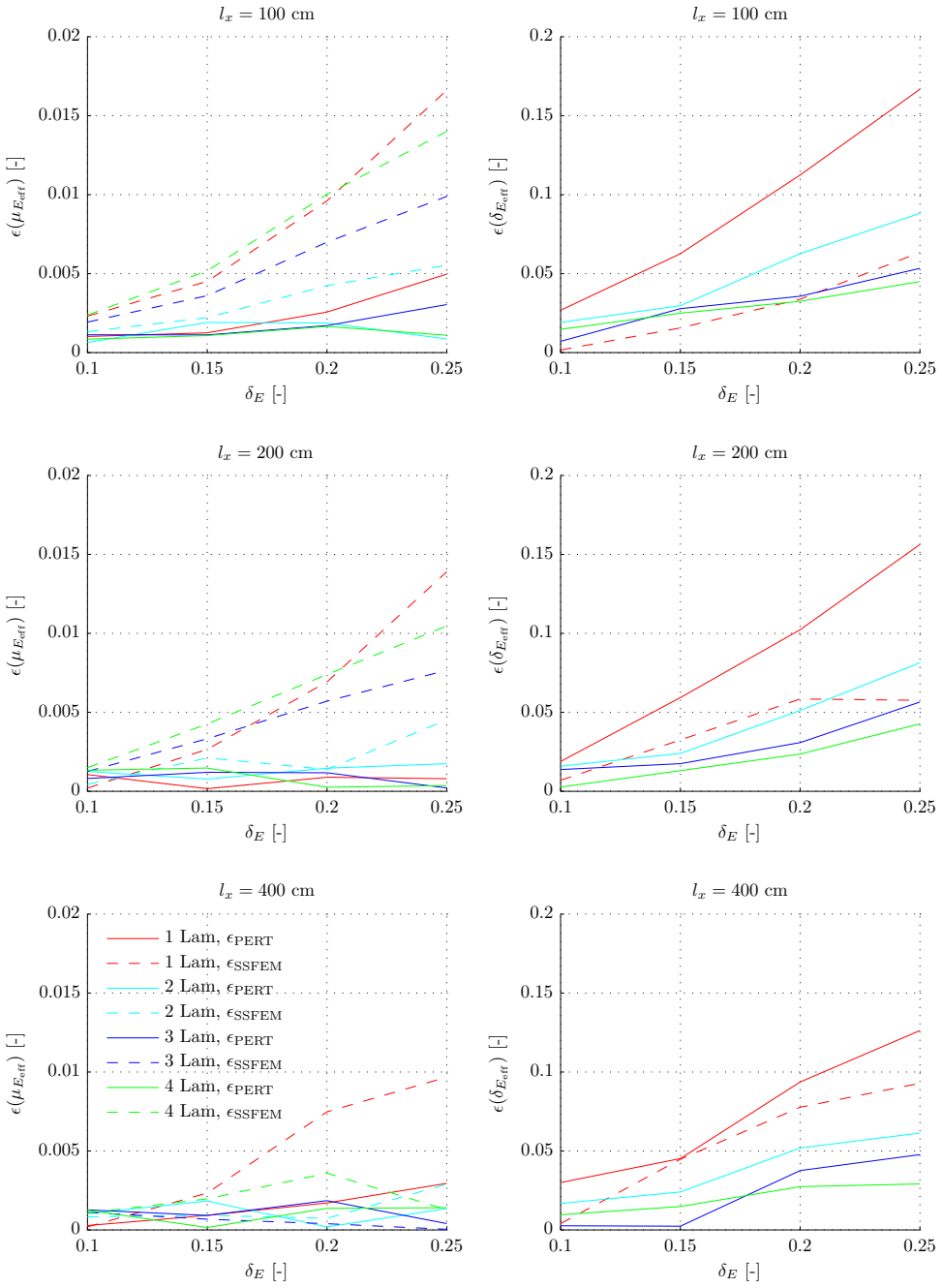

Figure 5.19: Estimation error of the mean and COV of E_{eff} as a function of the COV δ_E of the "raw" material and for three different correlation lengths l_x, for up to four laminations, and for two SFE methods (MCS (MP) and MCS (KL) with 20000 samples).

5.7.2 Results

The mean and the COV of the effective modulus E_{eff} are given as a function of the COV δ_E of the "raw" material and for three different correlation lengths l_x in Figures 5.17 and 5.18, respectively. For MCS, each sample is evaluated using (5.24), whereas results of PERT and SSFEM are computed according to Equations (5.25) and (5.26). In Figure 5.19 the relative errors ϵ_{PERT} and ϵ_{SSFEM} between PERT and SSFEM results and the corresponding MCS results are shown.

Regarding the Perturbation approach, related to the MCS the error of the estimate for the mean value $\mu_{E_{\text{eff}}}$ is fairly small ($\max(\epsilon_{\text{PERT}}) \leq 0.5\,\%$), where the maximal difference appears for one lamination. Since it is based on a first-order Taylor-series expansion, the PERT approach is not suitable to exactly reveal the increase of $\delta_{E_{\text{eff}}}$ with increasing material variability δ_E for one lamella, where the error is 17 %. However, in this particular case, with a maximal error of 9 % the estimate for $\delta_{E_{\text{eff}}}$ is of acceptable accuracy for all structural configurations with more than one lamination.

The SSFEM provides results for the mean value with a maximum error of approximately 1.5 %. Regarding the COV $\delta_{E_{\text{eff}}}$, the SSFEM estimation is less than 10 % for one lamination. However, this method fails to depict the lamination effect at all, which can not be explained by the author at this moment.

As can be seen throughout the data in Figures 5.17 and 5.18, increasing material variability δ_E results in a non-linear decrease of the mean value $\mu_{E_{\text{eff}}}$ and an almost linear increase of the COV $\delta_{E_{\text{eff}}}$, respectively. However, the absolute value of $\mu_{E_{\text{eff}}}$ does not deviate significantly from the "raw" material mean value $\mu_E = 1100\,\text{kN/cm}^2$, whereas the variability in terms of the coefficient of variation $\delta_{E_{\text{eff}}}$ changes substantially.

Furthermore, MCS (MP), MCS (KL), and PERT method nicely capture the so called lamination effect, which describes the decreasing variability of the compound product $\delta_{E_{\text{eff}}}$ with increasing number of laminations. In Figure 5.20 the variability of E_{eff} is plotted over the number of laminations for a COV of the "raw" material of 0.2. With increasing number of laminations, the variability of the structural response ($\delta_{E_{\text{eff}}}$) decreases significantly. From one to four laminations, a reduction in variability of more than 50 % is obtained. This effect stems from the lateral support of laminations by neighbouring laminations and the take-over of the load by other laminations in case of local weak spots.

Another effect with considerable impact results from different correlation lengths l_x. It can be seen in Figures 5.17, 5.18, and 5.20 that as l_x increases, so does $\delta_{E_{\text{eff}}}$. This can be explained by the fact, that the greater the correlation length, the more a realization of the random field fits an almost constant value along the lamination axis, as discussed in Subsection 2.7.1. This effect is demonstrated in Figure 5.21, where realizations with correlation lengths $l_x = \{100, 200, 400, 1200\}\,\text{cm}$ are shown for a GLT beam with three laminations. Since the stiffness within each lamination becomes more or less constant for a high correlation length, the ability of the laminations to redistribute the stresses deteriorates and in the end, as $l_x \to \infty$, reduces to the model of springs in parallel, resulting in a high variability $\delta_{E_{\text{eff}}}$.

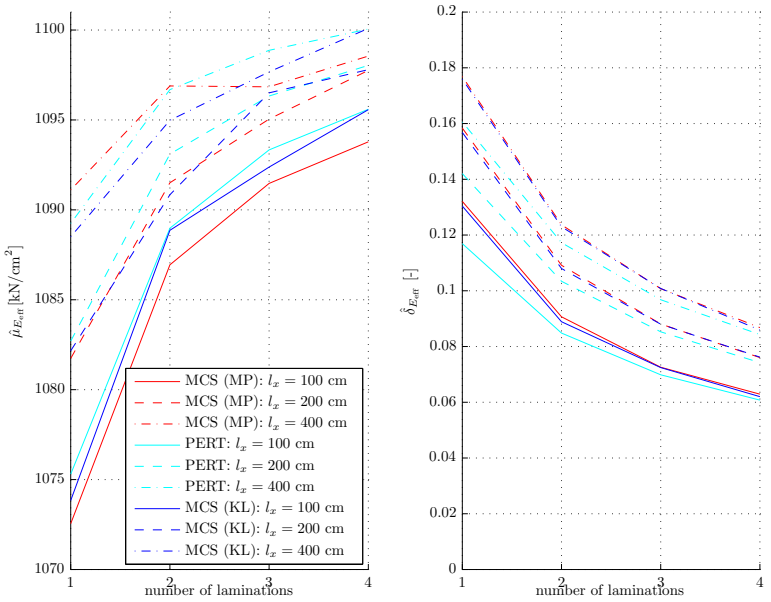

Figure 5.20: Mean value and COV of the effective elastic modulus E_{eff} plotted over the number of laminations, for $\delta_E = 0.2$.

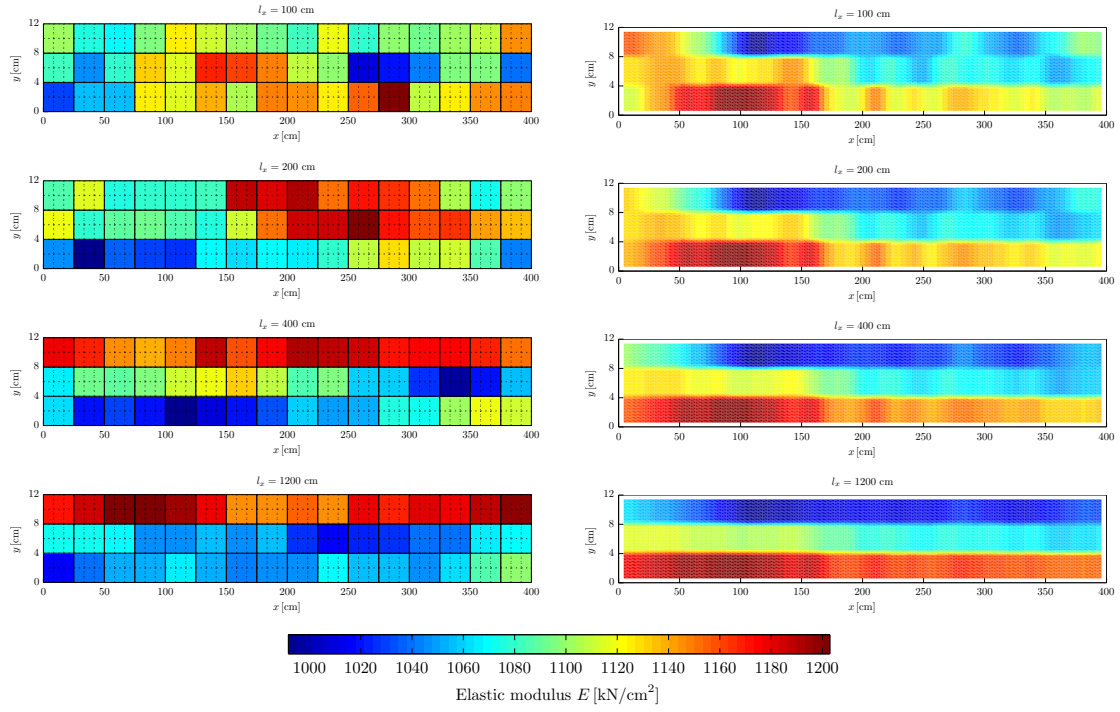

Figure 5.21: Realizations of the GLT-beam with $2, 3$, and 4 laminations using MP-discretization (left-hand side) with $N_e^{rf} = 16$ for each lamination and KL-expansion (right-hand side) of order $M = 16$, COV $\delta_E = 0.1$ and $l_x = 100\,\text{cm}$.

Chapter 6

Summary & conclusion

In this thesis, a brief introduction to probability theory was given (Chapter 2), followed by basic concepts of random field representation (Chapter 3). In Chapter 4, the application of probability theory in the framework of Finite-Element Methods was proposed. Therein, different so-called Stochastic-Finite-Element Methods were described, giving an idea of the strongly varying complexity and diversity of these approaches. Finally, in order to illustrate the performance of such methods, the three most prominent ones were applied to glued-laminated-timber elements (GLT), subjected to longitudinal loading (Chapter 5).

In different parameter studies, the influence of the variability of the "raw" material on the mechanical response on the structural scale is shown. Based on the obtained results, the following conclusions can be drawn:

- The coefficient of variation δ_E of the elastic modulus of the "raw" material has a major impact on the variability of the overall stiffness $\delta_{E_{\text{eff}}}$ of GLT, rather than the mean value $\mu_{E_{\text{eff}}}$.
- Similarly, $\delta_{E_{\text{eff}}}$ increases with the correlation length l_x. The acquisition of a correlation length suitable for depicting the stochastic phenomena of wood requires further research.
- With increasing number of laminations, the variability of the effective elastic modulus decreases substantially. This effect is known by the name "lamination effect", and is a result of load distributions in between the laminations of the GLT beam. This effect can be efficiently quantified using SFEM.
- The Monte Carlo simulation has been proven to be an universally applicable method, and therefore is used as benchmark model. However, the computational effort can be reduced significantly, while retaining the quality of the results, with the Spectral-Stochastic-Finite-Element Method or the Perturbation Method.

- The Spectral-Stochastic-Finite-Element Method gives accurate results for one lamination. However, the approach suggested in [8] failed to reveal the lamination effect, which could be a result of the Polynomial Chaos expansion with Hermite polynomials being inadequate for the response random field representation.
- The Perturbation Method delivers accurate results for two or more laminations with minimal computational effort. Therefore, it deserves further investigation regarding the improvements introduced in [15].

Summarized, it can be said that the Stochastic-Finite-Element Method is a powerful and valuable tool to gain understanding of the variability of the mechanical behaviour of wood-based products. Results, based on this methods, will become important in many fields, from grading and optimization of wood-based products to engineering design of wooden structures.

Bibliography

[1] R.J. Adler and J.E. Taylor. *Random fields and geometry*. Springer monographs in mathematics. Springer, 2007.

[2] Siu-Kui Au and James L. Beck. Estimation of small failure probabilities in high dimensions by subset simulation. *Probabilistic Engineering Mechanics*, 16(4):263 – 277, 2001.

[3] F. Beichelt. *Stochastische Prozesse für Ingenieure*. Teubner, 1997.

[4] R. Brandner and G. Schickhofer. Glued laminated timber in bending: new aspects concerning modelling. *Wood science and technology*, 42(5):401–425, 2008.

[5] R. Brandner and G. Schickhofer. Glued laminated timber in bending: thoughts, experiments, models and verification. In A. Ceccotti and J.-W. van der Kuilen, editors, *WCTE 2010 Conference Proceedings (DVD)*, 2010.

[6] C. Bucher. *Computational Analysis of Randomness in Structural Mechanics: Structures and Infrastructures Book Series*. Number 3 in Structures and Infrastructures Series. Taylor and Francis, 2009.

[7] C.G. Bucher and U. Bourgund. A fast and efficient response surface approach for structural reliability problems. *Structural Safety*, 7(1):57–66, 1990.

[8] Nian-Zhong Chen and C. Guedes Soares. Spectral stochastic finite element analysis for laminated composite plates. *Computer Methods in Applied Mechanics and Engineering*, 197(51-52):4830 – 4839, 2008.

[9] Seung-Kyum Choi, Ramana V. Grandhi, and Robert A. Canfield. Propagation of non-gaussian stochastic behavior using the polynomial chaos expansion. In K.J. Bathe, editor, *Computational Fluid and Solid Mechanics 2003*, pages 1896 – 1899. Elsevier Science Ltd, Oxford, 2003.

[10] Seung-Kyum Choi, Ramana V. Grandhi, and Robert A. Canfield. Structural reliability under non-gaussian stochastic behavior. *Computers and Structures*, 82(13-14):1113 – 1121, 2004. Advances in Probabilistic Mechanics and Structural Reliability.

[11] Armen Der Kiureghian and Jyh-Bin Ke. The stochastic finite element method in structural reliability. *Probabilistic Engineering Mechanics*, 3(2):83 – 91, 1988.

[12] O. Ditlevsen and B. Källsner. Statistical series system effects on bending strength of timber beams. In M.A. Maes and L. Huyse, editors, *Reliability and Optimization of Structural Systems*, pages 141–148. A.A. Balkema, 2004.

[13] O. Ditlevsen and H.O. Madsen. *Structural reliability methods*. Technical University of Denmark, 2007.

[14] Colling F.-Gölacher R. Ehlbeck, J. Einfluss keilgezinkter lamellen auf die biegefestigkeit von brettschichtholzträgern. *Holz als Roh- und Werkstoff*, 43:333–337, 369–373, 439–442, 1985.

[15] G. Falsone and N. Impollonia. A new approach for the stochastic analysis of finite element modelled structures with uncertain parameters. *Computer Methods in Applied Mechanics and Engineering*, 191(44):5067 – 5085, 2002.

[16] C.W. Gardiner. *Handbook of Stochastic Methods for Physics, Phemistry, and the Natural Sciences*. Springer series in synergetics. Springer, 1994.

[17] S. Ghahramani. *Fundamentals of probability with stochastic processes*. Pearson-/Prentice Hall, 2005.

[18] R.G. Ghanem and P.D. Spanos. *Stochastic Finite Elements: A Spectral Approach*. Springer-Verlag, 2003.

[19] A.A. Henriques. Efficient analysis of structural uncertainty using perturbation techniques. *Engineering Structures*, 30(4):990 – 1001, 2008.

[20] R. Hernandez, D. A. Bender, B.A. Richburg, and K. S. Kline. Probabilistic modeling of glued-laminated timber beams. *Wood and Fiber Science*, 24(3):294 – 306, 1991.

[21] T. Isaksson. Structural timber - variability and statistical modelling. In S. Thelandersson and H.J. Larsen, editors, *Timber Engineering*, pages 45–66. John Wiley & Sons, Chichester, 2003.

[22] D. Jackson. *Fourier Series and Orthogonal Polynomials*. Dover Books on Mathematics Series. Dover Publications, 2004.

[23] M. Kamiński. Generalized perturbation-based stochastic finite element method in elastostatics. *Computers and Structures*, 85(10):586–594, 2007.

[24] M. Kamiński and M. Kleiber. Perturbation based stochastic finite element method for homogenization of two-phase elastic composites. *Computers and Structures*, 78(6):811–826, 2000.

[25] M.M. Kamiński and P. Świta. Generalized stochastic finite element method in elastic stability problems. *Computers and Structures*, 89(11-12):1241 – 1252, 2011. Computational Fluid and Solid Mechanics 2011, Proceedings Sixth MIT Conference on Computational Fluid and Solid Mechanics.

[26] A. Der Kiureghian, T. Haukaas, and K. Fujimura. Structural reliability software at the university of california, berkeley. *Structural Safety*, 28:44 – 67, 2006. Structural Reliability Software.

[27] P.S. Koutsourelakis, H.J. Pradlwarter, and G.I. Schuëller. Reliability of structures in high dimensions, part i: algorithms and applications. *Probabilistic Engineering Mechanics*, 19(4):409 – 417, 2004.

[28] Chun-Ching Li and A. Der Kiureghian. Optimal discretization of random fields. *Journal of Engineering Mechanics*, 119(6):1136–1154, 1993.

[29] Hermann G. Matthies, Christoph E. Brenner, Christian G. Bucher, and C. Guedes Soares. Uncertainties in probabilistic numerical analysis of structures and solids-stochastic finite elements. *Structural Safety*, 19(3):283 – 336, 1997. Devoted to the work of the Joint Committee on Structural Safety.

[30] M.F. Ngah and A. Young. Application of the spectral stochastic finite element method for performance prediction of composite structures. *Composite Structures*, 78(3):447 – 456, 2007.

[31] Hyuk-Chun Noh and Taehyo Park. Monte carlo simulation-compatible stochastic field for application to expansion-based stochastic finite element method. *Computers & Structures*, 84(31-32):2363 – 2372, 2006.

[32] M.F Pellissetti and R.G Ghanem. Iterative solution of systems of linear equations arising in the context of stochastic finite elements. *Advances in Engineering Software*, 31(8-9):607 – 616, 2000.

[33] J.A. Rice. *Mathematical Statistics and data analysis*. Thomson Learning, 2006.

[34] G.I. Schuëller. Developments in stochastic structural mechanics. *Archive of Applied Mechanics*, 75(10-12):755–773, 2006.

[35] E. Serrano. *Adhesive joints in timber engineering - modelling and testing of fracture properties*. PhD thesis, Lund University, 2000.

[36] E. Serrano. Mechanical performance and modelling of glulam. In S. Thelandersson and H.J. Larsen, editors, *Timber Engineering*, pages 67–79. John Wiley & Sons, Chichester, 2003.

[37] G. Stefanou. The stochastic finite element method: Past, present and future. *Computer Methods in Applied Mechanics and Engineering*, 198(9-12):1031 – 1051, 2009.

[38] B. Sudret. *Uncertainty propagation and sensitivity analysis in mechanical models – Contributions to structural reliability and stochastic spectral methods*, 2007. Habilitation à diriger des recherches, Université Blaise Pascal, Clermont-Ferrand, France.

[39] B. Sudret and A. Der Kiureghian. *Stochastic finite element methods and reliability: a state-of-the-art report*. Report (University of California, Berkeley. Structural Engineering, Mechanics and Materials). Dept. of Civil and Environmental Engineering, University of California, 2000.

[40] P. E. Tissier. Bertrand's paradox. *The Mathematical Gazette*, 68(443):pp. 15–19, 1984.

[41] E. Vanmarcke. *Random Fields: Analysis and Synthesis*. World Scientific, 2010.

[42] D. Werner. *Funktionalanalysis*. Springer-Lehrbuch. Springer, 2007.

[43] Shinozuka Masanobu-Dasgupta Gautam Yamazaki, Fumio. Neumann expansion for stochastic finite element analysis. *Journal of Engineering Mechanics*, 114(8):1335–1354, 1988.

[44] Jun Zhang and Bruce Ellingwood. Orthogonal series expansions of random fields in reliability analysis. *Journal of Engineering Mechanics*, 120(12):2660–2677, 1994.